PhD-FSTC-2014-38

The Faculty of Sciences, Technology and Communication

DISSERTATION

Defense held on 27/10/2014 in Luxembourg

to obtain the degree of

DOCTEUR DE L'UNIVERSITÉ DU LUXEMBOURG
EN PHYSIQUE

by

Rymma SUSHKO

Born on 18 April 1984 in Kyiv (Ukraine)

THE EFFECT OF INTERPHASES CREATED BY AL_2O_3 NANOPARTICLES IN STYRENE BUTADIENE RUBBER

Dissertation defense committee

Dr Roland Sanctuary, dissertation supervisor
Professor, Université du Luxembourg

Dr Jörg Baller
Adjoint de recherche, Université du Luxembourg

Dr Phillip Dale, Chairman
Associate Professor, Université du Luxembourg

Dr Benoît Duez
External Exploration Concept Leader, Goodyear Innovation Center Luxembourg

Dr Jan-Kristian Krüger, Vice Chairman
Professor, Universität des Saarlandes

Table of contents:

Abstract

Elastomers are key-materials e.g. in tire industry. Nowadays it is common practice to enhance the mechanical performance of elastomers by introducing inorganic nanoparticles into the polymer matrix. Due to the extremely small filler size giant interfaces are created between the surfaces of the nanoparticles and the matrix molecules especially when the fillers are homogeneously distributed throughout the host material. Interfacial interactions can lead to the formation of regions with changed molecular mobility and/or morphology (so-called interphases) in the immediate vicinity of the fillers' surfaces. A challenging task consists in investigating and understanding the effect produced by interphases on the macroscopic properties of the polymer matrix.

In the frame of the present PhD research project an uncured styrene-butadiene rubber (SBR) was used as a matrix for three types of nanoparticles: native alumina, alumina coated with γ-mercaptopropyltrimethoxysilane (Mercapto) layers and finally alumina-Mercapto nanoparticles with SBR molecules grafted onto. The thermal and mechanical properties of the three families of nanocomposites were investigated using mechanical spectroscopy (rheometry and dynamical mechanic analysis). Electron microscopy was exploited for structural analysis.

Irrespective of the surface treatment of the nanoparticles an unexpected minimum of the glass transition temperature is found at small filler concentrations of about 2 wt.%. At higher filler contents each of the three families of nanocomposites is characterized by its own characteristic evolution of the glass transition temperature as a function of the filler content. Models are suggested to explain the different glass transition behaviors. Furthermore the influence of the surface treatment on the mechanical answer of the nanocomposites especially to low-frequency shear fields is discussed.

Acknowledgements

It would not have been possible to write my doctoral thesis without the help and support of the great people around me, to only some of whom it is possible to give particular mention here.

Firstly, I wish to express my sincere gratitude to my supervisors, Prof. Roland Sanctuary and Dr. Jörg Baller, for their kind help, guidance and constant encouragement throughout the course of the research project.

I am also very grateful to Prof. Jan-Kristian Krüger from the Saarland University for being part of my CET committee.

Furthermore, I would like to thank Dr. Phillip Dale from the University of Luxembourg and Dr. Benoît Duez from Goodyear Innovation Center Luxembourg for being part of the jury.

A special thanks goes to Dr. Marlena Filimon not only for microscopic measurements of my samples, but also for her constant help, advice and friendship. Another special thanks goes to our technician, Olga Astaschewa, for her constant (both technical and moral) support, and to Zornitza Tosheva.

Furthermore, I would like to thank Patrick Elens and Rick Dannert for doing rheology measurements for me in urgent mode. I'm also thankful to Anna Djemour for being a good companion at the conferences and for language lessons. I'm thankful to Carlo Di Giambattista for DLS measurements.

I would like to thank our secretary, Astrid Tobias, for making much simpler all of the complicated administrative things.

I'm thankful to Roby Wagener and Erny Apel for technical support.

I would like to acknowledge Fonds National de la Recherche Luxembourg (FNR) for funding and for interesting workshops.

I would like to express my thanks to my mom Tetiana and my brother Vlad for their motivation and continuous support. Special thanks to Sheyla.

I would like to thank Fabio and Anna for being with me when I had rough times.

Finally, much is owed to my colleagues and the technical staff within the department for their assistance and support.

Work done in conjunction with others

The work presented in this thesis was carried out by the author, with the following exceptions:

1. The TEM and ESEM measurements were done either by Marlena Filimon (University of Luxembourg) or Markus Ziehmer (University of Luxembourg), in collaboration with Jörg Schmauch (Saarland University).
2. The FT-IR measurements were done by the author together with Olena Litsis (National Taras Shevchenko University of Kyiv)
3. The rheological measurements were done by Rick Dannert (University of Luxembourg) and Patrick Elens (University of Luxembourg).

Introduction

Due to their unique mechanical properties, elastomers have a large spectrum of application: automotive and sports equipment, glues, different rubber products. As a function of application, a variety of formulations allows producing the specific materials. Very often in such formulations different fillers (such as carbon black, silica, clays etc.) are used. Those fillers improve significantly the wear properties of the composites and particularly their mechanical properties (elastic and shear moduli, impact strength, yield resistance etc.). Industry is highly interested in low-cost fillers that, already at small concentrations (negligible impact on mass), yield innovative properties or an improvement of the mechanical performance of the matrix. Although the composite materials already exist for a very long period of time, there is still no unambiguous explanation of the reinforcement effect produced by the fillers. In a large number of papers dealing with this subject, improved mechanical performances are attributed to the emergence of a filler network inside the polymer matrix requiring the existence of filler/filler and/or filler/matrix interactions inside the polymer matrix. In case of nanosized fillers such interactions can become extremely important because of the very large contact area (interface) [1-2] between the matrix and the fillers. In many cases the interfacial interactions lead to the formation of polymer layers with modified chain mobility in the immediate vicinity of the nanoparticles [3-5]. Very often these regions with changed molecular mobility and/or morphology are named interphases. By varying the size of the fillers or the chemical nature of the fillers' surfaces, the interactions with the polymer matrix can be influenced. Nowadays a lot of publications involving elastomers filled with carbon black or silica nanoparticles are available [1, 5-15]. To our best knowledge only little research work has so far be done on elastomer/alumina nanocomposites [10, 13, 26-27, 31].

As already pointed out, generally, the new or improved properties of the nanocomposites are linked to the modification of structure and dynamics of the polymer at and near the particle surface [5]. Because of the huge interfacial area this fraction of the polymer contributes significantly to the properties of the whole nanocomposite, even at low filler concentrations. Changes of molecular dynamics in the vicinity of the filler surfaces can be due to crowding and/or local ordering of chains as well as to loss of configurational entropy of the polymer segments near the solid surface (as a result of physico-chemical interactions e. g. [3-4]. Changes of molecular dynamics as a result of matrix/filler interactions can take influence on the mechanical reinforcement of the nanocomposites. Filler-filler interactions (network formation e.g.) represent an alternative mechanism able to take influence on the reinforcement of the polymer.

In many cases the glass transition (α-process) is exploited to investigate filler-induced changes of the molecular dynamics in the polymer matrix. Many different behaviors have been reported in literature: the glass transition temperature of the nanocomposite was found to increase, to decrease, not to be influenced at all, or the glass transition disappeared totally with increasing filler content [1,5,12-17].

Numerous experimental investigations [5,12,18] provide evidence for the existence of regions characterized by modified chain mobility. These domains do not extend throughout the whole nanocomposite but are restricted to layers with a thickness of a few nanometers located at the surfaces of the nanoparticles (interphases). For sure, reinforcement strongly depends on the properties of the interphases: it is largely influenced by the specific interactions between fillers and matrix molecules. Neutron scattering experiments realized on poly(dimethyl siloxane) filled with hydrophilic fumed silica have revealed the existence of two relaxation times – a slow process corresponding to restricted mobility near the filler surface and the α-process of the bulk polymer [20]. In a further work V. Arrighi et al. [12] exploited DMA (Differential Mechanical Analysis) to prove the existence of a second (slower) relaxation process in cured SBR samples filled with amorphous silica nanoparticles. This process emerging additionally to the α-process at temperatures about 40 °C above T_g was also brought into relation with reduced mobility of SBR molecules near the nanoparticle surface (constraints imposed by interactions with fillers/ confinement). Its intensity increases with the filler content. Double $\tan\delta$-peaks in poly(vinyl alcohol)/silica nanocomposites revealed by dynamical mechanical analysis are interpreted by a similar two-phase model (bulk polymer/polymer with reduced mobility near the silica) in the work of Lin Chen et al. [20].

In their highly cited work Tsagaropoulos et al [4] even claim the existence of three phases in polymer-based nanocomposites: a layer with tightly bound polymer at the surface of the nanoparticle, a second layer adjacent to the first one with loosely bound polymer and as a third phase bulk polymer. The authors justify that this double nanolayer model is appropriated to describe the emergence and complex evolution of two $\tan\delta$-peaks observed with DMA in a bunch of uncrosslinked polymers (PMMA, P4VP, PS, PDMS, PVAc, SBR) filled with nano-sized silica. The first “low-temperature” peak is associated to the glass transition of the bulk material. The second peak, occurring at temperatures as much as about 100 °C above the primary $\tan\delta$-peak is ascribed to the glass transition of loosely bound chains near the nanoparticles. In particular the shift of the slow process to lower temperatures and the reduction of the respective strengths of the glass transitions when the filler concentration increases is interpreted as a consequence of the progressive transformation of loosely bound polymer (exhibiting its own glass transition) into tightly bound polymer (showing any glass transition).

Support for the existence of polymer regions characterized by different mobility is provided by NMR relaxation time measurements on filled rubbers [21-24].

In their review article on glass transition and interfacial segmental dynamics in polymer-particle composites Robertson and Roland [25] point out that the “second glass transition” brought into play by Tsagaropoulos and Eisenberg [4] is located in the viscoelastic zone associated with terminal flow of the polymer. The authors suggest an alternate interpretation: the terminal relaxation process (chain diffusion) of un-crosslinked polymer can be suppressed by interaction with particles. This implies that only chains unaffected by the particles flow under usual terminal regime conditions. As a consequence terminal dispersion - reflected by a loss tangent peak – emerges instead of the usual divergence of tan δ towards infinity with increasing temperature (or decreasing frequency).

Robertson et al. [25] also stress that in case of the glass-rubber transition the interpretation of the maxima of the tan $\delta(f)$ or tan $\delta(T)$ curves as indicators of the glass transition can be problematic. As a matter of fact, in the softening region $\tan\delta$ is not only influenced by the local segmental dynamics, as reflected in the magnitude of the loss modulus at lower temperatures, but also by filler-induced changes in both G' and G'' at higher temperatures. In [6] the authors proved for BR reinforced with carbon black or SBR reinforced with silica, that the shape and position of the loss modulus peak (reflecting segmental motions) are unaffected by particle surface area and the intensity of the polymer-filler interaction, despite substantial changes in the loss tangent peaks.

Bindu and Thomas [17] studied viscoelastic behavior of the natural rubber (NR)/ZnO nanocomposites by DMA and discovered not only significant reinforcement effect, but also showed that the mobility of rubber chains in the proximity of nanoparticles is significantly reduced. The shift of the tan δ peak to the higher temperatures, as well as the lowering of the peak intensity compared to the neat NR has been observed.

The nanoparticles agglomeration and the lack of chemical bonding between the inorganic particles and organic matrix are the most prominent reasons impeding the reinforcement [26-27]. The interaction between the components of the nanocomposite can be promoted or inhibited by selection of the polymer and specifically modified filler [1, 26-27].

Chemical compatibility between fillers and rubber matrix is expected to play an important role in the dispersion of the fillers in the matrix and in the strong adhesion between the two phases [28-34]. Different fillers and rubbers require different coupling agents. For example, silane coupling agents work very well for silica and alumina-filled rubber composites [26, 31, 34].

Another method of enhancing the polymer-filler interaction consists in creating of the covalent bonds between these two components. It is believed that nanoparticles, which are tightly attached to the matrix, bring the wear resisting and friction reducing features of the particles into play. The feasibility of this concept has been partly proved by work of the Friedrich group on nano-silica filled epoxy systems [35-36]. Meanwhile, the approach proved to be an effective way for strengthening and toughening thermoplastics at rather low nano-filler loading [37-39].

In this work, three types of nanocomposites (styrene-butadiene rubber (SBR) filled with a) untreated Al_2O_3 nanoparticles, b) silanized Al_2O_3 nanoparticles, c) silanized Al_2O_3 nanoparticles grafted to the polymer chains) are investigated by Dynamic Mechanical Analysis (DMA) and Temperature-Modulated Differential Scanning Calorimetry (TMDSC) and structural investigation tools. As a matrix we choose a model rubber in form of physically cross-linked styrene butadiene. The aim of the investigation is to study the influence of the surface treatment of alumina nanoparticles on the glass transition behavior and on the reinforcement of the rubber matrix. How do molecular dynamics evolve when the filler concentration is changed or when, for a given nanoparticle concentration we modify the surfaces of the alumina nanoparticles? Does a second glass transition e.g. associated to the emergence of domains with altered molecular mobility, occur? What do we learn from changes of the glass transition temperature regarding interactions taking place inside the polymer matrix? Which influence do the different types of alumina have on the reinforcement of the SBR matrix, on the rheological behavior of the nanocomposites at the lowest probe frequencies? – such questions we will try to answer in this thesis.

References:

[1] Gauthier C., Reynaud E., Vassoille R., Ladoouce-Stelandre L., Analysis of the non-linear viscoelastic behaviour of silica filled styrene butadiene rubber, *Polymer,* 2004, 45, p.2761-2771.

[2] Pal K., Rajasekar R., Kang D.J., Zhang Z.X., Pal S.K., Das C.K., Kim J.K., Effect of fillers on natural rubber/high styrene rubber blends with nano silica: Morphology and wear, *Materials and Design*, 2010, 31, p.677–686.

[3] Tsagaropoulos G, Eisenberg A. Direct observation of two glass transitions in silica-filled polymers. Implications for the morphology of random ionomers, *Macromolecules*, 1995,28, p.396–398.

[4] Tsagaropoulos G, Eisenberg A. Dynamic mechanical study of the factors affecting the two glass transition behavior of filled polymers. Similarities and differences with random ionomers, *Macromolecules*, 1995, 28 (18), p.6067–6077.

[5] Sargsyan A., Tonoyan A., Davtyan S., Schick C. The amount of immobilized polymer in PMMA SiO_2 nanocomposites determined from calorimetric data, *European Polymer Journal*, 2007, 43, p.3113-3127.

[6] Robertson C.G., Lin C.J., Rackaitis M., Roland C.M., Influence of particle size and polymer-filler coupling on viscoelastic glass transition of particle-reinforced polymers, *Macromolecules*, 2008, 41, p. 2727-2731.

[7] Julien Ramier, PhD Thesis "Comportement mécanique d'élastomères chargés, Influence de l'adhésion charge-polymère, Influence de la morphologie", l'INSA de Lyon, 2004.

[8] Zhang A., Wang L., Zhou Y., A study on rheological properties of carbon black extended powdered SBR using a torque rheometer, *Polymer Testing*, 2003, 22, p.133-141.

[9] Marc Thomine, PhD Thesis "Relations viscoélasticité/tribology des élastomères chargés", l'INSA de Lyon, 2004.

[10] R. Sanctuary, J. Baller, J.K. Krüger, D. Schaefer, R. Bactavatchalou, B. Wetzel, W. Possart, P. Alnot, Complex specific heat capacity of two nanocomposite systems, *Thermochimica Acta,* 2006, 445 (2), 111-115.

[11] Vallés-Lluch A., Gallego Ferrer G., Monleón Pradas M., Effect of the silica content on the physico-chemical and relaxation properties of hybrid polymer/silica nanocomposites of P(EMA-co-HEA), *European Polymer Journal*, 2010, 46, p.910–917.

[12] Arrighi V., McEwen I.J., Qian H. and Prieto M.B.S., The glass transition and interfacial layer in styrene-butadiene rubber containing silica nanofiller, *Polymer*, 2003, 44, p.6259-66.

[13] Zhao S., Schadler L.S., Duncan R., Hillborg H. and Auletta T. Mechanisms leading to improved mechanical performance in nanoscale alumina filled epoxy, *Composites Science and Technology,* 2008, 68, p.2965-75.

[14] Alexandre M. and Dubois P. Polymer-layered silicate nanocomposites: preparation, properties and uses of a new class of materials, *Materials Science & Engineering R-Reports,* 2000, 28, p.1-63.

[15] Bansal A., Yang H., Li C., Benicewicz R.C., Kumar S.K. and Schadler L.S., Controlling the thermornechanical properties of polymer nanocomposites by tailoring the polymer-particle interface, *Journal of Polymer Science Part B-Polymer Physics,* 2006, 44, p.2944-50.

[16] Bansal A., Yang H.C., Li C.Z., Cho K.W., Benicewicz B.C., Kumar S.K. and Schadler L.S., Quantitative equivalence between polymer nanocomposites and thin polymer films, *Nature Materials*, 2005, 4, p.693-8.

[17] Bindu P. and Thomas S., Viscoelastic Behavior and Reinforcement Mechanism in Rubber Nanocomposites in the Vicinity of Spherical Nanoparticles, *Journal of Physical Chemistry B,* 2013, 117, p.12632-48.

[18] Lipatov Y.S. and Privalko V.P., Glass transition in filled polymer systems, *Polymer Sci. USSR*, 1972, 14 (7), p.1843.

[19] Arrighi V., Higgins J. S., Burgess A. N. and Floudas G. Local dynamics of poly(dimethyl siloxane) in the presence of reinforcing filler particles, *Polymer*, 1998, 39 (25), p.6369-6376.

[20] Chen L., Zheng K., Tian X., Hu K., Wang R., Liu C., Li Y. and Cui P., Double Glass Transitions and Interfacial Immobilized Layer in in-Situ-Synthesized Poly(vinyl alcohol)/Silica Nanocomposites, *Macromolecules*, 2010, 43 (2), p.1076–1082.

[21] Kaufman S., Slichter W. P., Davis D. D., Nuclear magnetic resonance study of rubber–carbon black interactions, *Journal of Polymer Science Part A-2: Polymer Physics*, 1971, 9 (5), p.829-39.

[22] O'Brien J., Cashell E., Wardell G. E., McBrierty V. J., An NMR investigation of the interaction between carbon black and cis-polybutadiene, *Macromolecules*, 1976, 9, p.653-660.

[23] Dutta N.K., Choudhury N.R., Haidar B., Vidal A., Donnet J. B., Delmotte L., Chezeau J.M., High resolution solid-state n.m.r. investigation of the filler-rubber interaction: 1. High speed ^{1}H magic-angle spinning n.m.r. spectroscopy in carbon black filled styrene-butadiene rubber, *Polymer,* 1994, 35, p.4293-99.

[24] Ito M., Nakamura T., Tanaka K., Pulsed NMR study on the silica-filled rubber systems, *Journal of Applied Polymer Science*, 1985, 30, p.3493-3504.

[25] Robertson C.G. and Roland C.M., Glass Transition and Interfacial Segmental Dynamics in Polymer-Particle Composites. Rubber Chemistry and Technology, 2008, 81 (3), p.506-522.

[26] Shukla D.K., Kasisomayajula S.V., Parameswaran V. Epoxy composites using functionalized alumina platelets as reinforcements Comp. Sci. Tech., V. 68, I.14, 2008, P. 3055–3063.

[27] Yang Y.-Ch., Jeong S.-B., Kim B.-G., Yoon P.-R. Examination of dispersive properties of alumina treated with silane coupling agents, by using inverse gas chromatography. Powder Technology, 191, 117–121 (2009).

[28] Suzuki N., Ito M., Yatsuyanagi F., Effects of rubber/filler interactions on deformation behavior of silica filled SBR systems, Polymer 46 (2005) 193–201.

[29] Gojny F.H., Wichmann M.H.G., Kopke U., Fiedler B., Schulte K. Carbon nanotube reinforced epoxy-composites: enhanced stiffness and fracture toughness at low nanotubes content. Comp Sci Tech 2004;64:2363–71.

[30] Yong V., Hahn H.T. Processing and properties of SiC/vinyl ester nanocomposites. Nanotechnology 2004;15:1338–43.

[31] Guo Z., Pereira T., Choi O., Wang Y., Hahn H.T. Surface functionalized alumina nanoparticle filled polymeric nanocomposites with enhanced mechanical properties. J Mater Chem 2006;16:2800–8.

[32] Tee D.I., Mariatti M., Azizan A., See C.H., Chong K.F. Effect of silane-based coupling agent on the properties of silver nanoparticles filled epoxy composites. Comp Sci Tech 2007;67:2584–91.

[33] Yuen S.M., Ma C.C.M., Chiang C.L., Chang J.A., Huang S.W., Chen S.C., et al. Silane-modified MWCNT/PMMA composites – preparation, electrical resistivity, thermal conductivity and thermal stability. Composites Part A: Applied Science and Manufacturing, V.38, I.12, 2007, 2527–2535.

[34] ten Brinke J.W., Debnath S.C., Reuvekamp L.A., Noordermeer J.W.M. Mechanistic aspects of the role of coupling agents in silica-rubber composites. Comp. Sci. Tech., 2003, 63(8), 1165-1174.

[35] Zhang M.Q., Rong M.Z., Yu S.L., Wetzel B., Friedrich K., Improvement of tribological performance of epoxy by the addition of irradiation grafted nano-inorganic particles, Macromol. Mater. Eng., 2002, 278, p.111-115.

[36] Rong M.Z., Zhang M.Q., Shi G., Ji Q.L., Wetzel B., Friedrich K., Graft polymerization onto inorganic nanoparticles and its effect on tribological performance improvement of polymer composites, Tribology International, 2003, 36, p.697-707.

[37] Rong M.Z., Zhang M.Q., Zheng Y.X., Zeng H.M., Walter R., Friedrich K., Structure-property relationships of irradiation grafted nanoinorganic particle filled polypropylene composites, Polymer, 2001, 42, p.167-183.

[38] Rong M.Z., Zhang M.Q., Zheng Y.X., Zeng H.M., Walter R., Friedrich K., Irradiation graft polymerization on nano-inorganic particles: an effective means to design polymer based nanocomposites. J Mater Sci Lett 2000;19:1159–61.

[39] Rong M.Z., Zhang M.Q., Zheng Y.X., Zeng H.M., Friedrich K., Improvement of tensile properties of nano-SiO_2/PP composites in relation to percolation mechanism, Polymer, 2001, 42, p.3301-3304.

Chapter I: Reinforcement of elastomers

I.1. Introduction to elastomer nanocomposites

Elastomer materials can undergo large, reversible elastic deformation, and offer novel possibilities for creating powerful materials. Structures consisting of soft materials such as elastomers have use in a variety of applications including automotive equipment, shoes, glues, MEMS devices, chemical or optical sensors [1]. Numerous recent studies (both experimental and theoretical) have explored the mechanical properties of such soft materials. The single most important property of elastomers - that from which their name derives - is their ability to undergo large elastic deformations, that is, to stretch and return to their original shape in a reversible way [2]. Often, this property appears to be unsufficient for an elastomer to be used at certain conditions. Many of the usual applications of elastomers could not be envisaged without the use of particulate fillers. The reinforcement of elastomers by such fillers has been extensively studied in the past, particularly in the 1960s-1970s. The main reason of such interest is the drastic changes in mechanical properties that filler introduction induces in polymer matrix. Unlike for plastics where reinforcement results in an increase in modulus and hardness, in case of elastomers the use of fillers induces simultaneous increase in modulus and deformation at break [2].

I.2. Fillers

Over the past few years polymer nanocomposites have been widely discussed by scientists by considering the number of potential nanoelements such as layered silicates, talc, silica, alumina, biofillers and carbon nanotubes. Although all these nanofillers have been in use in rubber nanocomposites for past 10 years, the major interest is on the use of layered silicates (clays), silica particles, carbon black and carbon nanotubes [3].

A fine dispersion of filler is needed to obtain a good adhesion at the polymer-filler interface, which is responsible for the reinforcement effect. Due to the large surface area of the nanosized fillers, their dispersion in polymers provides significantly improved properties compared to those of the pure polymer. Nowadays nanosized fillers can be found as layered structures (e.g. clays) [4-8], nanotubes (e.g. carbon nanotubes) [3, 9-16], isodimensional (or spherical) particles (e.g. silica) [17-23], POSS (polyhedral oligomeric silsesquioxane) [24-27] and fibers (e.g. wood fibers) [28-31].

Nanoparticles of spherical shape, which are of interest for the present thesis, have attracted a great attention nowadays due to the noticeable effect on polymer properties. It is generally believed that the change in behavior of the polymer matrix observed for nanocomposites containing spherical nanoparticles is associated with the greater specific interfacial area compared to conventional (i.e. micron-sized or larger) fillers. Different types of spherical nanoparticles are produced nowadays: SiO_2, Al_2O_3, TiO_2, V_2O_5, MoO_3, MgO, ZrO_2, ZnO, Fe_2O_3, SnO, carbon black, polymer nanoparticles etc. Oxide nanoparticles can exhibit unique physical and chemical properties due to their limited size and a high density. Bulk oxides are usually robust and stable systems with well-defined crystallographic structures. The preparation methods of such nanoparticles can be grouped in two main streams based upon the liquid-solid [17] and gas-solid [18] processes. The current knowledge on spherical nanoparticles allows affirming that most of their properties are size-dependent [19-23]. Similarly to the nanotubes, spherical nanoparticles exhibit a general trend towards aggregation.

I.3. Preparation methods of elastomer nanocomposites

The preparation methods of rubber nanocomposites could be divided into three groups:

1) dispersion of nanoparticles in the polymer matrix,
2) synthesis of the polymer in presence of nanofiller,
3) synthesis of nanoparticles in presence of polymer.

The first group includes the melt blending and the solution mixing of the polymer nanocomposites.

The melt blending is performed in extruders, two-roll mills or internal mixers at temperatures of the liquid state of polymer [32-38]. By control of mixing conditions the uniform distribution of the nanoparticles in the polymer matrix can be achieved. The high shear forces generated between extruder walls and screws or mill rolls allow obtaining almost perfect dispersion of the nanofiller in the polymer. This method is of great technical importance because of very simple upgrade from laboratory to industrial scales. The disadvantage is partial polymer chains degradation due to the shear forces or high temperatures. Control of molecular weight is therefore required.

The solution mixing uses polymer solution and nanoparticles dispersed in a solvent [39-41]. Such mixing allows obtaining relatively good dispersion of the nanoparticles in the polymer matrix. It is applicable to polymers that can be dissolved or swelled by the solvent [3, 42]. The stirring rate and the sonification of the solution are the factors influencing the filler dispersion in the nanocomposite. Ultrasound is often used in nanocomposite preparation [43-47]. The chemical effects of ultrasound derive primarily from acoustic cavitation [46]. The main advantage of this method in the context of the present work is the high level of kinetic energy which eventually is transferred to the nanoparticles resulting in desagglomeration. Therefore, the solution mixing method and the ultrasound treatment of nanoparticles have been used for nanocomposites preparation in this work.

If the rubber is obtained in the latex form, compounds added to the raw latex must be in the form of emulsions or dispersions [3]. Gelatin, casein, glues, soaps are frequently used as wetting or dispersing agents. The latex is usually stabilized with surfactants, which act by imparting a charge to the surface of the tiny rubber particles or by holding an envelope of water around the particle, thereby preventing any aggregation.

The second group of nanocomposite preparation methods includes chemical processes, in which polymerization is performed in the presence of the inorganic particles. Different types of polymerization can be performed using this method: radical [49, 59-60], ionic [61], emulsion [44-45, 50-56], suspension [48, 57-58] polymerization etc. Seeded (in the presence of nanoparticles) emulsion polymerization technology is commonly used in the production of nanocomposite emulsions [61]. Using this method, it is possible to control the reaction rate, particle size and morphology effectively [62].

The third group of methods is synthesis of nanoparticles in presence of monomers, oligomers or polymers. Different techniques can be used for this purpose. It was shown [63] that homogeneous dispersion of the nanoparticles in the polymer matrix can be achieved using this method because polymerization of organic monomer and formation of inorganic nanoparticles are simultaneous. Also, the presence of inorganic ions sometimes can catalyze the polymerization of the organic monomer [64]. At the same time, produced during reaction organic polymer matrices can efficiently prevent the produced inorganic nanoparticles from agglomeration. The polymer nanocomposites can be prepared also by synthesis of the nanoparticles in the polymer matrix [65-69]. Also here the polymer matrices efficiently prevent the formed inorganic nanoparticles from agglomeration [69].

Thus, the polymer nanocomposites can be obtained by various preparation methods. The properties of the final composites depend on different factors, such as nanoparticle size, polymer type and the interaction between the polymer and the nanoparticles.

I.4. Polymer-filler interactions

One of the most important factors influencing the composite properties is the polymer-filler interaction, which also depends on the degree of agglomeration of nanoparticles in the polymer matrix and the chemical compatibility of the components. The most popular type of the nanocomposites is hydrophilic inorganic filler/hydrophobic organic polymer. Often, due to the different chemical nature of the surfaces, the interactions between the components are not significant and do not result in desired modification of the properties. Many developments have been introduced as surface modifications for inorganic fillers. Typically, these modifications have aimed at achieving a higher organophilization of the filler surface, in order to promote the interactions with polymers [70]. Surface reactions on the inorganic materials have been studied extensively [71-79].

The most popular surface modifiers (or coupling agents) are silanes [71-84]. The generalized reaction scheme of the surface silanization is shown in Scheme I.1 [79].

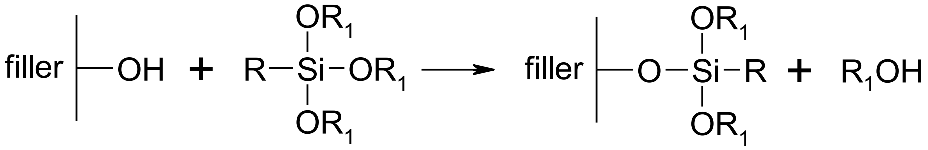

Scheme I.1. Generalized surface silanization reaction. R and R_1 are alkyl radicals, in some cases R_1=H.

Nowadays, different silane coupling agents are available. They can contain not only alkyl chains of various lengths, but also different functional groups (e.g. amino, mercapto, carboxyl etc.) that can change hydrophobicity/hydrophylicity of the filler surface [71-79, 82-85] or even be used in some further chemical reactions on the particle surface [80-81].

It was shown [70-85], that the significant change in nanocomposite properties can be achieved by appropriate functionalization of the nanofillers. The filler dispersion can be improved by the surface modification [74-75], which is very important for promoting the polymer-filler interactions.

For instance, a study involving the styrene butadiene rubber/organically modified clay (SBR/OMC) system confirmed that longer alkyl chains and a larger dosage of the surface modifier would facilitate the formation of a better dispersion state [82]. Probably, this is due to the better coverage of the nanoparticles surface by the surface modifier. The results of studies on nitrile-butadiene rubber NBR/OMC nanocomposites [83-84] have indicated that increasing the alkyl length of the surfactant would not only improve the filler dispersion, but also change the local structure in terms of intercalation and exfoliation [84]. Apart from the alkyl length of the surfactant, Zhang and coworkers also recognized that the intercalation extent increased with increasing surface modifier dosage in the ethylene propene diene monomer rubber EPDM/OMC nanocomposites [85].

Zunjarrao and Singh studied the fracture behavior of epoxy [78] and showed that both improved alumina particle dispersion and appropriate silane treatment lead to an increase in fracture toughness of the composite. Yang et al. [86] showed improved filler dispersion and interfacial compatibility of $CaCO_3$ nanoparticles with SBR after surface treatment with 3-methacryloxypropyltrimethoxysilane.

As can be seen, nanoparticle surface properties, which can be altered by means of surface modification, play a very important role in both dispersion and interfacial compatibility of nanoparticles. The surface properties of the filler after modification can be significantly changed, suggesting that surface modification is necessary sometimes before its application.

Another method of enhancing the polymer-filler interaction is creation of the covalent bond between filler and polymer. In this case, nanoparticles are tightly attached to the polymer matrix, which prevents them from agglomeration and increases the filler/matrix interfacial adhesion. It has been proved to be an efficient way for strengthening and toughening polymer at rather low filler content. In most cases [87-93] this method is about grafted polymerization of the monomer molecules onto the modified filler surface. Also, successful grafting of the polymer chains on the nanoparticle surface has been reported [94-98]. Direct grafting of preformed linear polymer molecules provides convenience in preparation of hybrid materials [95]. In this case the polymer "arms" form an organic domain to separate the silica particles and to prevent particle aggregation. Such hybrid materials exhibit good thermal stability compared to their ungrafted analogues [96].

Incorporation of nanoscale fumed silica particles modified with methacrylate surface groups to permit covalent bonding with the acrylate-terminated polymer chains, thereby forming tough hybrid nanocomposite materials, was found to improve the bulk modulus without affecting optical clarity and membrane selectivity [98].

Friedrich et al. [87] showed that the key effects of the grafting polymers lie in the strengthening of the loose nanoparticle agglomerates besides the increase of the filler/matrix interfacial adhesion.

I.5. Thermal and mechanical properties of the nanocomposites

As it was mentioned above, the interfacial interactions play an important role in modification of properties of the nanocomposites. In case of rubbers, thermal and mechanical properties are the most interesting due to the application possibilities of the rubber nanocomposites.

The glass transition (or α-relaxation) is often used to detect changes in molecular dynamics in polymers. It is generally believed [2-3, 37-38] that changes in molecular dynamics of the polymer molecules near the nanoparticle surface are responsible for the reinforcement effect. Different research works are dedicated to the studies of the glass transition of the nanocomposites [32, 37-38, 49-50, 99-133]. Some of them show increase in glass transition temperature compared to the pure polymer [32, 48, 102-105], other works show decrease in T_g [49, 99, 100-101], for some systems it was found that glass transition temperature is not affected by the filler presence [99-100, 102-103, 106-107]. Some authors [50, 99, 108-109] declare total suppression of the glass transition.

Many experimental results suggest that the restriction of the polymer chain mobility caused by the nanoparticles does not extend throughout the material but affects only the chains within a few nanometers of the filler surface. The existence of such an "interphase" has been shown for several polymer-filler systems [100, 106, 109-115]. For some nanocomposites this interphase has been identified as totally immobilized [50, 106, 111] while in other cases a second glass transition [116-118] has been observed at higher temperature.

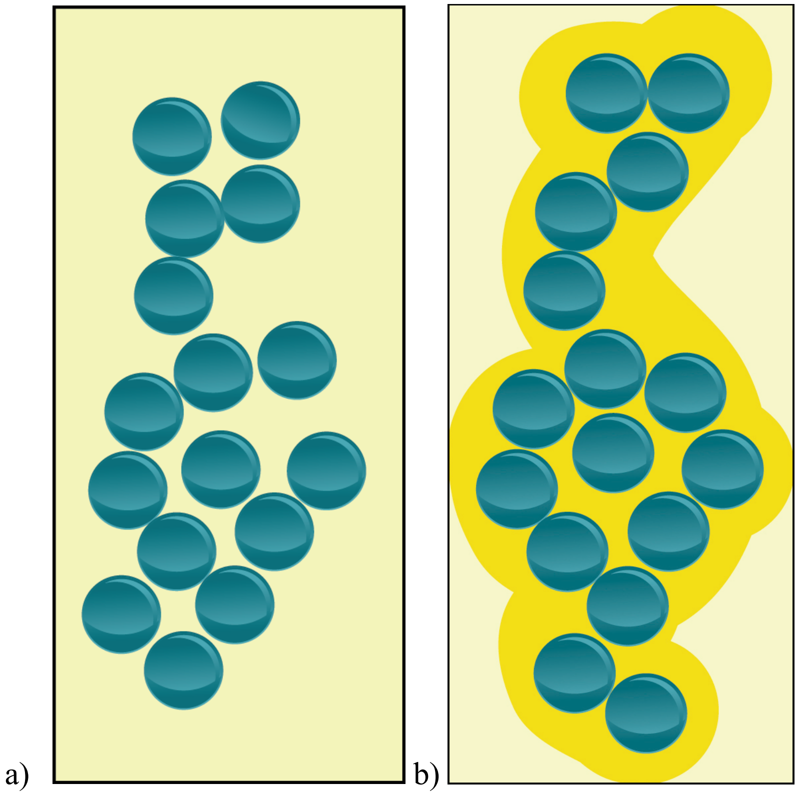

Figure 1.1.Illustration of the polymer-filler system: a) presents system where there is no "immobilized" polymer fraction; b) represents system with the "immobilized" polymer fraction.

Wunderlich approach [120-121] of identifying an immobilized interfacial fraction of the polymer has been recently used by Sargsyan et al. [38, 119] for PMMA/SiO_2 and PS/SiO_2 systems. The authors of [119] consider the immobilized polymer molecules near the nanoparticle surface as rigid amorphous fraction (RAF), known for semicrystalline polymers [120-121], and show that the thickness of the immobilized layer is similar to that found in semicrystalline polymers and independent from the shape of the nanoparticles (PMMA/Laponite (platelet-like filler) and PMMA/SiO_2 (spherical particles) systems were compared). The immobilized layer was found to be about 2nm thick. The glass transition temperature of the studied nanocomposites showed slight increase with growing filler concentration.

Flaifel and co-authors [122] also showed T_g increase for NR/NiZn nanocomposites, which is ascribed to the strengthening effect in which the nanoparticles have limited the mobility of the polymer chains. Also, decrease in damping peak values of the nanocomposites measured by DMA was observed when the filler loading increases, which was explained by lowering the degree of molecular motion and decrease in free volume provided by polymer matrix which is necessary to dissipate the vibrational energy [123].

The study of nitrile butadiene rubber (NBR) based layered double hydroxide (LDHs, untreated and surface-modified with sodium lignosulfonate, SLS) nanocomposites [124] showed that the glass transition temperature of NBR decreases as the LDH content increases. On the other hand, T_g of the SLS–LDH/NBR composites increased when compared with LDH/NBR composites indicating the enhancement of interactions between NBR chains and LDH particles in the presence of SLS. The study of mechanical properties of the composites showed that both pristine LDH and SLS–LDH can enhance the tensile strength and tear strength of NBR. This has been attributed to the strong interfacial interaction between the polar nitrile group of NBR and the hydroxyl group of LDH. Moreover, it was shown that both the tensile strength and tear strength of SLS–LDH/NBR composites are much superior to that of LDH/NBR at the same level of filler loading. This better enhancement in the tensile strength and tear strength has been ascribed to the better dispersion of LDH in the NBR matrix and interfacial interaction between filler and rubber in the presence of SLS.

As it was shown recently [125,126], glass transition process in polymers often leads to substantial change in stiffness, strength and other properties of polymeric materials. The thermal effects as well as fade and wear characteristics of rubber-based friction materials with and without reinforcements were examined [125]. The experimental data revealed that rubber-to-glass transition of rubber matrix in presence of the carbon fiber influenced significantly the fade behavior and wear rate of the composite.

The authors of the work [126] examined the effects of the glass transition of resin matrices on the friction and wear characteristics of friction materials. The increasing temperature and broadening width of *tan δ* peaks for resin based friction materials were owing to relatively stronger intermolecular interactions between relatively complete polymer crosslinking network and fibers. Both DMA and friction test results confirmed that changes in glass transition of the composites influenced significantly the friction behavior and wear rate of the composite friction materials.

Two kinds of hybrid composite systems, HNBR/La_2O_3/AA/MWNTs and HNBR/Sm_2O_3/AA/MWNTs, were analyzed in [127]. The glass transition temperature of the reinforced HNBR increased and the tensile strength tests indicated good reinforcement of the composites. These effects have been attributed to the combination of the increasing hindrance to molecular chain movements with increasing filler loading and the synergistic effect between MWNTs and filler.

In the above mentioned work of Flaifel [122] the value of storage modulus also moderately increases with the increase in filler content indicating an accompanying increase in the nanocomposite stiffness, which is resulted due to the reinforcement effect imparted by the magnetic nanofiller. The mechanism behind the enhancement of the stiffness of the nanocomposite samples when incorporating magnetic nanofiller is explained through the possible interfacial interactions that take place between the nanoparticles and the TPNR matrix, which could be visualized as transporting channels allowing higher amounts of stress to transfer [123].

Studies of carboxylated acrylonitrile-butadiene rubber composites containing silica nanoparticles revealed that the amount of the filler did not significantly influence either the temperature of the α-relaxation correlated with glass transition, or the activation energy [128]. The authors suggest that relaxation was caused by free, not bounded on the silica particles surface, polymer chains. Similar values of T_g were also confirmed by DSC. Although, the values of *tan* δ determined by DMA within T_g appeared to be silica amount dependent. Detected at higher temperature, α-relaxation resulted from the presence of domains, where polymer chains were affected by silica network, namely ionic bonds, geometrical restrictions and morphology of the silica-rich domains.

The vulcanized silicone rubber (HTVSR) with chitosan salt pretreated carbon nanotubes (CNTs) showed very uniform filler dispersion within the matrix, improving the thermal and mechanical properties of the HTVSR [129]. It was also shown that the nanocomposites could remain conductive without losing inherent properties after 100 times of repeated stretching/release cycles by 100%, 200%, and even 300%! The increasing of the tensile strength of the nanocomposites indicated that chitosan salt treated CNTs and HTVSR had very strong interfacial adhesions, and the CNTs helped to transfer some tensile force when the HTVSR/CNTs nanocomposite was stretched. It is also very interesting to notice that when the CNTs content in the HTVSR reached to 6 wt% or higher, the nanocomposites could be stretched to more than 200% of their original length, especially for the HTVSR/CNTs 8 wt% nanocomposite whose tensile strain was as high as 440%. Strong interactions between the chitosan salt treated CNTs and the HTVSR are also revealed from the enhanced thermal properties. It was shown that the HTVSR/CNTs nanocomposites are more thermally stable than the neat HTVSR hybrid.

The relaxed volume changes during heating have been investigated for PMMA/CB nanocomposites in [130]. Presence of carbon black particles in PMMA resulted in changes in thermal properties, such as increase in T_g and smaller Δc_p. From the point of view of volume relaxation, filler particles cause reduction of relaxation response and relaxation rate. The authors also indicate the presence of amorphous phase with modified properties by proximity of filler as immobilized polymer layer on their interface.

Friedrich et al. [131] published comparative study of epoxy/Al_2O_3 systems, where in order to enhance the interfacial interaction between the fillers and the matrix polymer, the nanoparticles were pretreated by either silane coupling agent or graft polymerization. The general trends described in this work manifest that the addition of the nanoparticles increases the stiffness of the polymer matrix. With increase in filler content, the elastic modulus increases mainly due to the contribution of the hard Al_2O_3 particles. It is worth to mention that the untreated nanoparticles exhibit higher stiffening efficiency, especially at high filler concentrations. The lower elastic moduli of the composites containing Al_2O_3 treated with γ-aminopropyltriethoxysilane was attributed to the "mask effect" of the relatively compliant interlayer constructed by the silane coupling agent or, in case of grafted systems, the grafted polymers adhered to the nanoparticles. It was shown that the introduction of grafting polymers can reduce the elastic moduli to the values which are even lower than that of pure epoxy. The authors made a conclusion that the untreated Al_2O_3/epoxy systems probably possess higher interfacial adhesion strength than systems with treated nanoparticles. The tribological performance tests revealed higher lubricating effect for grafted nanoparticles and also showed that the grafted nanoparticles accompanied by the homopolymer generated in the course of graft polymerization provide more obvious lubrication effect than the ones only with grafting polymer.

In another work of Friedrich and group [88] irradiation-grafted SiO_2/PP systems were studied. The authors concluded that the filler/matrix interaction is substantially enhanced by the entanglement of the grafting polymers and the matrix polymer. Also, it was shown that the direct contacts between the particles no longer appear because of the uniform coverage of grafted polymer chains on the surface of each nanoparticle. The tensile properties (strength, modulus and elongation at break) of PP were improved when the modified nanoparticles were incorporated. It was also found that the internal structure of the modified nanoparticles had an additional influence on the mechanical properties of the nanocomposites. For example, the optimum nanoparticle content was related to the optimum distribution of the particles. A considerable toughening effect could be observed at a rather low loading of the modified fillers which was interpreted by a hypothetical double-percolation model, which is based on: a) a percolation of the shear yielded zones inside the dispersed phases (consisting of the nanoparticles, the grafted and homopolymerized polymer) due to the superposition of stress volumes around the primary particles; and b) a percolation of the shear yielded zones throughout the matrix resin due to the superposition of stress volumes around the dispersed phases. According to the authors, such a multiple percolation process is beneficial to a low percolation threshold, i.e. a low brittle–ductile transition threshold. Regarding the percolation inside the modified nanoparticles, the significant decrease in impact strength with increasing weight ratio of styrene to SiO_2, has been interpreted by the fact that the stress volume fraction is reduced to a value lower than the percolation threshold. Another example is a significant decrease in impact strength with a rise in irradiation dose. As a higher irradiation dose might induce a crosslinking structure of the grafting polymers, shear deformation of the polymers adherent to the nanoparticles becomes more difficult. Consequently, a long-range connection of the deformed polymers is hindered.

The mechanical properties of SBR/SiO_2 nanocomposites with focus on the polymer-filler interfacial interactions were studied in [37]. The surface treatments used in this work apparently limited the physical interactions between filler and matrix, but promoted formation of covalent bonds in case where coupling agent has been used. The influence of the interactions filler-filler and filler-matrix on the Payne effect has been detected. To explain such effect, the authors proposed a model where the nanoparticle agglomerates are linked to each other by the layer of the "bound rubber". The rigidity of such structure depends on the filler-filler interactions in agglomerates and also on the amount of "bound rubber". The increase in temperature reduces the bound rubber fraction through desorption of the polymer chains at the SiO_2 surface, which diminishes the rigidity of the network and results in decrease of elastic moduli.

I.6. Conception of "bound rubber"

In several research works [37, 100-118] discussed above the authors ascribe the reinforcement effect to the formation of the "immobilized" polymer molecules near the nanoparticle surface. The term "bound rubber" characterizing this phenomenon appeared first more than 80 years ago. Nowadays, such regions with changed molecular mobility are called "interphases".

J.L. Leblanc [132] determined bound rubber as a gel of filler particles with the bonding agent consisting of the polymer molecules. The amount of bound rubber can be dependent on the surface area, structure and surface activity of the filler; the chemical structure of the polymer, as well as his macromolecular characteristics (molecular weight, polydispersity, degree of branching etc.) also play an important role in creation of the bound rubber layer. The filler dispersed in polymer matrix interacts with rubber, but the time scale of such interaction is always dependent on the characteristic response time of the polymer. The author says that a common sense in composite science is the assumption that bound rubber results from the adsorption of the polymer on the particle surface, but this would involve the existence of a physical equilibrium and consequently the possibility to completely recover the elastomer by suitable physical manipulations. Experimental proofs for the (partial) reversibility of bound rubber formation were obtained only recently by Wolff et al. [133], who performed measurements at temperatures ranging from room temperature to 100°C and showed that, above 80°C there is a severe drop in bound rubber content which however does not exclude the possibility that some rubber chains remain attached to filler particles. Many research works were dedicated to the bound rubber investigations, especially in 1950s-1960s [133-137], but the experiments were performed in conditions (polymer in solution) that are far from meeting those prevailing in an actual compound, i.e. a dense system, and it has been shown that bound rubber formed during mixing involves a greater amount of rubber than could be adsorbed from solution [137]. When a filler and rubber are dry mixed, the resulting quantity of bound rubber obviously reflects all possible adsorption mechanisms, as well as intermolecular entanglements. It was also shown [132-137] that chemical interaction between the polymer and the filler is not necessary for the development of bound rubber. But, as it was discussed above, much more pronounced effects are obtained when chemical interactions are produced between the components [87-98, 131].

In another work [138], Leblanc proposes a simple model of bound rubber formation: first of all, filler particles must have a good dispersion and be wetted by the polymer and only then bound rubber is formed (Fig.I.2).

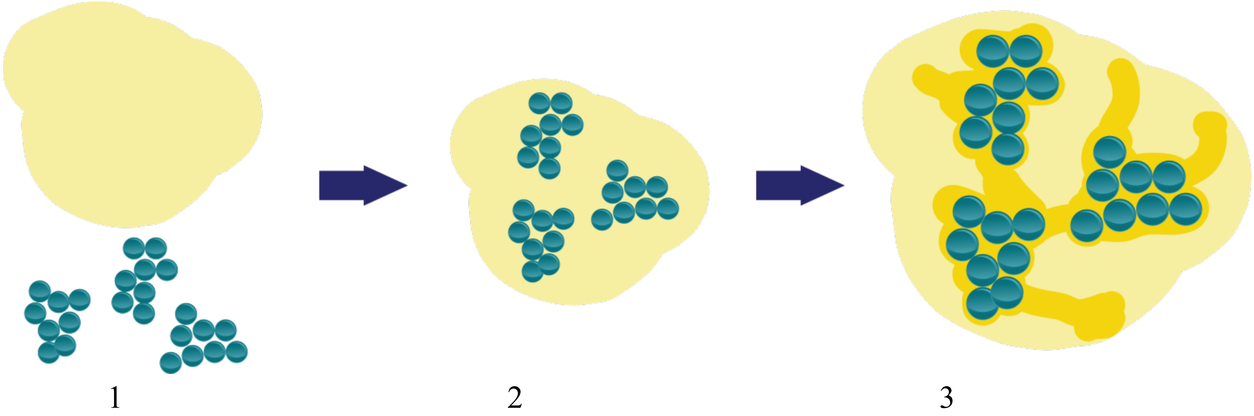

Figure 1.2.Illustration of the "bound rubber" formation: 1) mixing of rubber and filler; 2) wetting of filler by rubber molecules; 3) formation of the immobilized rubber layer (or "bound rubber").

The author points out that quite high level of mixing energy are needed for the full development of rubber–filler interactions. Because of the kinetic character of filler dispersion and bound rubber formation, one may expect the viscosity of a rubber formulation to strongly depend on the achievement of rubber–filler interactions, as indeed observed [139]. Despite the concomitance of events that take place during mixing process, the optimum adsorption of rubber segments on the filler surface is the ultimate controlling one. Direct relationships between bound rubber level and rheological properties are thus logically expected consequences. Uncured filled rubber compounds exhibit peculiar flow properties because, owing to strong rubber–filler interactions, they develop a three-dimensional morphology. Such materials can consequently be viewed as soft (filled) networks, interpenetrated by the extractable, unfilled elastomer [132].

Thus, the complex adsorption–desorption processes take place between the surface of filler particles and rubber segments. Because rubber segments belong to macromolecules, such localized effects of filler-polymer interactions, whilst occurring in the nanometer range, result in long-range modifications in terms of flow mechanics. In this context, bound rubber appears as a key property of filled rubber compounds, obviously an all-inclusive one, depending on the chemical nature of the elastomer, the size and structure of the filler, the mixing conditions and the storage time and temperature. At a given temperature and in rest conditions (i.e. no shear), there is a rubber–filler interphase whose dynamics reaches at best an equilibrium between adsorption and desorption of rubber segments on appropriate sites on filler particles. This means obviously that, if the temperature is changed or the material is submitted to shear, this equilibrium is likely to be displaced. This provides a qualitative explanation for many singularities in the flow properties of rubber compounds.

I.7. Glass transition

Glass transition process is a very important phenomenon in polymers. Almost all polymers form glasses, which are widely used in every day's life (lenses for glasses, bathtubs, plumbing pipes etc).

The glass transition is a transition between a liquid state and a glass [140-142].

The temperature, at which glass transition process occurs, is called glass transition temperature, or T_g. The knowledge of T_g is very important in the selection of materials for specific applications. In general, elastomers exhibit T_g values below room temperature. T_g values above room temperature define rigid polymers (plastics).

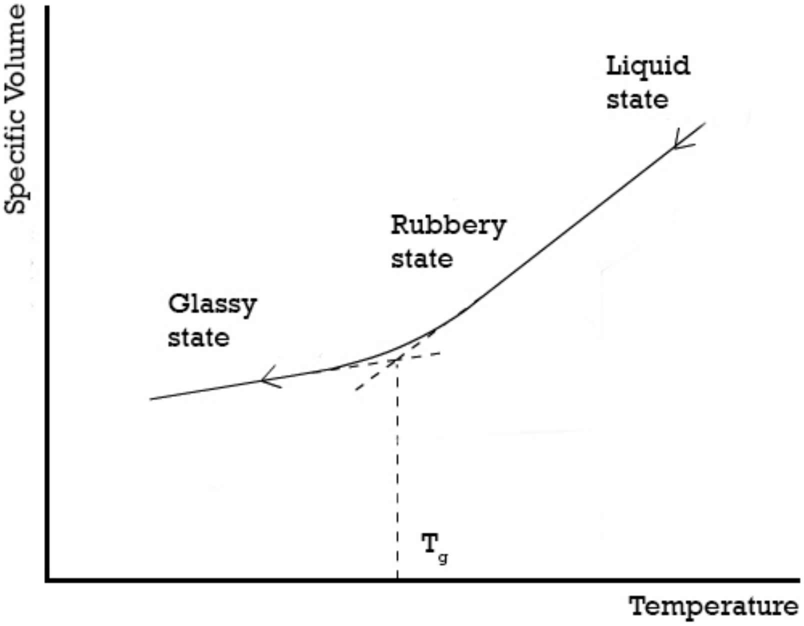

Figure 1.3.Volume changes on cooling a glass-forming polymer.

Glass transition process can be understood in terms of the structure of glass-forming materials, which usually consist of substances containing long chains and/or networks. Thus, glass-forming materials have a complex molecular structure. When rapid cooling occurs, molecular movement of the long chains is too slow to adopt the conformation which allows producing the crystalline state; in this case glass formation is observed. [140].

Figure 1.3 illustrates the volume dependence as a function of temperature and shows that the transition from liquid to glass in case of glass-forming system does not present a sudden change in volume (which is characteristic of freezing of the crystalline materials). Instead, glass-formers present a change in slope of the curve at the glass transition temperature. The intersection of the two straight-line segments of the curve defines the glass transition temperature T_g [140-141].

The glass transition temperature T_g is an essential polymer characteristic, which determines the bulk properties of the polymer material. As it was mentioned above, a wide number of research works is dedicated to determining T_g by different physical methods [32, 37-38, 49-50, 99-133, 140-143]. Glass transition reminds second-order phase transition, but it is not considered to be a real thermodynamic phase transition [140]. This is due to the fact that experimental T_g value depends on the conditions of the experiment (e.g. cooling/heating rate, frequency) [2-3, 140]. The most popular method of detecting T_g remains so far DSC (Differential Scanning Calorimetry). Also, among the popular methods are: DTA (Differential Thermal Analysis), DMA (Dynamic Mechanical Analysis), rheometry, dielectric spectroscopy, dilatometry [32, 37-38, 49-50, 99-133, 140-145]. In this thesis, the glass transition process in rubber nanocomposites has been studied by TMDSC (Temperature-Modulated Differential Scanning Calorimetry), DMA and rheometry. These methods will be considered in subchapters II.5, III.4 and III.5.

At the material level, there are also some factors influencing the glass transition temperature [146-147]:

a) molecular weight: for a given polymer, a sample with higher molecular weight will exhibit higher T_g;
b) molecular structure: polymers having stiff backbone exhibit higher T_g than polymers having flexible chains; polymers having double bonds in their backbone have lower T_g due to decreased bond rotation;
c) degree of cross-linking: the higher the cross-linking degree, the higher the T_g;
d) moisture/solvent presence: lower T_g observed due to the plasticizing effect;
e) filler presence: as it was discussed above (subchapter I.5), different polymer/filler combinations exhibit different shifts in T_g (increase in T_g [32, 48, 102-105], decrease in T_g [49, 99, 100-101], no T_g change [99-100, 102-103, 106-107] or suppression of the glass transition process [50, 99, 108-109]).

Therefore, T_g is a very important parameter of a polymeric material. T_g is a measure of flexibility of the polymers chains. T_g value indicates the temperature region at which a given polymer transforms from solid to a viscous state; it is very useful in choosing not only the processing conditions, but also conditions at which a given material can be used.

References:

[1] Krishnan D., Johnson H.T., Light-induced deformation in a liquid crystal elastomer photonic crystal, *Journal of the Mechanics and Physics of Solids*, 2014, 62, p.48–56.

[2] Mark J.E., Erman B., Eirich F.R., Science and Technology of rubber, 3rd Ed., 2005, Elsevier Inc., USA.

[3] Thomas S., Stephen R., Rubber nanocomposites. Preparation, properties and applications, 2010, John Wiley & Sons (Asia) Pte Ltd, Singapore.

[4] Messersmith P.B., Giannelis E.P., Polymer-layered silicate nanocomposites: in situ intercalative polymerization of ε-caprolactone in layered silicates, *Chemistry of Materials*, 1993, 5 (8), p.1064–1066.

[5] Giannelis E.P., Polymer-layered silicate nanocomposites, *Advanced Materials*, 1996, 8, p. 29-35.

[6] Komarneni S., Nanocomposites, *Journal of Materials Chemistry*, 1992, 2, p.1219-1230.

[7] Ruiz-Hitzky E., Conducting polymers intercalated in layered solids, *Advanced Materials*, 1993, 5, p.335-340.

[8] Luo J.J., Daniel I.M., Characterization and modeling of mechanical behavior of polymer/clay nanocomposites, *Composites Science and Technology*, 2003, 63, p.1607–1616.

[9] Thostenson E.T. et al., Advances in the science and technology of carbon nanotubes and their composites: a review. *Composites Science and Technology*, 2001, 61, p.1899-1912.

[10] Coleman J.N. et al., Small but strong: A review of the mechanical properties of carbon nanotube–polymer composites, *Carbon*, 2006, 44, p.1624-1652.

[11] Lau K.T., Gu C., and Hui D., A critical review on nanotube and nanotube/nanoclay related polymer composite materials, *Composites Part B: Engineering*, 2006, 37, p. 425-436.

[12] Dickey M.D., Weiss E.A., Smythe E.J., Chiechi R.C., Capasso F. and Whitesides G., Fabrication of Arrays of Metal and Metal Oxide Nanotubes by Shadow Evaporation, *ACS Nano*, 2008, 2 (4), p 800–808.

[13] Satishkumar B.C., Govindaraj A., Natha M. and Rao C. N. R., Synthesis of metal oxide nanorods using carbon nanotubes as templates, *Journal of Materials Chemistry*, 2000, 10, p.2115-2119.

[14] Cochran R.E., Shyue J.J., Padture N.P., Template-based, near-ambient synthesis of crystalline metal-oxide nanotubes, nanowires and coaxial nanotubes, *Acta Materialia*, 2007, 55, p.3007-3014.

[15] Liu M., Guo B., Du M., Cai X. and Jia D., Properties of halloysite nanotube–epoxy resin hybrids and the interfacial reactions in the systems, *Nanotechnology*, 2007, 18, p. 455703-455711.

[16] Du M., Guo B., Liu M. and Jia D., Preparation and Characterization of Polypropylene Grafted Halloysite and Their Compatibility Effect to Polypropylene/Halloysite Composite, *Polymer Journal*, 2006, 38, p.1198–1204.

[17] D'Souza L., Richards R. Synthesis of Metal-Oxide Nanoparticles: Liquid-Solid transformations in "Synthesis, Properties and Applications of Oxide Nanoparticles" (Rodríguez J.A., Fernández-García M., Eds.), Wiley: N.J., 2007. Ch. 3.

[18] Buzby S., Franklin R., Shah, S.I., Synthesis of Metal-Oxide Nanoparticles: Liquid-Solid transformations in "Synthesis, Properties and Applications of Oxide Nanoparticles" (Rodríguez, J.A., Fernández-García, M; Eds.). Wiley: N.J., 2007. Ch. 4.

[19] Mather G.C., Martinez-Arias A., Transport properties and Oxygen Handling in "Synthesis, Properties and Applications of Oxide Nanoparticles" (Rodríguez J.A., Fernández-García M; Eds.). Wiley: N.J., 2007. Ch. 13.

[20] Chiang Y.M., Lavik E.B., Kosacki I., Tuller H.L. and Ying J.Y., Nonstoichiometry and Electrical Conductivity of Nanocrystalline CeO_{2-x}, *Journal of Electroceramics*, 1997, 1, p.7-14.

[21] Franke M.E., Koplin T.J., Simon U., Metal and Metal Oxide Nanoparticles in Chemiresistors: Does the Nanoscale Matter? *Small*, 2006, 2, p.36-50.

[22] Kosacki I, Anderson H.U. The structure and electrical properties of $SrCe_{0.95}Yb_{0.05}O_3$ thin film protonic conductors, *Solid State Ionics*, 1997, 97, p.429-436.

[23] Maekawa H., Tanaka R., Sato T., Fujimaki Y., Yamamura T., Size-dependent ionic conductivity observed for ordered mesoporous alumina-LiI composite, *Solid State Ionics*, 2004, 175 (1-4), p.281-285.

[24] Ayandele E., Sarkar B. and Alexandridis P., Polyhedral Oligomeric Silsesquioxane (POSS)-Containing Polymer Nanocomposites, *Composite Nanomaterials*, 2012, 2, p.445-475.

[25] Li G., Wang L., Ni H. and Pittman C.U. Polyhedral oligomeric silsesquioxane (POSS) polymers and copolymers: a review, *Journal of Inorganic and Organometallic Polymers*, 2001, 11, p.123-154.

[26] Illescas S., Sánchez-Soto M., Milliman H., Schiraldi D.A. and Arostegui A., The morphology and properties of melt-mixed polyoxymethylene/monosilanolisobutyl-POSS composites, *High Performance Polymers*, 2011, 23 (6), p. 457-467.

[27] Liang K., Li G., Toghiani H., Koo J.H. and Pittman C.U., Cyanate Ester/Polyhedral Oligomeric Silsesquioxane (POSS) Nanocomposites: Synthesis and Characterization, *Chemistry of Materials*, 2006, 18 (2), p.301–312.

[28] Bhatnagar N. and Sain M. Processing of cellulose nanofiber-reinforced composites, *Journal of Reinforced Plastics and Composites*, 2005, 24, p.1259-1368.

[29] Angellier H., Molina-Boisseau S., Lebrun L. and Dufresne, A. Processing and structural properties of waxy maize starch nanocrystals reinforced natural rubber, *Macromolecules*, 2005, 38, p.3783-3792.

[30] Angellier H., Molina-Boisseau S. and Dufresne, A. Mechanical properties of waxy maize starch nanocrystal reinforced natural rubber, *Macromolecules*, 2005, 38, p.9161-9170.

[31] Lapa V.L.C., de Oliveira P.D., Visconte L.L.Y. and Nunes R.C.R. Investigation of NBR-cellulose II nanocomposites by rheometric and equilibrium swelling properties, *Polymer Bulletin*, 2008, 60, p.281-290.

[32] Liu, X. and Q. Wu, PP/clay nanocomposites prepared by grafting-melt intercalation. *Polymer*, 2001. 42, p.10013-10019.

[33] Cho, J.W. and D.R. Paul, Nylon 6 nanocomposites by melt compounding. *Polymer*, 2001, 42: p. 1083-1094.

[34] Karaman, J.V., et al., Structure/Property Relationships for Polyamide 6/Organoclay Nanocomposites in the Melt and in the Solid State. *Macromolecular Symposia*, 2005. 221: p. 85-94.

[35] Liu, S.L., et al., Fabrication and properties of polyp32ropylene/organoclay nanocomposites. *SIMTech techn. reports*, 2005, 6 (1), p.33-38.

[36] Stéphanie, E., et al., Effects of incorporation of modified silica nanoparticles on the mechanical and thermal properties of PMMA. *Journal of Thermal Analysis and Calorimetry*, 2007, 87 (1), p.101-104.

[37] Julien Ramier, PhD Thesis "Comportement mécanique d'élastomères chargés, Influence de l'adhésion charge-polymère, Influence de la morphologie", l'INSA de Lyon, 2004.

[38] Albert Sargsyan, PhD thesis "Quantification of the immobilized fraction in polymer inorganic nanocomposites", Universität Rostock, 2007.

[39] Chen, L., et al., Fabrication and characterization of polycarbonate/carbon nanotubes composites. *Composites Part A*: *Applied Science and Manufacturing*, 2006, 37, p.1485-1489.

[40] Chae, D.W. and B.C. Kim, Characterization on polystyrene/zinc oxide nanocomposites prepared from solution mixing. *Polymers for Advanced Technologies*, 2005, 16, p.846-850.

[41] Yeun, J.H., et al., Poly(vinyl alcohol) Nanocomposite Films: Thermooptical Properties, Morphology, and Gas Permeabilit,. *Journal of Applied Polymer Science*, 2006, 101, p.591-596.

[42] Brandrup, J., E.H. Immergut, and E.A. Grulke, Polymer Handbook 4th Ed. Vol. 1. 1999: John Wiley & Sons.

[43] Franco, F., L.A. Pérez-Maqueda, and J.L. Pérez-Rodríguez, Influence of the Particle-Size Reduction by Ultrasound Treatment on the Dehydroxylation Process of Kaolinites. *Journal of Thermal Analysis and Calorimetry*, 2004, 78, p.1043-1055.

[44] Qiu, G., et al., Ultrasonically initiated miniemulsion polymerization of styrene in the presence of Fe3O4 nanoparticles. *Polymer International*, 2006, 55, p.265-272.

[45] Mahdavian, A.R., M. Ashjari, and A.B. Makoo, Preparation of poly(styrene–methyl methacrylate)/SiO2 composite nanoparticles via emulsion polymerization. An investigation into the compatiblization. *European Polymer Journal*, 2007, 43, p.336-344.

[46] Suslick, K.S. and G.J. Price, Applications of ultrasound to materails chemistry, *Annual Review of Materials Science*, 1999, 29 (1), p. 295-326.

[47] Ballav N., Biswas M. Preparation and evaluation of a nanocomposite of polythiophene with Al_2O_3. *Polymer International,* 2003, 52, p.179-184.

[48] X. Huang and W.J. Brittain, Synthesis and Characterization of PMMA Nanocomposites by Suspension and Emulsion Polymerization. *Macromolecules,* 2001, 34 (10), p.3255-3260.

[49] B.J. Ash, L.S. Schadler, and R.W. Siegel, Glass transition behavior of alumina/polymethylmethacrylate nanocomposites. *Materials Letters*, 2002. 55, p.83-87.

[50] Lee D.C. and L.W. Jang, Preparation and Characterization of PMMA/Clay Hybrid Composite by Emulsion Polymerization. *Journal of Applied Polymer Science*, 1996, 61, p.1117-1122.

[51] Negrete-Herrera N., J.L. Putaux, and E. Bourgeat-Lami, Synthesis of polymer/Laponite nanocomposite latex particles via emulsion polymerization using silylated and cation-exchanged Laponite clay platelets. *Progress in Solid State Chemistry*, 2006, 34, p. 121-137.

[52] Zhou, J., et al., Synthesis of SiO_2/Poly(styrene-co-butyl acrylate) Nanocomposite Microspheres via Miniemulsion Polymerization. *Journal of Polymer Science Part A: Polymer Chemistry*, 2006, 44, p.3202-3209.

[53] Qi, D.M., et al., Preparation of acrylate polymer/silica nanocomposite particles with high silica encapsulation efficiency via miniemulsion polymerization. *Polymer,* 2006, 47, p. 4622-4629.

[54] Yan, F. and J. Texter, Capturing nanoscopic length scales and structures by polymerization in microemulsions. *Soft Matter*, 2006, 2, p.109-118.

[55] Xu, P., et al., Preparation and morphology of SiO2/PMMA nanohybrids by microemulsion polymerization. *Colloid Polymer Science*, 2006, 284, p.755-762.

[56] Hwu, J.M., et al., Synthesis and Properties of Polystyrene–Montmorillonite Nanocomposites by Suspension Polymerization. *Journal of Applied Polymer Science*, 2004, 91, p.101-109.

[57] Zhao, Q. and E.T. Samulski, In Situ Polymerization of Poly(methylmethacrylate)/Clay Nanocomposites in Supercritical Carbon Dioxide. *Macromolecules*, 2005, 38, p.7967-7981.

[58] Hajji, P., et al., Synthesis, Structure, and Morphology of Polymer–Silica Hybrid Nanocomposites Based on Hydroxyethyl Methacrylate. *Journal of Polymer Science Part B: Polymer Physics*, 1999, 37, p.3172-3187.

[59] Okamoto, M., et al., Synthesis and structure of smectic clay/poly(methylmethacrylate) and clay/polystyrene nanocomposites via in situ intercalative polymerization. *Polymer*, 2000, 41(10), p.3887-3890.

[60] Zhang, Z., et al., Styrene–Butadiene–Styrene/Montmorillonite Nanocomposites Synthesized by Anionic Polymerization. *Journal of Applied Polymer Science*, 2006, 99, p.2273-2278.

[61] Ni, K.F., et al., Kinetics and Modeling of Hybrid Core-Shell Nanoparticles Synthesized by Seeded Emulsion (Co)polymerization of Styrene and Methacryloyloxypropyltrimethoxysilane. *Macromolecules*, 2005, 38 (22), p. 9100-9109.

[62] Faai Zhang, Y.W.C.C., Preparation of styrene-acrylic emulsion by using nano-SiO_2 as seeds. *Polymer International,* 2004, 53 (9), p.1353-1359.

[63] Hao, L.Y., et al., Inorganic-organic polymer nanocomposites fabricated by ultraviolet irradiation. *Rare Metal Materials and Engineering*, 2001, 30 (2), p.138-140.

[64] Sanctuary R., Baller J., Zielinski B., Becker N., Krüger J.K., Pholipp M., Müller U. and Ziehmer M., Influence of Al_2O_3 nanoparticles on the isothermal cure of an epoxy resin, *Journal of Physics: Condensed Matter,* 2009*,* 21, p.035118-125.

[65] Burke, N.A.D., et al., Preparation and characterization of polymer-coated magnetic nanoparticles. Magnetics, *IEEE Transactions*, 2001, 37 (4), p.2660-2662.

[66] Leslie-Pelecky, D.L., X.Q. Zhang, and R.D. Rieke. Self-stabilized magnetic colloids: Ultrafine Co particles in polymers. in "The 40th annual conference on magnetism and magnetic materials". 1996, Philadelphia, Pennsylvania (USA): AIP.

[67] Toshiharu Teranishi, I.K.M.M., Synthesis of Monodisperse Gold Nanoparticles Using Linear Polymers as Protective Agents. *Advanced Materials*, 1998, 10 (8), p.596-599.

[68] Yang, T.I. and P. Kofinas, Dielectric properties of polymer nanoparticle composites. *Polymer,* 2007, 48, p.791-798.

[69] Bouyer, F., et al., Role of double-hydrophilic block copolymers in the synthesis of lanthanum-based nanoparticles. *Colloids and Surfaces A: Physicochemical and Engineering Aspects*, 2003, 217 (1-3), p.179-184.

[70] Mittal V., Optimization of Polymer Nanocomposite Properties, 2010, WILEY-VCH Verlag GmbH & Co. KGaA, Weinheim.

[71] Shukla D.K., Kasisomayajula S.V., Parameswaran V. Epoxy composites using functionalized alumina platelets as reinforcements, *Composites Science and Technology*, 2008, 68, 14, p.3055–3063.

[72] Yang Y.-Ch., Jeong S.-B., Kim B.-G., Yoon P.-R. Examination of dispersive properties of alumina treated with silane coupling agents, by using inverse gas chromatography. *Powder Technology*, 2009, 191, p.117–121.

[73] Tee D.I., Mariatti M., Azizan A., See C.H., Chong K.F. Effect of silane-based coupling agent on the properties of silver nanoparticles filled epoxy composites. *Composites Science and Technology,* 2007, 67, p.2584–91.

[74] Yuen S.M., Ma C.C.M., Chiang C.L., Chang J.A., Huang S.W., Chen S.C., et al. Silane-modified MWCNT/PMMA composites – preparation, electrical resistivity, thermal conductivity and thermal stability. *Composites Part A: Applied Science and Manufacturing*, 2007, 38, 12, p. 2527–2535.

[75] Shukla D.K., Kasisomayajula S.V., Parameswaran V. Epoxy composites using functionalized alumina platelets as reinforcements, *Composites Science and Technology, 2008,* 68, 14, p.3055–3063.

[76] ten Brinke J.W., Debnath S.C., Reuvekamp L.A., Noordermeer J.W.M. Mechanistic aspects of the role of coupling agents in silica-rubber composites. *Composites Science and Technology,* 2003, 63 (8), p.1165-1174.

[77] Guo Z, Pereira T, Choi O, Wang Y, Hahn HT. Surface functionalized alumina nanoparticle filled polymeric nanocomposites with enhanced mechanical properties. *Journal of Materials Chemistry*, 2006, 16, p.2800–8.

[78] Zunjarrao SC, Singh RP. Characterization of the fracture behavior of epoxy reinforced with nanometer and micrometer sized aluminum particles. *Composites Science and Technology,* 2006, 66, p.296–305.

[79] Dai J.C., Huang J.T., Surface modification of clays and clay-rubber composite, *Applied Clay Science*, 1999, 15, p.51-65.

[80] Rong M.Z., Ji Q.L., Zhang M.Q., Friedrich K., Graft polymerization of vinyl monomers onto nanosized alumina particles, *European Polymer Journal*, 2002, 38, p.1573–1582.

[81] Matinlinna J.P., Lassila L.V.J., Vallittu P.K., The effect of five silane coupling agents on the bond strength of a luting cement to a silica-coated titanium, *Dental Materials*, 2007, 23, p.1173–1180.

[82] Schön F., Thomann R., Cronski W., Shear controlled morphology of rubber/organoclay nanocomposites and dynamic mechanical analysis, *Macromolecular Symposia*, 2002, 189, p.105-110.

[83] Kim J., Oh T., Lee D. Morphology and rheological properties of nanocomposites based on nitrile rubber and organophilic layered silicates, *Polymer International*, 2003, 52 (7), p.1203 – 1208.

[84] Kim J., Oh T., and Lee D. Preparation and characteristics of nitrile rubber (NBR) nanocomposites based on organophilic layered clay, *Polymer International*, 2003, 52 (7), p.1058 – 1063.

[85] Zheng H., Zhang Y., Peng Z., and Zhang Y. Influence of the clay modification and compatibilizer on the structure and mechanical properties of ethylene–propylene–diene rubber/montmorillonite composites, *Journal of Applied Polymer Science*, 2004, 92 (1), p.638 – 646.

[86] Yang Z., Tang Y., Zhang J., Surface modification of $CaCO_3$ nanoparticles with silane coupling agent for improvement of the interfacial compatibility with styrene-butadiene rubber (SBR) latex, *Chalcogenide Letters*, 2013, 10 (4), p.131-141.

[87] Rong M.Z., Zhang M.Q., Shi G., Ji Q.L., Wetzel B., Friedrich K., Graft polymerization onto inorganic nanoparticles and its effect on tribological performance improvement of polymer composites, *Tribology International*, 2003, 36, p.697-707.

[88] Rong M.Z., Zhang M.Q., Zheng Y.X., Zeng H.M., Walter R., Friedrich K., Structure-property relationships of irradiation grafted nanoinorganic particle filled polypropylene composites, *Polymer*, 2001, 42, p.167-183.

[89] Rong M.Z., Zhang M.Q., Zheng Y.X., Zeng H.M., Walter R., Friedrich K., Irradiation graft polymerization on nano-inorganic particles: an effective means to design polymer based nanocomposites, *Journal of Materials Science Letters*, 2000, 19, p.1159–61.

[90] Rong M.Z., Zhang M.Q., Zheng Y.X., Zeng H.M., Friedrich K., Improvement of tensile properties of nano-SiO2/PP composites in relation to percolation mechanism, *Polymer*, 2001, 42, p.3301-3304.

[91] Yu J., Ryu S.H., Ultraviolet-Initiated Photografting of Glycidyl Methacrylate onto Styrene–Butadiene Rubber, *Journal of Applied Polymer Science*, 1999, 73, p.1733–1739.

[92] Radu, D.R.; Lai, C.Y.; Wiench, J.W.; Pruski, M.; Lin, V.S.Y. Gatekeeping layer effect: A poly(lactic acid)-coated mesoporous silica nanosphere-based fluorescence probe for detection of amino-containing neurotransmitters. *Journal of the American Chemical Society*, 2004, 126, p.1640-1641.

[93] Chen X., Zhu Y., Zhou B., Guo Y., Gao W., Ma Y., Guan S., Wang L., Wang Z., Hydrophilic CaCO3 nanoparticles designed for poly (ethylene terephthalate), *Powder Technology*, 2010, 204, p.21–26.

[94] Hou Y.H., Zhang M.WQ., Rong M.Z., In situ melt grafting in carbon black/polyolefin composites and its influence on conductive performance, *Polymer International*, 2004, 53, p.944-950.

[95] Zou H., Wu S., Shen J., Polymer/Silica Nanocomposites: Preparation, Characterization, Properties, and Applications, *Chemical Reviews*, 2008, 108, p.3893-3957.

[96] Liu Y.L., Li S.H. Poly(dimethylsiloxane) Star Polymers Having Nanosized Silica Cores, *Macromolecular Rapid Communications*, 2004, 25, p.1392-1395.

[97] Gomes D., Buder I., Nunes, S.P. Sulfonated silica-based electrolyte nanocomposite membranes *Journal of Polymer Science Part B: Polymer Physics,* 2006, 44, p.2278-2298.

[98] Patel N.P., Zielinski J.M., Samseth J., Spontak R., Effects of Pressure and Nanoparticle Functionality on CO2-Selective Nanocomposites Derived from Crosslinked Poly(ethylene glycol), *Macromolecular Chemistry and Physics*, 2004, 205 (18), p.2409-2419.

[99] Bershtein V.A., et al., Molecular Dynamics in Nanostructured Polyimide–Silica Hybrid Materials and Their Thermal Stability. *Journal of Polymer Science Part B: Polymer Physics*, 2002. 40, p.1056-1069.

[100] Arrighi V., et al., The glass transition and interfacial layer in styrene- butadiene rubber containing silica nanofiller. *Polymer,* 2003. 44, p.6259-6266.

[101] Ash, B.J., R.W. Siegel, and L.R. Schadler, Glass-Transition Temperature Behavior of Alumina/PMMA Nanocomposites. *Journal of Polymer Science Part B: Polymer Physics*, 2004. 42, p.4371-4383.

[102] Privalko, V.P. and G.V. Titov, The Heat Capacity of Filled, Amorphous Polymers. *Polymer Science U.S.S.R.*, 1978, 21, p. 380-387.

[103] Lipatov, Y.S. and V.P. Privalko, Glass Transition in Filled Polymer Systems. *Polymer Science U.S.S.R.*, 1972, 14 (7), p.1843.

[104] Kalogeras, I.M. and N.R. Neagu, Interplay of surface and confinement effects on the molecular relaxation dynamics of nanoconfined poly(methyl methacrylate) chains. *European Physical Journal E*, 2004, 14, p.193- 204.

[105] Tabtiang, A., S. Lumlong, and R.A. Venables, The influence of preparation method upon the structure and relaxation characteristics of poly(methyl methacrylate)/clay composites. *European Polymer Journal*, 2000, 36 (12), p.2559-2568.

[106] Miwa, Y., A.R. Drews, and S. Schlick, Detection of the Direct Effect of Clay on Polymer Dynamics: The Case of Spin-Labeled Poly(methyl acrylate)/Clay Nanocomposites Studied by ESR, XRD, and DSC. *Macromolecules*, 2006, 39 (9), p.3304–3311.

[107] Mijovic, J., et al., Dynamics in Polymer-Silicate Nanocomposites As Studied by Dielectric Relaxation Spectroscopy and Dynamic Mechanical Spectroscopy. *Macromolecules*, 2006, 39, p.2172-2182.

[108] Giannelis, E.P., R. Krishnamoorti, and E. Manias, Polymer-Silicate Nanocomposites: Model Systems for Confined Polymers and Polymer Brushes. *Advances in Polymer Science*, 1999, 138, p.107-147.

[109] Privalko, V.P., Y.S. Lipatov, and Y.Y. Kercha, Calorimetric Study of the Phase Boundary Effect on Oligo-Ethylene Glycol Adipate (Oega) Properties. *Polymer Sci. U.S.S.R.*, 1970, 12 (6), p. 1520.

[110] Mammeri, F., et al., Elaboration and mechanical characterization of nanocomposites thin films Part II. Correlation between structure and mechanical properties of SiO_2-PMMA hybrid materials. *Journal of the European Ceramic Society*, 2006, 26, p.267-272.

[111] Vieweg, S., et al., Kinetic structure of glass transition in polymer interfaces between filler and SBR matrix. *Journal of Non-Crystalline Solids*, 1998, 235, p.470-475.

[112] Kirst K.U., F. Kremer, and V.M. Litvinov, Broad-Band Dielectric Spectroscopy on the Molecular Dynamics of Bulk and Adsorbed Poly(dimethylsi1oxane). *Macromolecules*, 1993, 26, p.975-980.

[113] Litvinov V.M. and H.W. Spies, ^{2}H NMR Study of molecular motions in polydimethylsiloxane and its mixtures with aerosils. *Macromolecular Chemistry and Physics*, 1991, 192, p.3005-3019.

[114] Yagrarov M.S., V.S. Ionikin, and Z.G. Gizatullina, Study of the Low- Temperature Thermal Behaviour of Filled Polydimethylsiloxanes. *Polymer Sci. U.S.S.R.,* 1969, 11 (10), p.2626.

[115] Haraguchi, K. and H.J. Li, Mechanical Properties and Structure of Polymer-Clay Nanocomposite Gels with High Clay Content. *Macromolecules*, 2006, 39, p.1898-1905.

[116] Tsagaropoulos, G. and A. Eisenberg, Dynamic Mechanical Study of the Factors Affecting the Two Glass Transition Behavior of Filled Polymers. Similarities and Differences with Random Ionomers. *Macromolecules*, 1995, 28 (18), p.6067-6077.

[117] Fragiadakis, D., P. Pissis, and L. Bokobza, Glass transition and molecular dynamics in poly(dimethylsiloxane)/silica nanocomposites. *Polymer*, 2005, 46, p.6001-6008.

[118] Tsagaropoulos, G. and A. Eisenberg, Direct Observation of Two Glass Transitions in Silica-Filled Polymers. Implications for the Morphology of Random Ionomers. *Macromolecules*, 1995, 28, p.396-398.

[119] Sargsyan, A.G., Tonoyan, A.O., Davtyan, S.P., Schick, C. The amount of immobilized polymer in PMMA-SiO_2 nanocomposites determined from calorimetric data. *European Polymer Journal*, 2007, 43, p.3113-3127.

[120] Suzuki, H., J. Grebowicz, and B. Wunderlich, Glass transition of poly(oxymethylene). *British Polymer Journal*, 1985, 17 (1), p.1-3.

[121] Wunderlich, B., Reversible crystallization and the rigid-amorphous phase in semicrystalline macromolecules. *Progress in Polymer Science*, 2003, 28 (3), p.383-450.

[122] Flaifel M.H., Ahmad S.H., Hassan A., Bahri S., Taravneh M.A., Yu L.J. Thermal conductivity and dynamic mechanical analysis of NiZn ferrite nanoparticles filled thermoplastic natural rubber nanocomposite, *Composites Part B: Engineering,* 2013, 52, p.334–339.

[123] Hassan A, Rahman NA, Yahya R. Extrusion and injection-molding of glass fiber/MAPP/polypropylene: effect of coupling agent on DSC, DMA and mechanical properties. *Journal of Reinforced Plastics and Composites*, 2011, 30 (14), p.1223–1232.

[124] Xiao S., Tan Y., Xu J., Xiong C., Wang X., Su S., Lignosulfonate as dispersant for layered double hydroxide in nitrile–butadiene rubber composites, *Applied Clay Science*, 2014, 97–98, p.91–95.

[125] Saffar A., Shojaei A., Arjmand M., Theoretical and experimental analysis of the thermal, fade and wear characteristics of rubber-based composite friction materials, *Wear*, 2010, 269, p.145-151.

[126] Wu Y., Zeng M., Xu Q., Hou S., Jin H., Fan L., Effects of glass-to-rubber transition of thermosetting resin matrix on the friction and wear properties of friction materials, *Tribology International*, 2012, 54, p.51–57.

[127] Wu W., Zhai Y., Zhang Y., Ren W., Mechanical and microwave absorbing properties of in situ prepared hydrogenated acrylonitrile–butadiene rubber/rare earth acrylate composites, *Composites Part B: Engineering*, 2014, 56, p.497-503.

[128] Pietrasik J., Gaca M., Zaborski M., Okrasa L., Boiteux G., Gain O., Studies of molecular dynamics of carboxylated acrylonitrile-butadiene rubber composites containing in situ synthesized silica particles, *European Polymer Journal*, 2009, 45, p.3317–3325.

[129] Shang S., Gan L., Yuen M., Jiang S., Luo N.M., Carbon nanotubes based high temperature vulcanized silicone rubber nanocomposite with excellent elasticity and electrical properties, *Composites Part A: Applied Science and Manufacturing*, 2014, 66, p.135–141.

[130] Hadac J., Slobodian P., Saha P., Riha P., Evaluation relaxed volume of α-PMMA and α-PMMA/CB from heating, *Chemické listy*, 2014, 108, p.50–58.

[131] Shi G., Zhang M.Q., Rong M.Z., Wetzel B., Friedrich K., Sliding wear behavior of epoxy containing nano-Al_2O_3 particles with different pretreatments, *Wear,* 2004, 256, p.1072–1081.

[132] Leblanc J.L., Rubber–filler interactions and rheological properties in filled compounds, *Progress in Polymer Science*, 2002, 27, p.627-687.

[133] Wolff S., Wang M.-J., Tan E.-H., Filler-elastomer interactions. Part VII. Study on bound rubber, *Rubber Chemistry and Technology*, 1993, 66, p.163–177.

[134] Kida N., Ito M., Yatsuyanagi F., Kaido H., Studies on the structure and formation mechanism of carbon gel in the carbon black filled polyisoprene rubber composite, *Journal of Applied Polymer Science*, 1996, 61, p.1345–1350.

[135] Kolthoff I.M., Kahn A., Sorption of GR-S-type rubber by varbon black I. Sorption from benzene solution by Graphon, *Journal of Physical and Colloid Chemistry*, 1950, 54, p.251–256.

[136] Jenckel E., Rumbach B.,Formation of bound rubber of GRS-S type polymer with carbon blacks, *Zeitschrift für Elektrochemie*, 1950, 55, p.612–618.

[137] Sweitzer C.W., Goodrich W.C., Burgess K.A., The carbon black gel complex in cold rubber reinforcement, *Rubber Age*, 1949, 65, p.651–662.

[138] Leblanc J.L., Barrès C., Bound rubber: a key factor in understanding the rheological properties of carbon black filled rubber compounds. Rub Div Mtg, Am. Chem. Soc. Chicago, Illinois, Paper#70, 1999.

[139] Cotten G.R., Mixing of carbon black with rubber I. Measurement of dispersion rate by changes in mixing torque, *Rubber Chemistry and Technology*, 1984, 57, p.118–133.

[140] R.A.L. Jones, Soft Condensed Matter, Oxford University Press, 2002, 196p.

[141] A.J. Kovacs, Transition vitreuse dans les polymères amorphes. Etude phénoménologique, *Advances in Polymer Science*, 1964, 3(3), p. 394-507.

[142] D.R. Burfield, Polymer glass transition temperatures, *Journal of Chemical Education*, 1987, 64 (10), p. 875.

[143] D.R. Burfield and K.L Lim, Differential scanning calorimetry analysis of natural rubber and related polyisoprenes. Measurement of the glass transition temperature, *Macromolecules,* 1983, 16 (7), p. 1170–1175.

[144] F. Kremer, A. Schönhals, Broadband Dielectric Spectroscopy, Springer, 2003 ed., 729 p.

[145] C. Riedel, A. Alegria, J. Colmenero and P. Tordjeman. Polymer Rheology by Dielectric Spectroscopy, Rheology, Dr. Juan De Vicente (Ed.), 2012, InTech.

[146] D. E. Packham, Handbook of Adhesion, John Wiley & Sons, 2006, Technology & Engineering, 692 p.

[147] V.Chaudhary, PhD thesis "Fundamental studies of the effect of glass transition temperature on enzymatic activity in high-solid biomaterials", 2013, RMIT University, Melbourne, Australia.

Chapter II: Materials and Methods

II.1. Polymer matrix

Poly(styrene-co-butadiene) (SBR) from Aldrich with 45% wt. styrene was used in this work. It is random linear copolymer of styrene and butadiene which was used as received. Figure II.1. illustrates the chemical structure of the copolymer. All of the samples (both pure SBR and SBR/nanoparticles) were prepared from the same chunk in order to avoid the variations of the composition.

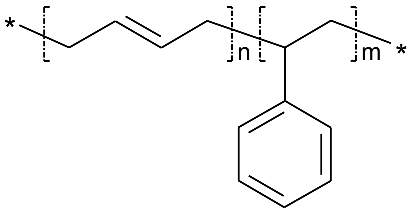

Figure II.1. Chemical structure of the SBR copolymer.

SBR chains are characterized by the very high flexibility at room temperature; the absence of the polar groups means that there are no significant intermolecular interactions. Placed under stress, those entangled SBR molecules just slide against each other resulting in general deformation of the sample. It was proposed long time ago that the introduction of the filler particles should modify the properties of a polymer matrix, because they cause an increase in the number of entanglements in filled systems [1]. We investigated these effects by introducing the alumina nanoparticles.

II.2. Nanoparticles

II.2.1. Unmodified nanoparticles

Aluminium oxide nanoparticles (γ-Al_2O_3) were obtained in form of powder from Evonik Industries AG (Germany), trade name is Aeroxide Alu C. According to the producer [2, 3], the average diameter of the primary particles produced by noble gas condensation at 343K is about 13 nm. During the production process, primary particles sinter to irregularly shaped, chemically bonded aggregates. This leads to nanoparticles with linear dimensions between 13 and 200 nm [3, 4]. The specific surface area of the particles is (100±15) m^2/g. The untreated Alu C nanoparticles have OH-groups at the surface which implies the hydrophilic character of these nanoparticles.

II.2.2. Modified nanoparticles

To investigate the influence of the chemical nature of the filler's surface, the nanoparticles were functionalized using γ-mercaptopropyltrimethoxysilane (supplied by Sigma-Aldrich). Chemical structure of the γ-mercaptopropyltrimethoxysilane is shown in Fig. II.2. All of the solvents used in this work (Chloroform, Methanol and Ethanol) were of spectroscopic purity grade, supplied by Carl Roth GmbH.

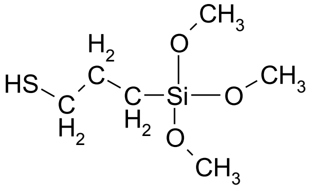

Figure II.2. Chemical structure of γ-mercaptopropyltrimethoxysilane.

Surface-modified Alu C nanoparticles were prepared using method described in [5] and [6]. The suitable solvent (Table II.1.), silane coupling agent and alumina were combined in a flask equipped with reflux condenser. The mixture was refluxed at the boiling temperature of the solution during 5h. The reaction products were centrifuged and soxhlet-extracted with ethanol for 16h [6] to remove the excess silane adsorbed on the alumina surface. Then the surface-treated alumina was air-dried and kept at 80°C under vacuum for 24h [6].

Table II.1. Conditions of the surface modification reaction.

Silane	Solution	Range of suitable pH
γ-Mercaptopropyltrimethoxysilane	80% MeOH+20% H_2O	4,5-5,0

Surface modification reaction is shown in the Scheme II.1. At the first stage the hydrolysis of silane molecule occurs, resulting in replacement of the alkoxy groups by the OH-groups which are needed for further reactions. Second stage of the process is the polycondensation with neighboring silane molecules; this process occurs in parallel with grafting to the nanoparticle surface (reactions 3-4 in the Scheme II.1): at that stage first the hydrogen bonds between OH-groups of the hydrolyzed silane molecules and alumina surface appear, then, when high temperature is applied, these physical bonds are replaced by the covalent bonds [5].

1) $HS\text{-}(CH_2)_3\text{-}Si\text{-}(OCH_3)_3 + 3H_2O \rightarrow 3CH_3\text{-}OH + HS\text{-}(CH_2)_3\text{-}Si\text{-}(OH)_3$ (hydrolysis)

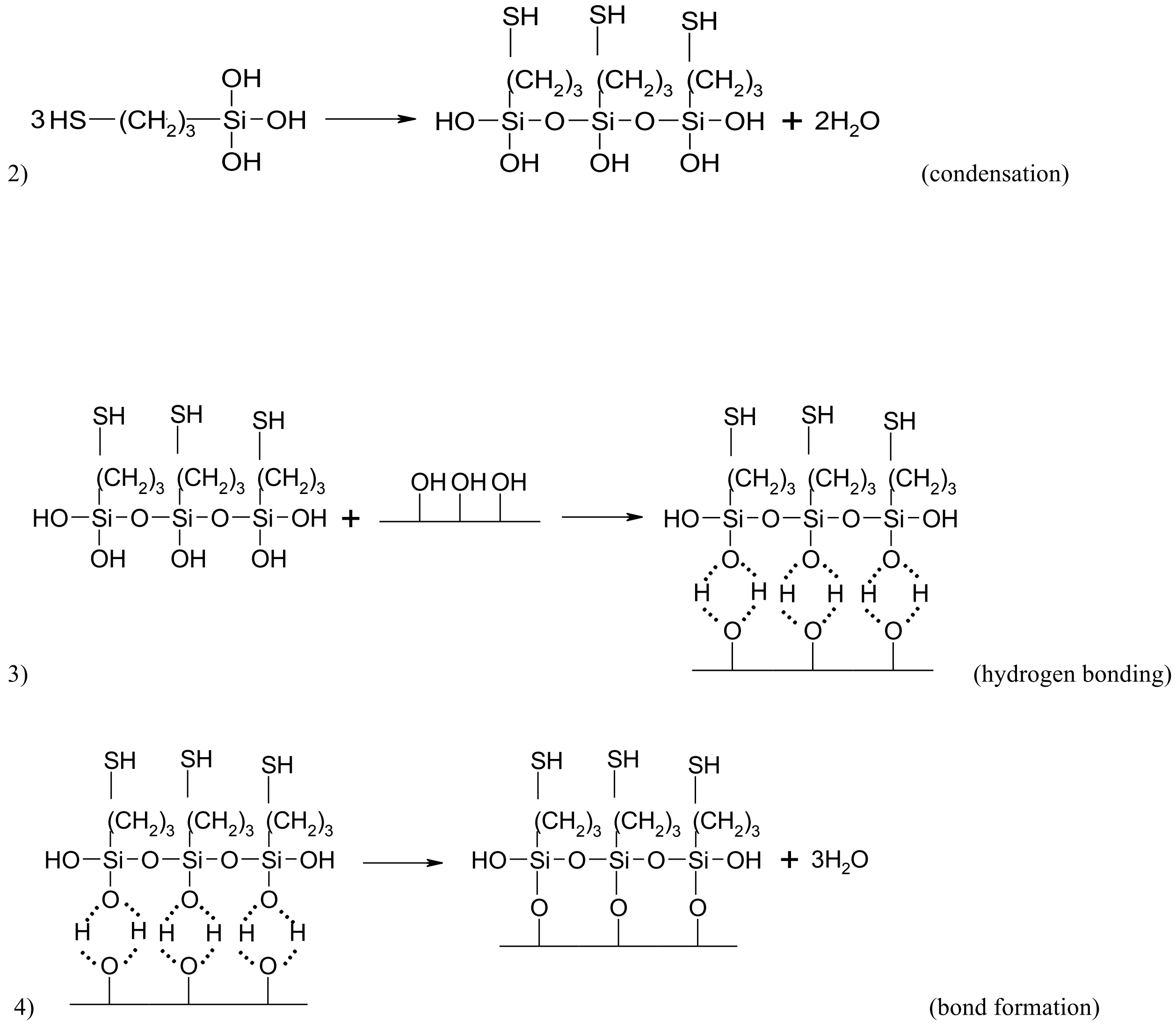

Scheme II.1. Surface modification reactions: 1) Stage of the hydrolysis of silane molecules; 2) Condensation stage, when silane molecules form "n-mers"; 3) Stage of the hydrogen bonding, when condensed silane molecules approach the alumina surface and form hydrogen bonds with OH-groups at the surface of the particles; 4) Chemical bond formation stage, when silane molecules form covalent bond with the OH-groups of the alumina surface.

Figure II.3. schematically illustrates how the modified nanoparticle looks like: it has an aluminium oxide-"core" and a silane-"corona"; in reality the "core" has bigger size than "corona", the area occupied by a single silane molecule at the surface is approximately 0.5-1 nm^2 [5].

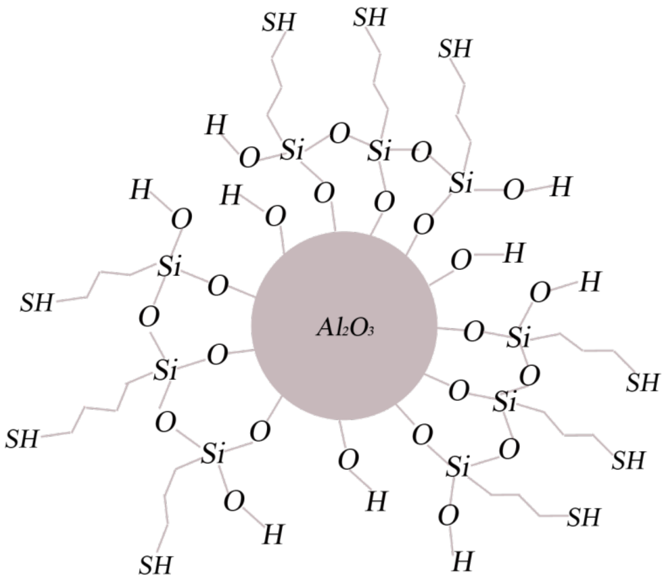

Figure II.3. Schematic representation of the nanoparticle modified with γ-mercaptopropyltrimethoxysilane (size proportions are omitted for clearness).

II.3. Nanocomposites

To produce the SBR/Alu C and SBR/modified Alu C nanocomposites, the following procedure was used [7]: a known mass of Alu C nanoparticles was dispersed and sonicated in Chloroform, after which 10% SBR solution in Chloroform was injected. This mixture was stirred in a planetary mixer for 15 minutes and then freeze-dried. It was shown (see Chapter III) that this method allows obtaining a homogeneous distribution of the nanoparticles in the SBR matrix. The samples for investigations were molded into pellets in a vacuum oven at 85°C during 24h. Some technical issues related to the sample preparation procedure are described in Annex VI.

Thus, three series of nanocomposites containing 1%, 1.5%, 2%, 3%, 4%, 10%, 20% and 30% (wt.) of Alu C or modified Alu C nanoparticles were prepared.

II.4. Grafted nanocomposites SBR/silanized Alu C

The functional group SH of the γ-mercaptopropyltrimethoxysilane, used for surface-modification of the Alu C nanoparticles, allows making covalent bond with the styrene-butadiene rubber. The SH-group can be used in the frame of the radical-mediated polymer modification [8]: the addition to double bonds of a thiol radical is considered a specific and selective reaction not directly involving the formation of polymeric alkyl radical species which, especially in the case of polyolefins, can undergo side reactions depending on feed conditions and polymer structure [9].

Scheme II.2 illustrates grafting reactions:

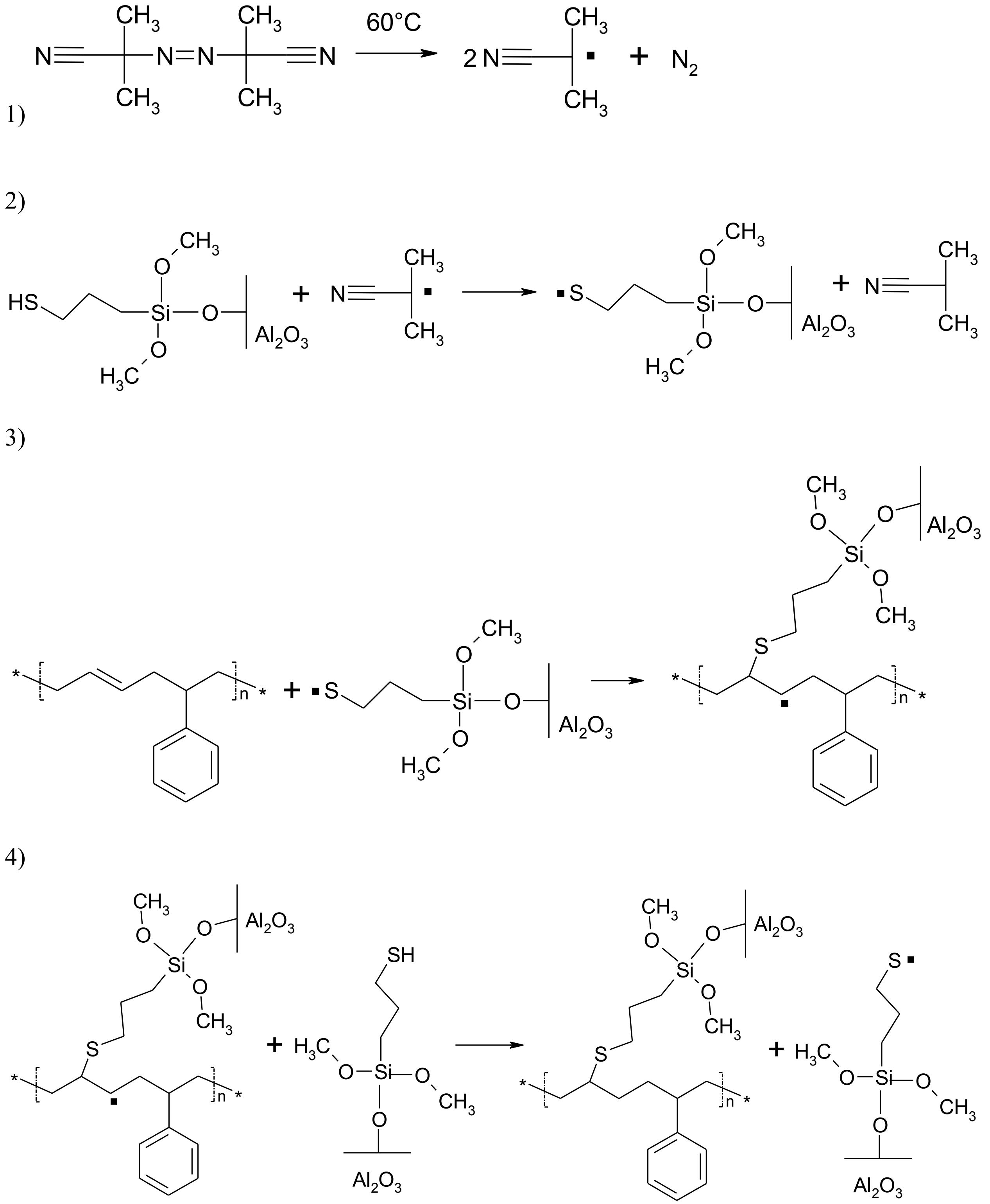

Scheme II.2. Grafting reaction between SBR and Alu C modified with γ-mercaptopropyltrimethoxysilane.

At the first stage of the reaction the initiator AIBN (azobisisobutyronitrile) at 90°C forms radicals which initiate grafting reaction at the second stage; third stage of the reaction represents bond formation between polymer and silanized nanoparticle; fourth reaction is a transfer of radical from polymer to the silane molecule at the surface of the Alu C nanoparticle. Grafting reactions have been performed at 90°C in Helium atmosphere using 10% SBR solution in Toluene and the same amounts of silanized nanoparticles that were used for preparation of the ungrafted nanocomposites. AIBN amount used for the reaction was proportional to the total amount of silane molecules at the nanoparticles surface (taken from TGA, see Annex I), calculated for each nanoparticle concentration. The molar ratio [AIBN$^{\cdot}$]:[silane] was 1:1.

This way, another series of the nanocomposites containing 1%, 1.5%, 2%, 3%, 4%, 10%, 20% and 30% (wt.) of the Alu C nanoparticles grafted to the SBR macromolecules was prepared.

II.5. Experimental techniques

II.5.1. Thermogravimetric Analysis

Thermogravimetric Analysis (TGA) was used to confirm the concentration of alumina nanoparticles in the final SBR/Alu C nanocomposites.

TGA is an essential laboratory method used for material characterization. It is a technique in which the mass of a substance is monitored as a function of temperature or time as the sample specimen is subjected to a controlled temperature program in a controlled atmosphere. Upon heating a material, its weight increases or decreases. TGA measures a sample's weight as it is heated or cooled in a furnace.

A TGA consists of a sample pan that is supported by a precision balance. That pan resides in a furnace and is heated or cooled during the experiment. The mass of the sample is monitored during the experiment. A sample purge gas controls the sample environment. This gas may be inert or a reactive gas that flows over the sample and exits through an exhaust [12].

For my measurements, TGA 2950 from TA Instruments was used. It is a bottomloading (hangdown) model of instrument, which supports the sample pan via a "hangdown" below the balance. The measurements were performed in the temperature range 25÷500°C, with a heating rate of 5°C/min and 10°C/min, in the air atmosphere.

II.5.2. Transmission Electron Microscopy

To examine the dispersion of surface-treated, as well untreated alumina nanoparticles in SBR matrix, the Transmission Electron Microscope has been used.

Transmission electron microscopy (TEM) is a microscopy technique in which a beam of electrons is transmitted through an ultra-thin specimen, interacting with the specimen as it passes through. As a result of the interaction of the electrons transmitted through the specimen the image is produced; the image is magnified and focused onto an imaging device, such as a fluorescent screen, on a layer of photographic film, or to be detected by a sensor such as a CCD camera [13].

The transmission electron microscope operates on the same basic principles as the light microscope but uses electrons instead of light. What you can see with a light microscope is limited by the wavelength of light. TEMs use electrons as “light source” and their much lower wavelength (de Broglie wavelength) make it possible to get a resolution a thousand times better than with a light microscope.

With TEM it is possible to see objects to the order of a few angstroms (10^{-10} m). The possibility for high magnifications has made the TEM a valuable tool in both medical, biological and materials research.

A "light source" (electron gun) at the top of the microscope emits the electrons that travel through vacuum in the column of the microscope. Instead of glass lenses focusing the light in the light microscope, the TEM uses electromagnetic lenses to focus the electrons into a very thin beam. The electron beam then travels through the specimen. Depending on the density of the material present, some of the electrons are scattered and disappear from the beam. At the bottom of the microscope the un-scattered electrons hit a fluorescent screen, which gives rise to a "shadow image" of the specimen with its different parts displayed in varied darkness according to their density. The image can be studied directly by the operator or photographed with a camera [13-14].

The morphology of cross-sectioned areas at the specimen surface was examined using transmission electron microscope (JEOL JEM 2011-HRTEM), which was operated at an acceleration voltage of 100 kV.

II.5.3. Temperature Modulated Differential Scanning Calorimetry

Temperature-Modulated Differential Scanning Calorimetry (TMDSC) is a calorimetric technique which was first introduced in 1971 [15-16]. The use of a modulated temperature profile with DSC, combined with a deconvolution procedure in order to obtain the same information as conventional DSC plus, at the same time, the response to the modulation, was first proposed by Reading and co-workers [17–23]. In TMSDC, a sine wave modulation is applied to the standard linear temperature program (Fig. II.4).

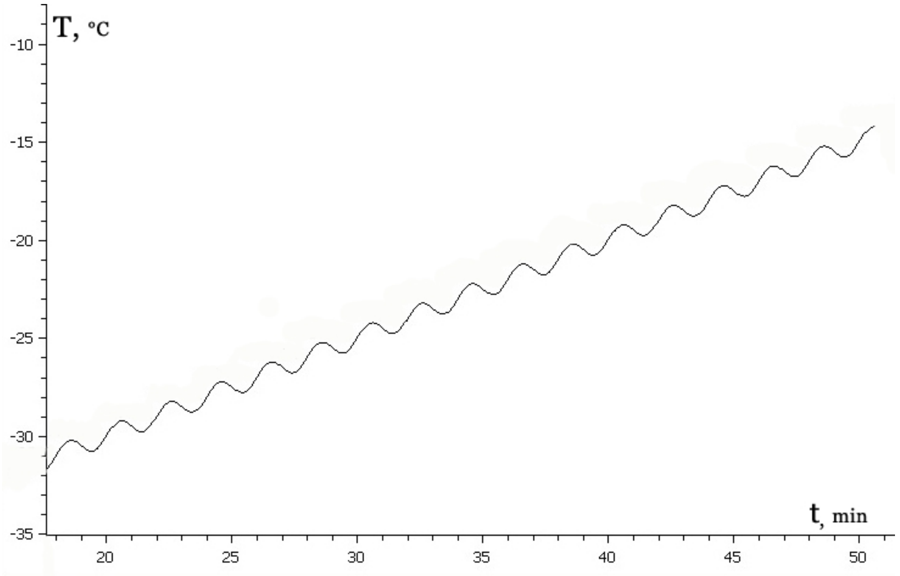

Figure II.4. Example of the sinusoidal modulation of temperature in TMDSC.

TMDSC technique, as well as conventional DSC, may be used to characterize physical and chemical processes via changes in their enthalpy or heat capacity of a sample. Like other thermal methods, calorimetry involves manipulation of temperature to produce some measured parameter (e.g. heat flow) during thermal process.

Thermal processes detectable by DSC can be endothermic (e.g. melting) or exothermic (e.g. crystallization). Some processes may involve noticeable heat capacity changes (e.g. glass transition).

The basic DSC setup consists of a sample and reference positioned in a furnace (Fig. II.5).

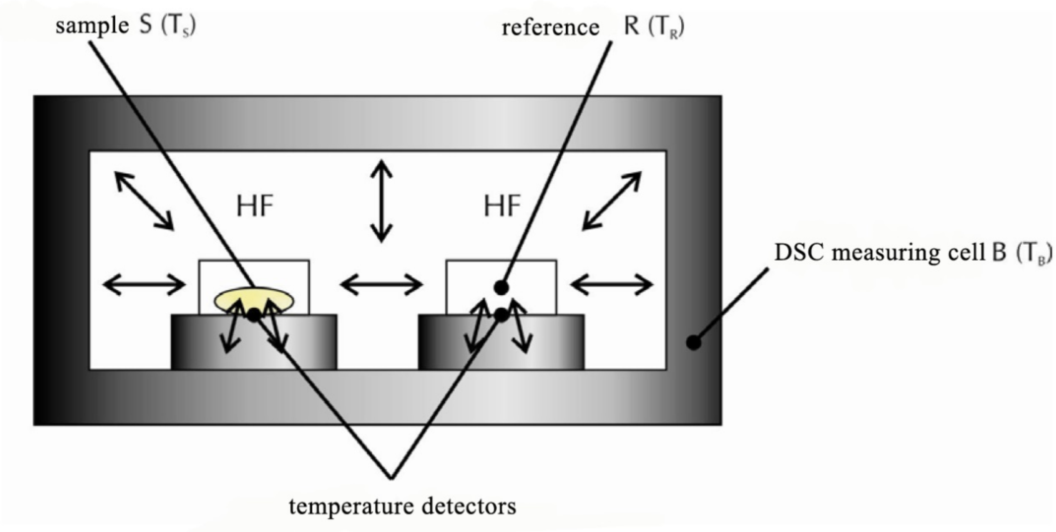

Figure II.5. Illustration of the basic DSC setup. "HF" designates Heat Flow.

The sample and reference pans are heated from the same source and the temperature difference between both crucibles is measured. An assumption is made that the thermal gradients within the components of the cell are negligible. In this case the cell temperature changes linearly:

(Eq. II.5) $$T_B(t) = T_0 + \beta t \ ,$$

where $T_0 = T(0)$ and $\beta = \frac{\partial T_B}{\partial t}$. The temperature difference between reference and sample pans is

(Eq. II.6) $$\Delta T(t) = T_R(t) - T_S(t) \ ,$$

The temperature difference between the cell B and the sample S (or reference R) produces the heat flow *HF_S(t)* (or *HF_R(t)*)

(Eq. II.7) $$HF_{S/R}(t) = \frac{\partial Q_{S/R}}{\partial t} \ ,$$

between the respective setup elements. According to Fourier's law

(Eq. II.8) $$HF_{S/R}(t) = k(T_B(t) - T_{S/R}(t)) \ ,$$

where k is a characteristic constant of the instrument.

The heat capacity is defined as (index p indicates that we measure the heat capacity at constant pressure)

(Eq. II.9) $$C_{pS/R} = \frac{\partial Q_{S/R}}{\partial T_{S/R}} \ ,$$

which after integration transforms to

(Eq. II.10) $$Q_{S/R}(t) = C_{pS/R}(T_{S/R}(t) - T_0) \ ,$$

$$\frac{\partial(Q_{S/R}(t))}{\partial t} = c_{pS/R} \frac{\partial(T_{S/R}(t))}{\partial t} \ .$$

Comparing to Eq. II.7 and taking into account Eq. II.5 and Eq. II.8, we obtain

(Eq. II.11) $$\frac{\partial(T_{S/R}(t))}{\partial t} + \frac{k}{c_{pS/R}} T_{S/R}(t) = \frac{k}{c_{pS/R}} (T_0 + \beta t) \ .$$

Partial integration with respect to t allows obtaining the following equation (taking into account limiting conditions):

(Eq. II.12) $$\ln\left(\frac{\beta - \frac{k}{C_{pS/R}}(T_0 + \beta t - T_{S/R}(t))}{\beta - \frac{k}{C_{pS/R}}(T_0 + \beta \cdot 0 - T_{S/R}(0))}\right) = -\frac{k}{C_{pS/R}} t \ .$$

Taking the exponential and isolating $T_{S/R}(t)$ we get

(Eq. II.13) $$T_{S/R}(t) = T_0 + \beta t + \frac{\beta C_{pS/R}}{k}\left(e^{-\frac{k}{C_{pS/R}}t} - 1\right).$$

For a long period of time comparing to the time constant $\tau = \frac{C_{pS/R}}{k}$, the exponential in brackets becomes negligible which allows writing

(Eq. II.14) $$T_{S/R}(t) = T_0 + \beta t - \frac{\beta C_{pS/R}}{k}, \text{ where } t \gg \tau.$$

We observe that the change in sample (and reference) temperature lags behind the one of the cell. Temperature difference between the reference and the sample is described as follows:

(Eq. II.15) $$T_R(t) - T_S(t) = \frac{\beta}{k}(C_{p_S} - C_{p_R}).$$

If we admit that the crucibles are identical:

(Eq. II.16) $$\varDelta T = \frac{\beta m c_p}{k},$$

where c_p is the specific heat capacity of the sample under study.

(Eq. II.17) $$c_p = \frac{k\varDelta T}{\beta m}.$$

Eq. II.16 indicates that the measured temperature difference is proportional to the heating rate β. Thus, in order to obtain $\varDelta T$ high enough, β should also be sufficiently high. At the same time, high heating rates might result in a bad temperature resolution. Also, if β vanishes the signal disappears, which means that isothermal DSC measurements do not allow c_p to be determined.

The TMDSC mathematical model is based on the model which describes conventional DSC, only with addition of the temperature modulation term.

In that case, the TMDSC cell temperature will be described as follows:

(Eq. II.18) $$\check{T}_B(t) = T_0 + \beta t + iA_{T_B} \cdot e^{-i\omega t},$$

where A_{T_B} is the temperature modulation amplitude of the cell, β the heating rate of the oven, and $\omega = \frac{2\pi}{P}$ (period P of the modulation) the angular frequency. Then

(Eq. II.19) $$T_B(t) = R\left(\check{T}_B(t)\right) = T_0 + \beta t + A_{T_B}\sin(\omega t),$$

whereby

(Eq. II.20) $$\check{T}_B(0) = T_0 + iA_{T_B}$$

is the complex temperature at the start of the experiment. Using the same mathematical procedures as we used previously to get the equations for conventional DSC, we obtain the following [20]:

a) The expression for the temperature difference between the reference and the sample is given by:

(Eq. II.21) $$\Delta T = \frac{\beta m c_p}{k} + A_{\Delta T}\sin(\omega t - \delta),$$

where c_p is the specific heat capacity of the sample, $A_{\Delta T}$ is the amplitude of the temperature difference between the reference and the sample, and δ represents the phase difference between $\Delta T(t)$ and $T_B(t)$.

Eq. II.21 shows that the temperature difference $\Delta T(t)$ comprises two terms: the DSC term (Eq. II.16) and the second term generated by the temperature modulation.

b) The heat flow resulting from the temperature difference between sample and reference

(Eq. II.22) $$HF = \beta m c_p + \mathrm{k}A_{\Delta T}\sin(\omega t - \delta).$$

c) After measuring the heat flow, the specific heat capacity c_p can be determined as

(Eq. II.23) $$c_p = \frac{A_{\Delta T}}{m\omega A_{T_S}}\sqrt{k^2 + \omega^2 C_{p_R}^2}\ ,$$

where c_{p_R} is the specific heat capacity of the reference crucible, A_{T_S} is the amplitude of the temperature modulation of the sample, and k is the DSC cell constant.

Eq. II.23 shows c_p can be determined from isothermal TMDSC measurements.

In the frame of my PhD thesis I mainly used TMDSC to investigate the glass transition behavior of SBR/alumina nanocomposites. Vitrification is a process depending on the experimental time/frequency scale (e.g. it is well known that the glass transition temperature depends on the cooling rate used in the experiment). In such a situation the specific heat capacity has to be treated as a complex magnitude

(Eq. II.24) $$c_p^*(T,\omega) = c'_p(T,\omega) - ic''_p(T,\omega).$$

The modulated temperature program can be considered as an external perturbation. In the frame of Linear Response Theory, the investigated system reacts to the external perturbation by a heatflow [25]:

(Eq. II.25) $$HF\big(T(t)\big) = C_\beta(T)\beta + \omega A_{T_S}\left|mc_p^*(T,\omega)\right|\cos(\omega t - \varphi),$$

where φ is the phase angle between the sinusoidal heat flow and the sinusoidally modulated heating rate ($\varphi = \delta + \frac{\pi}{2}$).

If the heat capacity is independent of time, we consider c_β equal to c_p. Comparing Eq.II.25 and Eq. II.22 ($A_{HF}=kA_{\Delta T}$) yields

(Eq. II.26) $$\left|c_p^*(T,\omega)\right| == \frac{|C^*(T,\omega)|}{m} = \frac{A_{HF}}{m\omega A_{TS}},$$

(Eq. II.27) $$\varphi = arctan\frac{A_{HF}}{A_{TS}}.$$

The prerequisite for the use of the equation II.26 is a heating rate $\beta = \frac{\partial T}{t}$, which has to be slower than 1K/min.

The real part of the specific heat capacity

(Eq. II.28) $$c_p' = \left|c_p^*\right| \cos\varphi$$

is considered as "storage" heat capacity [24, 28-30]; it describes the periodic heat exchange between the sample and the environment.

The imaginary part of the specific heat capacity

(Eq. II.29) $$c_p'' = \left|c_p^*\right| \sin\varphi$$

is called "loss" specific heat capacity [24, 28-30]; it describes the increase of entropy inside the sample during irreversible processes and dissipation phenomena in the system.

In my research, I have used a Mettler Toledo DSC 821e instrument. Samples of 8-10 mg were weighed and sealed in aluminum pans. Thermal measurements were performed in helium atmosphere in the temperature range from 193 to 298 K with a cooling rate of -0.5 K/min, temperature modulation amplitude of 0.5 K and a modulation period of two minutes. The real and imaginary parts of the specific heat capacity were evaluated using standard methods [24].

II.5.4. Dynamic Mechanical Analysis and Rheometry

II.5.4.1 Stress response of dynamically sheared viscoelasic samples. Boltzmann's super-position principle

In all of the mechanical experiments realized in this PhD project the samples were sheared. Fig. II.6 schematically shows the typical set-up:

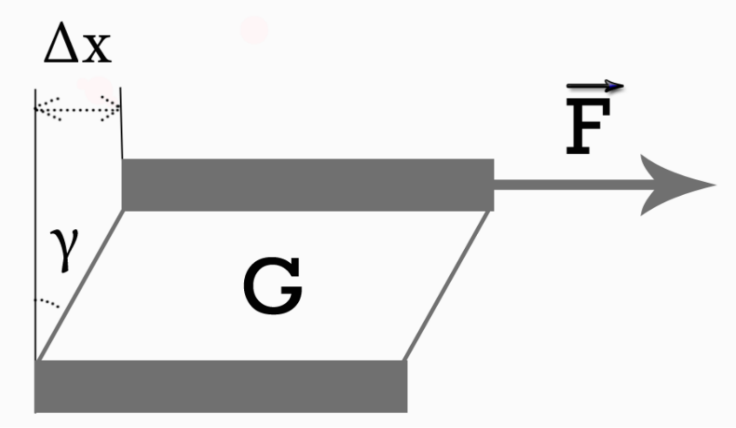

Figure II.6. Typical experimental set-up for shear experiments.

The sample with thickness h is placed between two parallel plates of area S. The lower plate is fixed and the upper one is mobile. Applying a tangential force on the upper plate yields a deformation

(Eq. II.30)
$$\gamma \approx \tan\gamma = \frac{\Delta x}{h}.$$

The shear modulus G of the sample is defined as

(Eq. II.31)
$$G = \frac{\sigma}{\gamma},$$

where σ is representing the shear stress:

(Eq. II.32)
$$\sigma = \frac{F}{S}\,.$$

Many polymers behave as viscous liquids at high temperatures and as elastic solids when they are cooled below the glass transition temperature T_g. In the intermediary temperature range the long chain molecules react to strains or stresses by combining viscous and elastic elements of response. In this case the polymer sample behaves viscoelastically.

Viscoelasticity can best be evidenced in a stress-step strain experiment like the one illustrated in Fig. II.7:

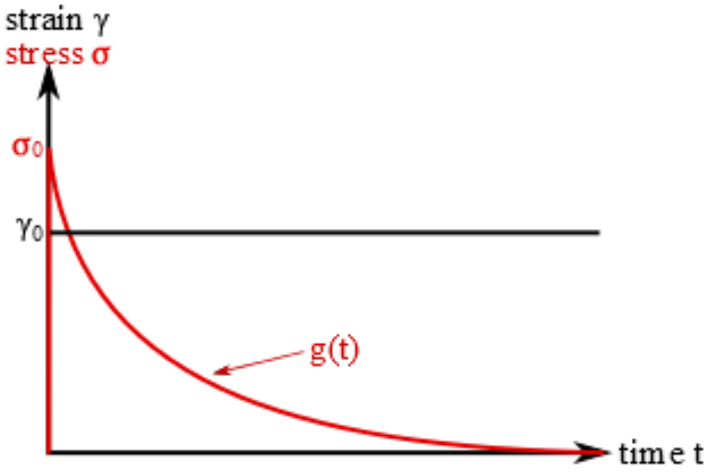

Figure II.7. Stress σ and strain γ as a function of time in a stress-step strain experiment.

Imposing a step-strain γ_0 to the sample at a given time point *t'* yields a stress decay which can be described by the so-called relaxation modulus

(Eq. II.33)
$$g(t) = \frac{\sigma(t)}{\gamma_0}.$$

Obviously, in the viscoelastic regime, the shear modulus *G=g(t)* is a time-dependent quantity. While at short times the material behaves solid-like, at long times this behavior switches to liquid-like.

In a shear experiment, linear response conditions are respected when upon doubling, tripling, …, the deformation, the stress also gets twice, three times, … larger. All of the mechanical tests carried out in the present project were realized under linear regime conditions.

Following Boltzmann, in a shear experiment the stress at any time point *t* depends on the entire strain story up to that time (causality); each strain change makes an independent contribution to the stress at time point *t* and these contributions add to give the total observed stress (linearity).

According to Boltzmann superposition principle, shear stress *σ(t)* at the time point *t* is equal to the total of the infinitesimal stress contributions

(Eq. II.34)
$$d\sigma(t) = g(t-t')d\gamma,$$

generated by infinitesimal step-strains $d\gamma$ at time points $-\infty < t' < t$:

(Eq. II.35) $$\sigma(t) = \int_{-\infty}^{t} g(t-t')d\gamma \;.$$

With $\gamma' = \frac{d\gamma}{dt}$ the equation II.35 becomes

(Eq. II.36) $$\sigma(t) = \int_{-\infty}^{t} g(t-t')\gamma'(t')dt' \;.$$

Eq. II.36 corresponds to the mathematical formulation of Boltzmann's superposition principle. According to the latter the stress response of a viscoelastic sample to an arbitrary strain is entirely determined by the relaxation modulus *g(t)*, i.e. the stress response of the material to a step-strain.

II. 5.4.2 Dynamic mechanical analysis. Rheometry

To carry out the shear experiments, a Dynamic Mechanical Analysis equipment (Mettler Toledo DMA/SDTA 861e) and a rheometer (Anton Paar MCR 302), both available at LPM were used. In the following I will succinctly describe the working principles of both machines.

1) DMA

The DMA/SDTA 861e instrument (Fig. II.8) works in the temperature range from -150°C to 500°C, at frequencies comprised between 0.001 Hz and 1000 Hz, and force range from 1 mN to 40N. In the shear mode two identical disk-like samples are needed, these samples are located between 3 parts of the shear clamp as shown in Fig.II.9. The two external parts of the clamp are immobile while the internal part can be moved up and down by the motor. Unfortunately, such sample holder can only poorly be adapted to the changing thickness of the sample, which is especially important at low temperatures near or below the thermal glass transition. The sample diameter can be 15mm maximum and the sample thickness can be up to 6.5mm. The diameter of my samples was around 8mm and the thickness about 1mm.

The shear modulus can be calculated from the measured force (F_a) and displacement (D_a) amplitudes (Fig.II.10) and their phase shift (δ). The phase shift δ is calculated from the time delay Δ (Fig.II.10), using the equation

(Eq. II.37) $$\delta = 2\pi f \Delta \;.$$

The value of *tan* δ corresponds to the ratio of $''/G'$. The moduli are calculated from the measured stiffness according to the following equations:

(Eq. II.38) $$|G^*| = S \cdot g = \frac{F_a}{D_a} g,$$

where g is the geometry factor calculated from the sample dimensions (for disk-like samples $g = \frac{2T}{\pi d^2}$, where T is the sample thickness and d is the diameter), S is the stiffness of the sample ($S = \frac{F_a}{D_a}$); the stiffness of the sample can be influenced by the change in sample geometry.

The storage modulus *G'* is determined by the equation

(Eq. II.39) $$G' = |G^*| \cos \delta$$

and is a characteristic of the energy stored elastically and reversibly. Loss modulus G" is proportional to the energy transformed into heat and irreversibly lost and is calculated using the following equation:

(Eq. II.40) $$G'' = |G^*| \sin \delta$$

The measurements of *G'* and *G"* moduli on my samples were performed as a function of frequency (from 0.008 to 800Hz) with the displacement of 5μm and the force of 1N.

Figure II.8. Mettler Toledo DMA/SDTA 861e instrument.

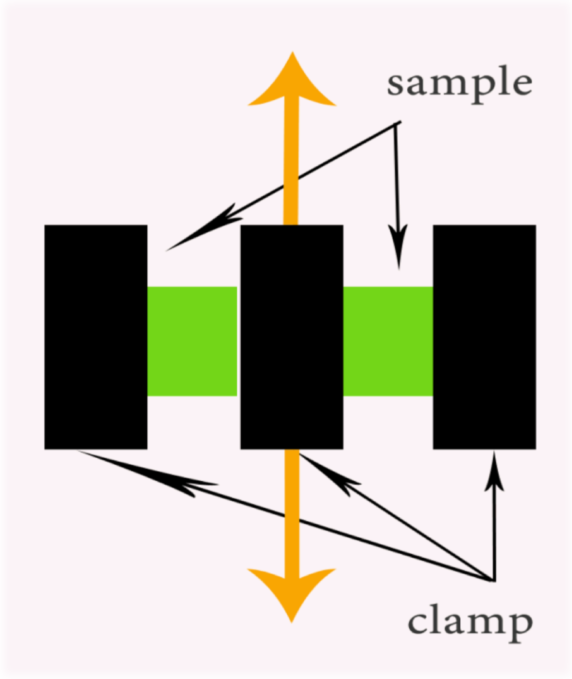

Figure II.9. Schematical drawing of the DMA shear clamp.

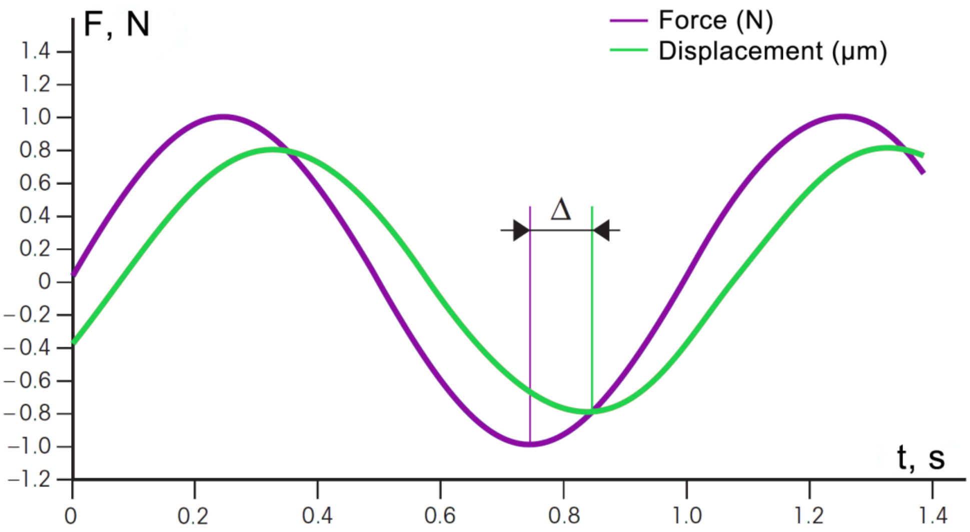

Figure II.10. Force F and displacement D dependence upon time t at a frequency f.

2) Rheometry

The Anton Paar MCR2 (Fig.II.11) instrument is a rotational rheometer working in the temperature range from -150°C to 1000°C, at frequencies extending from 10^{-3} to 628 rad/s. We used the device with plate-plate geometry. In this configuration the sample holder comprises two horizontal plane disks of radius R (R = 8 mm) separated by a gap of width h. The lower disk is immobile while the upper one can be rotated around the vertical z-axis (Fig. II.12).

Figure II.11. Anton Paar MCR2 instrument.

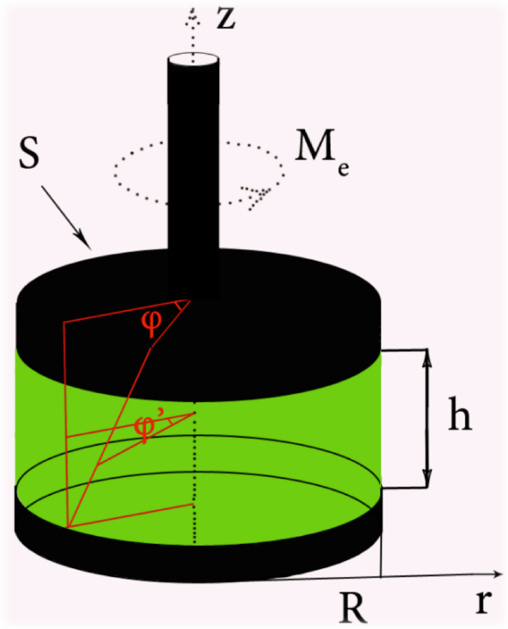

Figure II.12. Geometry of a parallel plate rheometer.

The sample to be investigated is filled into the gap. During the measurements on our samples, the normal force was kept constant at 2N and the gap size h (usually between 1 and 2 mm) was allowed to adapt to the thermal expansion of the samples. When wall slip can be neglected, the angular deformation of the sample layer in contact with the upper disk corresponds to the rotation angle φ imposed by the rheometer on the upper plate. The angular deformation progressively decreases with diminishing height in the sample (e.g. $\varphi' < \varphi$). The layer in contact with the lower immobile plate is not deformed ($\varphi'' = 0$). To establish the described deformation profile in the sample, a torque M_e has to be exerted on the rheometer axis. Our rheometer determines M_e and measures φ as well as the angular velocity $\dot{\varphi}$. As described in [49], these quantities are linked to the deformation rate $\dot{\gamma}(R)$, the deformation $\gamma(R)$ and the stress $\sigma(R)$ by the following relations [49]:

(Eq. II.41)
$$\dot{\gamma}(R) = \frac{R\dot{\varphi}}{h},$$

(Eq. II.42)
$$\gamma(R) = \frac{R\varphi}{h},$$

(Eq. II.43)
$$\sigma(R) = \frac{M_e}{2\pi R^2}\left(3 + \frac{d\ln M_e}{d\ln\dot{\gamma}(R)}\right).$$

The $\frac{d\ln M_e}{d\ln\dot{\gamma}(R)}$ term in the Eq.II.43 is called Rabinowitch-Mooney term. For ideal viscous liquids $\frac{d\ln M_e}{d\ln\dot{\gamma}(R)} = 1$. For non-Newtonian samples this term is automatically evaluated by the rheometer.

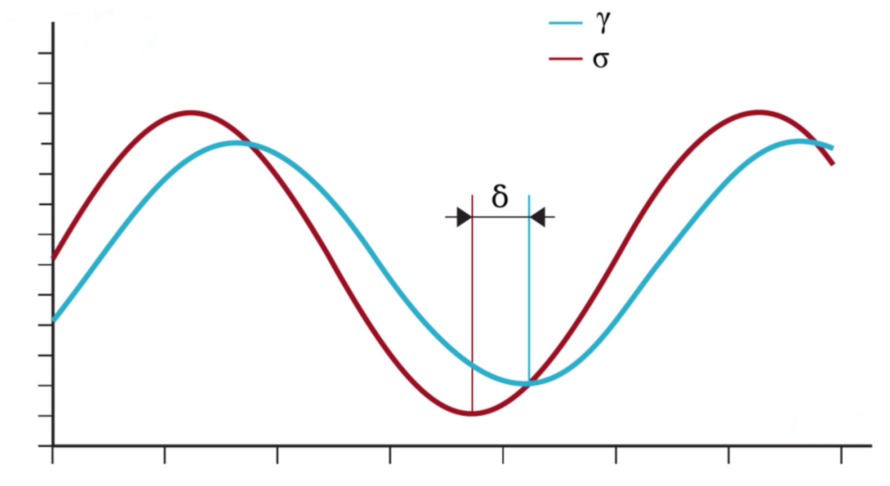

Figure II.13. Stress response to a sinusoidal deformation at constant frequency.

Fig. II.13 illustrates a typical stress response

(Eq. II.44) $$\sigma(t) = \sigma_0 \sin(\omega t + \delta)$$

to a sinusoidal deformation

(Eq. II.45) $$\gamma(t) = \gamma_0 \sin(\omega t)$$

applied by the DMA or rheometer to a viscoelastic sample under linear response conditions: σ_0 – stress amplitude; γ_0 – strain amplitude; $\omega=2\pi f$ – angular frequency (f is frequency); δ – phase shift angle between stress and strain at a given angular frequency, δ is provided by the rheometer.

II. 5.4.3. Shear storage and loss moduli

As already mentioned, in a dynamic mechanical experiment carried out by DMA or rheometry, the deformation γ varies sinusoidally as a function of time (Eq. II.45). According to Boltzmann's superposition principle (Eq. II.36), the stress of a viscoelastic sample obeys to

(Eq. II.46) $$\sigma(t) = \int_{-\infty}^{t} g(t-t') \cdot \gamma_0 \cdot \omega \cdot \cos \omega t' \cdot dt'.$$

Using the new variable $s = t - t'$ yields

(Eq. II.47) $$\sigma(t) = \int_0^\infty g(s) \cdot \gamma_0 \cdot \omega \cdot \cos\omega(t-s) \cdot ds$$

or

(Eq. II.48) $$\sigma(t) = G'(\omega)\gamma_0 \sin\omega t + G''(\omega)\gamma_0 \cos\omega t \;,$$

with

(Eq. II.49) $$G'(\omega) = \omega \int_0^\infty g(s)\sin(\omega s)\,ds,$$

(Eq. II.50) $$G''(\omega) = \omega \int_0^\infty g(s)\cos(\omega s)\,ds.$$

Obviously the stress response (Eq. II.48) comprises an "in-phase" term and a second term being out of phase with the deformation by $\pi/2$.

While the in-phase term is characterized by the storage shear modulus *G'(ω)*, the out-of-phase term depends on the loss shear modulus *G"(ω)*. The storage modulus *G'* describes the ability of the material to store potential energy and release it upon deformation; it is known as a measure of the elastic character or solid-like nature of the material. The loss modulus *G"* is associated with energy dissipation in the form of heat upon deformation and is known as a measure of the viscous character or liquid-like nature of the material. The larger *G'* is relative to *G"*, the more of the energy required to deform the sample is elastically recoverable. The larger *G"* is relative to *G'*, the more of the deformation energy is viscously dissipated as heat. Most interestingly the storage modulus and the loss modulus can correspond to the sin- and cos - Fourier transforms of the relaxation modulus *g(t)* respectively. Hence *g(t)* contains the integral information on the shear behavior of the material the sample is made of.

In case of a sinusoidal deformation (Eq. II.45), DMA or rheometry deliver a stress response which can be written as Eq. II.44 or

(Eq. II.51) $$\sigma(t) = \sigma_0 \sin(\omega t) cos\delta + \sigma_0 \cos(\omega t) sin\delta.$$

Comparing to the Eq. II.48 the results obtained from dynamical measurements can be used to determine the frequency dependence of storage and loss shear moduli according to

(Eq. II.52) $$G' = \frac{\sigma_0}{\gamma_0}\cos\delta$$

(Eq. II.53) $$G'' = \frac{\sigma_0}{\gamma_0}\sin\delta.$$

The loss factor is defined as

(Eq. II.54) $$\tan\delta = \frac{G''}{G'}.$$

Tan δ ranges from zero for an ideal elastic solid to infinity for an ideal liquid. It represents the ratio of energy dissipated to energy stored per cycle of deformation. For an ideal elastic solid, the phase lag δ is zero. Thus, the shear modulus reduces to *G'*; the loss modulus *G"* is zero. An ideal viscous liquid, for which the phase lag is 90° (π/2) radians, cannot store elastic potential energy. In a physical sense, the storage modulus is related to the stiffness of the material and the loss modulus is reflected in the damping capacity of the material [47]. The dynamic loss modulus is often associated with "internal friction" and is sensitive to different kinds of molecular motions, relaxation processes, transitions, morphology and other structural heterogeneities. Thus, the dynamic properties provide information at the molecular level to the understanding of the polymer's mechanical behavior.

Liquid viscoelastic samples show universal low-frequency behavior under linear regime conditions. Considering Eq. II.49-II.50, when $\omega \to 0$ ($\sin \omega s \to \omega s$; $\cos \omega s \to 1$):

(Eq. II.55) $$G'(\omega) \approx \omega^2\left[\int_0^\infty s g(s) ds\right] \propto \omega^2,$$

(Eq. II.56) $$G''(\omega) \approx \omega\left[\int_0^\infty g(s) ds\right] \propto \omega.$$

Terminal regime behavior manifests itself by the power laws $G'(\omega) \propto \omega^2$ and $G''(\omega) \propto \omega$. Violations of the terminal regime behavior are generally due to structural changes (e.g. gelation, network formation) occurring in the samples or to the emergence of additional relaxation processes (e.g. bound rubber in elastomer-based nanocomposites).

Using a complex notation to describe the time dependencies of strain and stress, the shear modulus equation can be rewritten as a complex number:

(Eq. II.57) $$G^* = G' + iG''.$$

II. 5.4.4. Frequency-temperature equivalence. Master curves

Generally the viscoelastic response of a polymer material extends over many decades of frequency. However, our equipment (DMA and rheometer) can only measure in frequency windows with limited widths (10^{-3} to 628 rad/s for rheometer; 0.001 to 1000 Hz for DMA). To significantly increase the frequency range, the results obtained from isothermal frequency sweeps realized at different temperatures can be superposed in master curves at a reference temperature T_0. This construction is justified by the frequency-temperature equivalence principle. The essence of the concept is, that if all the relaxation phenomena involved in *g(t)* have the same temperature dependency, then changing the temperature of a measurement will have the same effect on the data as shifting the data horizontally on the log(frequency) axis.

To illustrate the procedure we have represented in Fig. II.14 the results gained on a neat SBR sample from DMA. The left part of the figure shows storage modulus data *G'(f)* obtained from isothermal frequency sweeps realized at different temperatures. The right hand side of Fig. II.14 clearly documents various shifts operated along the *log(f)* axis to achieve the overlapping of the different pieces of curve with the data set at the reference temperature $T_0 = 273\ \mathrm{K}$. The construction yields the master curve *G'(f·a*$_T$*)* of neat SBR at $T_0 = 273\ \mathrm{K}$. Vertical shifts were not necessary to achieve the construction of the master curve.

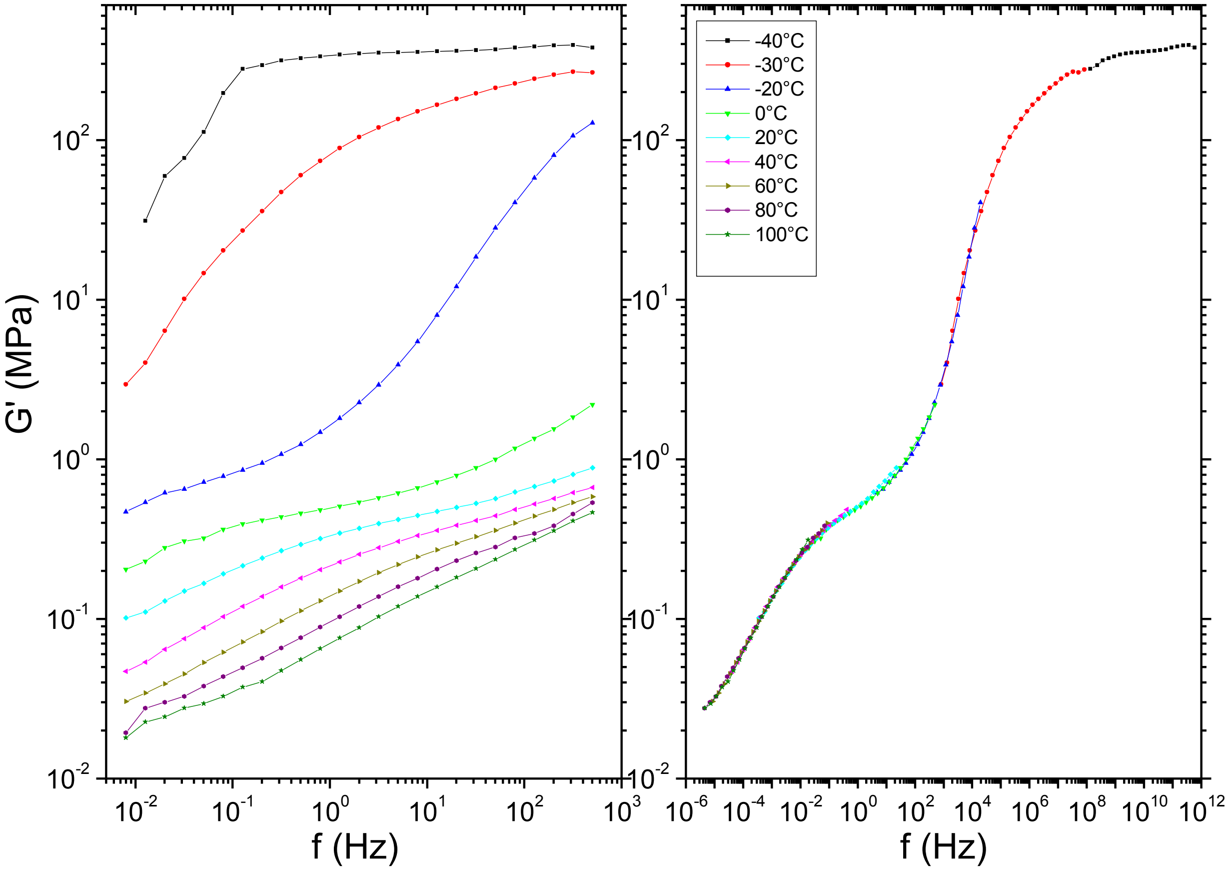

Figure II.14. Storage modulus G' dependence upon frequency: left part shows experimental data from isothermal frequency sweeps at different temperatures; right part shows the final mastercurve.

To construct the master curves, Williams–Landel–Ferry (WLF) equation [52] has been used for the shift factors:

(Eq. II.58) $$\log a_T = \frac{-C_1(T-T_R)}{C_2+(T-T_R)},$$

(Eq. II.59) $$C_1 = \frac{B}{2.303 f_g} \quad \text{and} \quad C_2 = \frac{f_g}{\alpha_f},$$

where B is the constant, f_g is the fractional free volume at the glass transition temperature and α_f is the coefficient of expansion of the fractional free volume [57]. Williams, Landel, and Ferry found that C_1 and C_2 were similar for many amorphous polymers with C_1=17.44 and C_2=51.6 in the temperature range between T_g and T_g+100K. When C_1 and C_2 assume these values, the equation is called "universal" WLF equation. While this equation is not truly universal, it was developed from a large database for various polymers. When the equation is written in this form (Eq. II.58), it is clear that T_g serves as a corresponding state for viscoelastic behavior. Although, the WLF equation is sometimes applied over temperatures outside the recommended temperature range, including polymers below T_g [47].

I relied on the following transformation (holding also true for the shear loss modulus):

(Eq. II.60)
$$G'(T, \log f) = G'(T_0, log a_T + \log f).$$

In rheology, the sample viscosity η is usually measured. The horizontal shift factors obey the following rule [58]:

(Eq. II.61)
$$a_T = \frac{\eta(T)}{\eta(T_0)},$$

where $\eta(T)$ represents the viscosity of the sample at temperature T. For many polymer systems, the viscosity obeys to an empirical equation known as Vogel-Fulcher-Tamman law [58]:

(Eq. II.62)
$$\eta(T) = Be^{-\frac{T_A}{T-T_V}},$$

where B is the viscosity at $T\to\infty$, T_A is the activation temperature (linked to activation energy), T_V is Vogel temperature (making up the difference to Arrhenius's law). Introducing Eq. II.62 into Eq. II.61 and taking the logarithm of both members of the equation yields the WLF equation (Eq. II.58), where

(Eq. II.63)
$$C_1 = \frac{T_A}{T_R - T_V}\log e \text{ and } C_2 = T_R - T_V.$$

II. 5.4.5. Typical shear modulus dependence

Fig. II.15 illustrates the transitions which can be observed for polymers using DMA method [39, 48]:

a) The area of sub-T_g (or higher-order) transitions consists of β-transition (which corresponds to the side group movements), γ-transition (bond bending and stretching), δ-transition (local motions). These sub-T_g transitions are associated with the materials properties in the glassy state. The strength of these transitions is related to how strongly polymer responded to those processes.

b) The glass transition (or α-transition) zone, where large segments of the chain start moving. This region is characterized by the temperature of glass transition T_g or T_α. The T_g represents a major transition for many polymers, as physical properties change drastically as the material goes from a hard glassy to a rubbery state. Changes in the T_g are commonly used to monitor changes in the polymer.

c) The so called "rubbery plateau" is the area above the T_g and below the melt. The length of it as well as its viscosity is dependent on the molecular weight between entanglements or cross-links [49]. The modulus in the plateau region is often expressed as

$$G' = \frac{\rho RT}{M_c}, \qquad \text{(Eq. II.64)}$$

where ρ is the polymer density and M_c is the molecular weight between entanglements. This modulus provides the information about the changes in M_c or the number of cross-links compared to the initial sample.

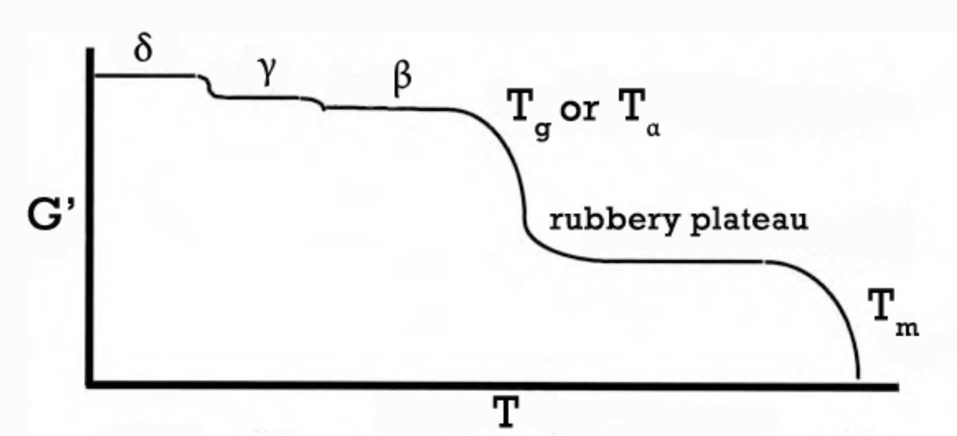

Figure II.15. Ideal case of the G' dependence upon temperature measured by DMA.

d) The terminal region is observed at the point where the free volume has increased so much that polymer chains are able to slide past each other and the material flows. This ability to flow is dependent on the molecular weight of the polymer. Degradation, polymer structure, and environmental effects all influence what changes occur. Polymers that degrade by cross-linking will look very different from those that exhibit chain scissoring. Very highly cross-linked polymers will not melt, as they are unable to flow.

References:

[1] F. Bueche In “Reinforcement of Elastomers”; G. Kraus, Ed.; Interscience: New York, 1965.

[2] Product Information Aeroxide AluC, Aerosil Degussa, März 2004

[3] Wetzel B, PhD Thesis: Mechanische Eigenschaften von Nanoverbundwerkstoffen aus Epoxydharz und keramischen Nanopartikeln, Universität Heidelberg, Germany, 2006.

[4] Baller J., Thomassey M., Ziehmer M., Sanctuary R. The catalytic influence of alumina nanoparticles on epoxy curing. *Thermochimica Acta,* 2011, 517, p.34–39

[5] Yang Y.-Ch., Jeong S.-B., Kim B.-G., Yoon P.-R. Examination of dispersive properties of alumina treated with silane coupling agents, by using inverse gas chromatography. *Powder Technology*, 2009, 191, p.117–121.

[6] Rong M.Z., Ji Q.L., Zhang M.Q., Friedrich K. Graft polymerization of vinyl monomers onto nanosized alumina particles, *European Polymer Journal*, 2002, 38, p.1573-1582.

[7] Ballav N., Biswas M. Preparation and evaluation of a nanocomposite of polythiophene with Al_2O_3. *Polymer International*, 2003, 52, p.179-184.

[8] E. Passaglia, F. Donati, Functionalization of a styrene/butadiene random copolymer by radical addition of L-cysteine derivatives. *Polymer,* 2007, 48, p.35-42.

[9] Passaglia E, Ghetti S, Picchioni F, Ruggeri G. Grafting of diethyl maleate and maleic anhydride onto styrene-b-(ethylene-co-1-butene)-b-styrene triblock copolymer (SEBS). *Polymer*, 2000, 41, p.4389-4400.

[10] J. Coates, Interpretation of Infrared Spectra, A Practical Approach. Encyclopedia of Analytical Chemistry. p. 10815–10837. Published by John Wiley & Sons Ltd, Chichester, 2000.

[11] Infrared and Raman Spectroscopy: Methods and Applications. Ed. B. Schrader. Published jointly by VCH Verlagsgesellschaft mbH, Weinheini (Federal Republic of Germany) and VCH Publishers. Inc., New York, NY (USA), 1995.

[12] M. E. Brown, Introduction to Thermal Analysis, Techniques and Applications. Published by Chapman and Hall Ltd, London, United Kingdom, 1988.

[13] P.J. Goodhew, J. Humpheys, R. Beanland, Electron Microscopy and Analysis, 3rd edition. Published by Taylor and Francis, London, United Kingdom, in 2001.

[14] L. Reimer, H. Kohl, Transmission Electron Microscopy. Physics of Image Formation. Springer Series in Optical Sciences, Vol. 36, 5th ed. 2008.

[15] H. Gobrecht, K. Hamann and G. Willers, Complex plane analysis of heat capacity of polymers in the glass transition region, *Journal of Physics E: Scientific Instruments*, 1971, 4, p.21.

[16] M.Reading, D.J Hourston, Modulated Temperature Differential Scanning Calorimetry. Theoretical and Practical Applications in Polymer Characterisation. Published by Springer, P.O. Box 17, 3300 AA Dordrecht, The Netherlands, 2006.

[17] P.S. Gill, M. Reading, I.M. Salin and J.C. Seferis, *Proceedings of the Greek Academy of Science*, 1992, 67, p.311.

[18] M. Reading, B.K. Hahn and B.S. Crowe, Method and Apparatus for Modulated Differential Analysis. 1993, US patent 5, 224, 775.

[19] M. Reading, Modulated Differential Scanning Calorimetry - A New Way Forward in Materials Characterization, *Trends in Polymer Science*, 1993, 1, p.248-253.

[20] M. Reading, D Elliott and V.L.Hill, A new approach to the calorimetric investigation of physical and chemical transitions, *Journal of Thermal Analysis and Calorimetry*, 1993, 40, p.949-955.

[21] P.S. Gill, S.R. Sauerbrunn and M. Reading, Modulated differential scanning calorimetry, *Journal of Thermal Analysis and Calorimetry*, 1993, 40, p.931-939.

[22] M. Reading, R. Wilson and H.M. Pollock, *Proceedings of the Twenty-third Conference of the North American Thermal Analysis Society*, 1994, 22, p.2.

[23] M. Reading, A. Luget and R. Wilson, Modulated differential scanning calorimetry, *Thermochimica Acta*, 1994, 238, p.295-307.

[24] J.E.K. Schawe, A comparison of different evaluation methods in modulated temperature DSC, *Thermochimica Acta*, 1995, 260, p.1-16.

[25] J.E.K. Schawe Principles for the interpretation of modulated temperature DSC measurements. Part 1. Glass transition, *Thermochimica Acta,* 1995, 261, p.183-194.

[26] J.E.K. Schawe, G.W.H. Höhne The analysis of temperature modulated DSC measurements by means of the linear response theory, *Thermochimica Acta,* 1996, 287, p.213-223.

[27] R. Sanctuary, J. Baller, J.K. Krüger, D. Schaefer, R. Bactavatchalou, B. Wetzel, W. Possart, P. Alnot, Complex specific heat capacity of two nanocomposite systems, *Thermochimica Acta*, 2006, 445 (2), p.111-115.

[28] J.M. Hutchinson, S. Montserrat The application of modulated differential scanning calorimetry to the glass transition of polymers. I. A single-parameter theoretical model and its predictions, *Thermochimica Acta*, 1996, 286 (2), p.263-296.

[29] Z. Jiang, C.T. Imrie, J.M. Hutchinson Temperature modulated differential scanning calorimetry. Part I: Effects of heat transfer on the phase angle in dynamic ADSC in the glass transition region, *Thermochimica Acta*, 1998, 315, p. 1-9.

[30] J.M. Hutchinson, Characterising the glass transition and relaxation kinetics by conventional and temperature-modulated differential scanning calorimetry, *Thermochimica Acta*, 1998, 324, p.165-174.

[31] N.O. Birge, S.R. Nagel, Specific-heat spectroscopy of the glass transition, *Physical Review Letters*, 1985, 54 (25), p.2674.

[32] J.K. Nielsen, J.C. Dyre Fluctuation-dissipation theorem for frequency-dependent specific heat, *Physical Review. B. Condensed Matter*, 1996, 54 (22), p.15754-15761.

[33] M. Beiner, J. Korus, H. Lockwenz, K. Schroter, E. Donth, Heat-capacity spectroscopy compared to other linear-response methods at the dynamic glass transition in poly(vinyl acetate) *Macromolecules*, 1996, 29, p.5183-5189.

[34] E. Donth et al., Fine structure of the main transition in amorphous polymers – entanglement spacing and characteristic length of the glass transition – discussion of examples, *Macromolecules*, 1996, 29 (20), p.6589-6600.

[35] J. Jäckle, Heat conduction and relaxation in liquids of high viscosity, *Physica A*, 1990, 162, p.377–404.

[36] W. Gotze, A. Latz, Generalised constitutive equations for glassy systems, *Journal of Physics: Condensed Matter*, 1989, 1, p.4169.

[37] S. L. Simon and G.B. McKenna, Interpretation of Dynamic Heat Capacity in Glass-Forming Liquids, *Journal of Chemical Physics*, 1997, 107 (20), p.8678 - 8685.

[38] S.L. Simon temperature-modulated differential scanning calorimetry: theory and application, *Thermochimica Acta*, 2001, 374, p.55-71.

[39] K.P. Menard Dynamic Mechanical Analysis. A Practical Introduction. Published by CRC Press LLC, US.

[40] A. L. Kimball and D. E. Lovell. Internal friction in solids. *Transactions of ASME*, 1926, 48, p.479-500.

[41] K. te Nijenhuis, Rheology, V.1. Principles, G. Astarita et al., Eds., Plenum Press, New York, 263, 1980.

[42] M.L. Miller, The Structure of Polymers, Reinhold, New York, 1966.

[43] J. Ferry, Viscoelastic Properties of Polymers, 3rd ed., Wiley, New York, 1980.

[44] J. Gilham and J. Enns, Trends in Polymer Science, 2, 406, 1994.

[45] T. Murayama, Dynamic Mechanical Analysis of Polymeric Materials, Elsevier, New York, 1977.

[46] B. E. Read and G. D. Brown, The Determination of the Dynamic Properties of Polymers and Composites, Wiley, New York, 1978.

[47] J.D. Menczel and R. Bruce Prime, Thermal Analysis of Polymers. Fundamentals and Applications. Published by John Wiley & Sons, Inc., NJ, US, 2009.

[48] N. McCrum, G. Williams and B. Read, Anelastic and Dielectric Effects in Polymeric Solids, Dover, New York, 1967.

[49] C. W. Macosko, Rheology: principles, measurements and applications, VCH Publishers Inc., Minneapolis, 1994.

[50] A.V. Tobolsky, Properties and Structure of Polymers, John Wiley Intersciences, New York, (1960).

[51] L.E. Nielson, Mechanical Properties of Polymers, Reinhold, New York, (1962).

[52] M.L. Williams, R.F. Landel, and J.D. Ferry, The Temperature Dependence of Relaxation Mechanisms in Amorphous Polymers and Other Glass-forming Liquids, *Journal of American Chemical Society*, 1955, 77 (14), p.3701-3707.

[53] Ferry J. D., Viscoelastic Properties of Polymers, 3rd ed., 1980, Wiley, New York .

[54] A. Y, Goldman, Prediction of the Deformation Properties of Polymeric and Composite Materials, ACS, Washington, D.C., 1994.

[55] R. Tanner, Engineering Rheology, Oxford Science Publishers, Oxford, 1985, 352–353.

[56] J.J. Aklonis and W.J. MacKnight, Introduction to Polymer Viscoelasticity, 2nd ed., Wiley-Science Publication, New York. (1983).

[57] U.W. Gedde, Polymer Physics, Kluwer Academic Publishers, Dordrecht, Netherlands, 1999.

[58] G.R. Strobl, The Physics of Polymers, Concepts for Understanding Their Structures and Behavior, 3rd ed. 2007, XIV, 518, 295p.

Chapter III: Characterization of the nanocomposites

This chapter deals with investigations carried out on neat SBR and three series of SBR/AluC nanocomposites. TGA, electron microscopy, FT-IR, TMDSC and DMA/rheometry were used as experimental tools.

III.1. *Concentration of alumina nanoparticles*

Thermogravimetry (TGA) was used to accurately determine the filler concentration of the final SBR/Alu C nanocomposites.

SBR is an organic copolymer which shows initial decomposition at 330°C and the final decomposition at 500°C [1], [Annex I]. Alumina nanoparticles are stable at these temperatures and remain unchanged after thermal treatment of the sample. Thanks to this fact it is possible to determine the nanoparticles concentration in the sample.

The measurements were performed under atmospheric pressure in the temperature range extending from 25 to 500°C, with a heating rate of 5°C/min, in the air atmosphere.

Table III.1 illustrates the results of the degradation experiments.

Table III.1. Experimental filler concentration for SBR/Alu C and SBR/Alu C-modified nanocomposites. The absolute measurement error is within 5%.

Sample	W_{filler} (experimental), %		Sample	W_{filler} (experimental), %
SBR+1% Alu C	1.08		SBR+1% Alu C-Mercapto	1.3
SBR+1.5% Alu C	1.62		SBR+1.5% Alu C-Mercapto	1.58
SBR+2% Alu C	2.5		SBR+2% Alu C-Mercapto	1.87
SBR+3% Alu C	3.2		SBR+3% Alu C-Mercapto	2.83
SBR+4% Alu C	4.3		SBR+4% Alu C-Mercapto	3.68
SBR+10% Alu C	10.7		SBR+10% Alu C-Mercapto	9.9
SBR+20% Alu C	17		SBR+20% Alu C-Mercapto	19.55
SBR+30% Alu C	28.7		SBR+30% Alu C-Mercapto	27.4

Sample	W_{filler} (experimental), %
SBR+1% Alu C-Mercapto grafted	0.88
SBR+1.5% Alu C-Mercapto grafted	1.48
SBR+2% Alu C-Mercapto grafted	2.9
SBR+3% Alu C-Mercapto grafted	3.2
SBR+4% Alu C-Mercapto grafted	3.73
SBR+10% Alu C-Mercapto grafted	12.6
SBR+20% Alu C-Mercapto grafted	20.23
SBR+30% Alu C-Mercapto grafted	30.4

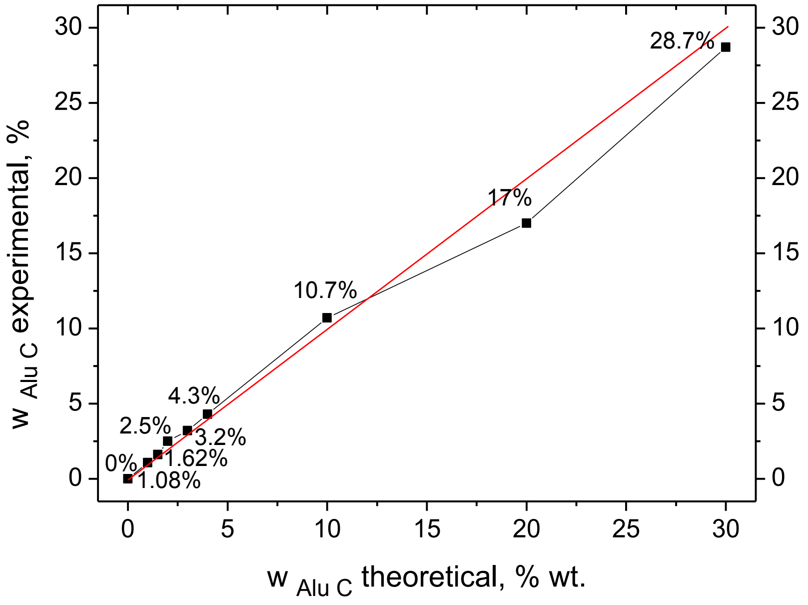

Figure III.1. Alu C concentrations obtained from TGA versus the expected Alu C concentrations in SBR/Alu C nanocomposites. The red line illustates the "perfect" case, when theoretical and experimental concentrations coincide.

From the results presented in Table III.1 it becomes clear that the experimentally obtained filler concentrations correspond to the expected concentrations within the limits of experimental accuracy.

Fig. III.1 shows the Alu C concentrations obtained from experiment versus the expected concentrations for the investigated SBR/AluC nanocomposites.

III.2. Dispersion of alumina nanoparticles in SBR/Alu C nanocomposites

The morphology, i.e. the dispersion state of fillers is known to strongly affect the mechanical behavior of nanocomposites [2]. Thus information on the distribution of the alumina inside the SBR matrix and on structure formation is needed to improve the understanding of filler-induced properties of the nanocomposites. Cross-section samples were cut using a microtome. The cross-sectioned areas were examined by transmission electron microscopy (TEM). The TEM (JEOL JEM 2011-HRTEM at Saarland University) was operated at an acceleration voltage of 1000 kV. Fig. III.2 shows TEM pictures of SBR filled with 1, 2, 4 and 10% of alumina nanoparticles at four different magnifications.

We observe aggregates and agglomerates (clusters of aggregates) of nanoparticles with heterogeneous morphology. This observation is in line with results reported by [2] for SBR/SiO_2 nanocomposites (SBR with 25% of styrene; highly structured silica nanoparticles). The highest magnification of the 1% sample depicts the chemical aggregation of the quasi-spherical primary particles (13 nm) to fractal nanoparticles (up to 200 nm in diameter). It has been shown that these aggregates cannot be broken even by high shear forces [3]. Prior investigations [4] have shown that the agglomerates can easily be broken by applying shear forces, e. g. in Alu C/epoxy resin nanocomposites. Therefore we assume that the agglomerates are held together by weak Van der Waals forces.

The images shown in Fig. III.2 suggest that with increasing filler content the number of agglomerates grows. This observation is in line with the results obtained by Mélé et al. [2]. In contrast to the findings of Mélé et al. the size of the agglomerates in our nanocomposites increases with the alumina concentration. Mélé et al. associate the break-down of the silica clusters to the mixing process. The authors argue that with increasing silica content collisions between agglomerates occur more frequently.

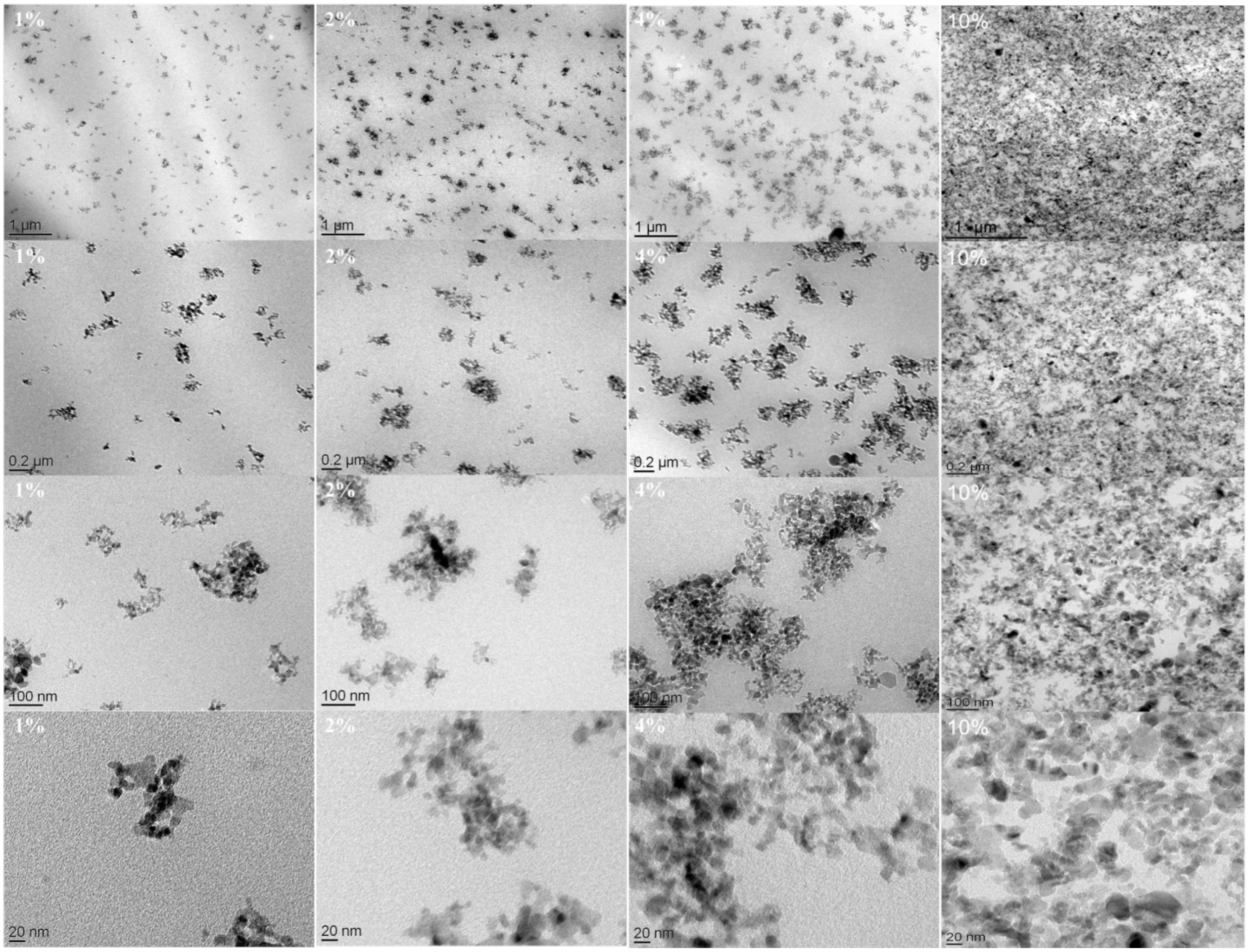

Figure III.2. TEM micrographs of the SBR/Alu C nanocomposites containing (from left to right) 1%. 2%, 4% and 10% alumina nanoparticles. Magnifications (from top to bottom): 1µm, 0.2µm, 100nm, 20nm.

The different results could of course be explained by different preparation procedures of the nanocomposites. We however believe that the main reason for the discrepancy lies in the difference between the matrices used by Mélé et al. and ourselves: SBR used in the work of Mélé et al. was extended with 37.5 parts per hundred rubber of oil; furthermore their compounds contained ingredients such as ZnO and vulcanizing agents.

The microscopic investigation for silanized and grafted nanocomposites are presented in Annex II. The ESEM pictures of these samples show rather homogeneous filler dispersion and also increase in the number of agglomerates with increasing filler concentration.

III.3. FT-IR analysis

FT-IR analysis (Perkin-Elmer Spectrum BX instrument) has been used in order to confirm the silanization of the Alu C nanoparticles. Samples for FTIR spectroscopy were prepared: a) by mixing KBr powder with the nanoparticles in a pestle and by grinding them into a uniform powder, then the sample pellets were prepared by pressing the powder into a disk; b) for the SBR pure and nanocomposite samples films were prepared by solvent casting method. The scanning was performed in the wavenumber range from 4000 to 400 cm^{-1}.

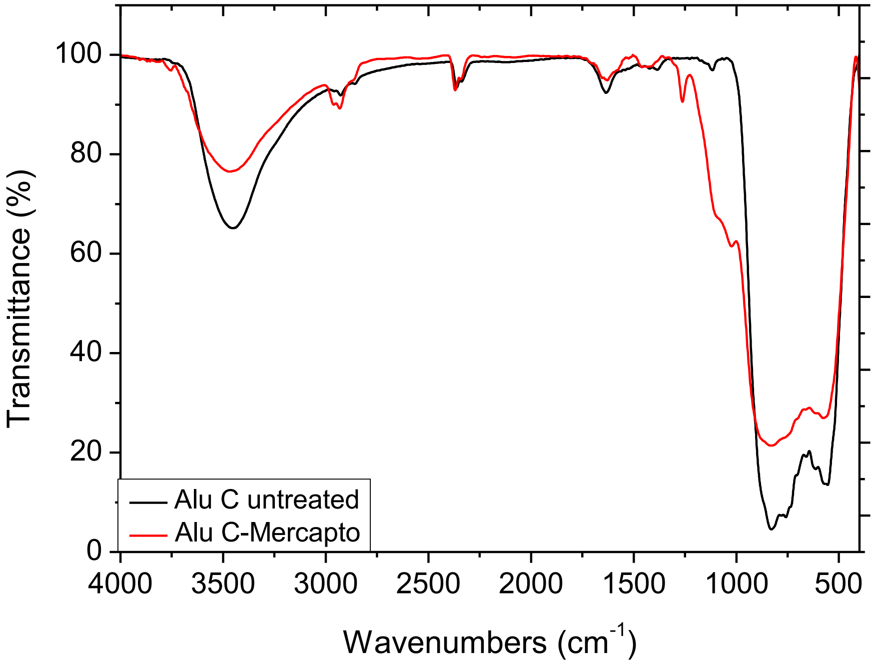

Figure III.3. FTIR spectra of Alu C and Alu C treated with γ-mercaptopropyltrimethoxysilane.

FTIR spectra realized on modified Alu C nanoparticles show characteristic peaks of functional groups of silanes (Fig.III.3). The common peaks on all of the spectra of modified nanoparticles are:

i. 566 cm^{-1} corresponds to stretching vibration of Al-O in octahedral coordination [5].
ii. 756 cm^{-1} corresponds to Al-O-Al stretching vibration in tetrahedral and octahedral coordination [5].
iii. 828 cm^{-1} corresponds to stretching vibration of Al-O in tetrahedral coordination [5].
iv. 1040-1020 cm^{-1} corresponds to the stretching vibration of the C-C bond.
v. 1099 cm^{-1} broad peak corresponds to asymmetrical Si-O stretch (from Si-O-H, Si-O-Al and Si-O-Si) [6].
vi. 1462 cm^{-1} corresponds to asymmetrical deformation of CH_3 and scissoring deformation of CH_2.
vii. 1636 cm^{-1} corresponds to O-H group bending vibrations.
viii. 2350-2300 cm^{-1} corresponds to the CO_2 vibrations (air).

ix. 2844 cm^{-1} and 2926 cm^{-1} correspond to symmetrical and asymmetrical stretching of CH_3 and CH_2.

x. 3451 cm^{-1} corresponds to O-H group stretching vibration (surface hydroxyl groups of the Alu C nanoparticles and hydroxyl groups of absorbed water molecules).

In case of Alu C modified with γ-mercaptopropyltrimethoxysilane, unfortunately, we do not observe any S-H peak at 2620-2550 cm^{-1}. Perhaps, because S-H group stretching vibration peak is usually weak, it is due to the limited resolution of the instrument. The peak of the C-S bond which has to appear at 710-570cm^{-1} is probably hidden behind broad peaks of the Al-O stretching vibrations. The presence of the C-C and C-H peaks in this case can be accepted as a proof of silanization.

FT-IR spectra of the nanocomposites can be found in Annex III.

III.4. Investigations of the neat SBR

III.4.1. Results from TMDSC

TMDSC measurements were performed in helium atmosphere in the temperature range from 193 to 298 K with a heating rate of +1 K/min, temperature modulation amplitude of 0.5 K and a modulation period of two minutes. The real and imaginary parts of the specific heat capacity were evaluated using standard methods [7]. Fig. III.4 shows the evolution of c_p' and c_p'' as a function of temperature. SBR undergoes a glass transition which, upon heating, manifests itself by a step-like increase of the storage specific heat capacity and the emergence of a loss peak (culminating in the maximum of the imaginary part c_p'').

Several parameters can be used to characterize the glass transition:

- the relaxator strength Δc_p,
- the *FWHM* (full width at half maximum) of the loss peak,
- the loss peak area A_{peak},
- the loss peak height h_{peak} and
- the glass transition temperature T_g.

Δc_p is a measure for the number of configurational degrees of freedom freezing during the glass transition. *FWHM* characterizes the width of the distribution of relaxators involved in the structural α-process. A_{peak} yields information on the number of relaxators per gram SBR which take part in the relaxation process. Finally, the height h_{peak} of the loss peak can be considered as a measure of the number of relaxators with a relaxation time $\tau = \omega^{-1}$ (ω: angular frequency of the temperature modulation).

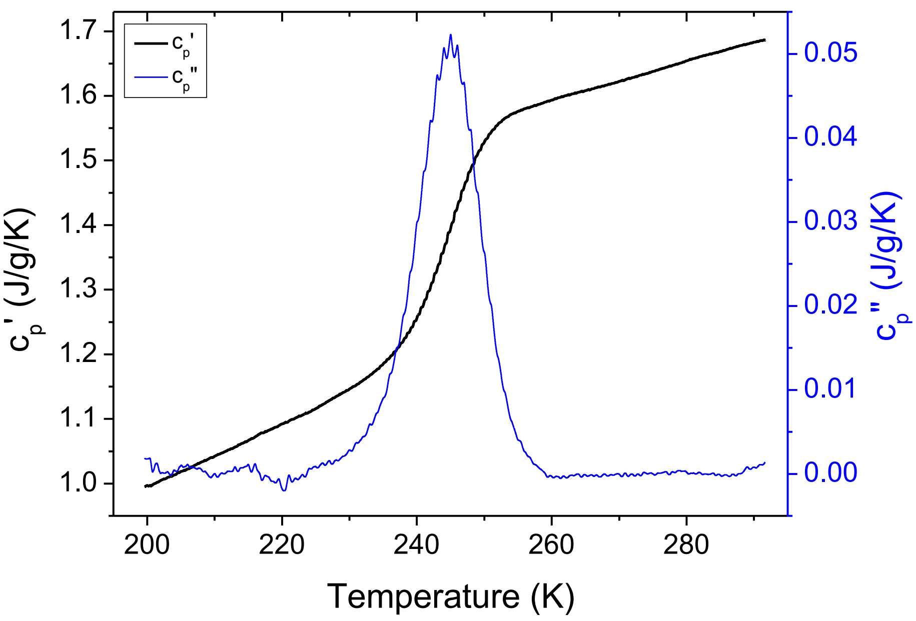

Figure III.4. Real (c_p') and imaginary (c_p") part of the complex specific heat capacity (c_p) of neat SBR. The specific heat capacity has been measured upon heating by TMDSC in helium atmosphere in the temperature range from 193 to 298 K with a heating rate of +1 K/min, temperature modulation amplitude of 0.5 K and a modulation period of two minutes.*

In Fig. III.5 *a* and *b* we illustrate how the various parameters have been determined. The glass transition temperature T_g has been determined as a maximum of the first derivative of the *cp'*. The relaxator strength Δc_p has been determined by ASTM method.

Table III.2 shows TMDSC parameters for neat SBR.

Table III.2. TMDSC parameters determined for neat styrene-butadiene rubber.

T_g, K	Δc_p, J/(g·K)	A_{peak}	h_{peak}	FWHM
244.68	0.3089	0.93	0.082	10.66

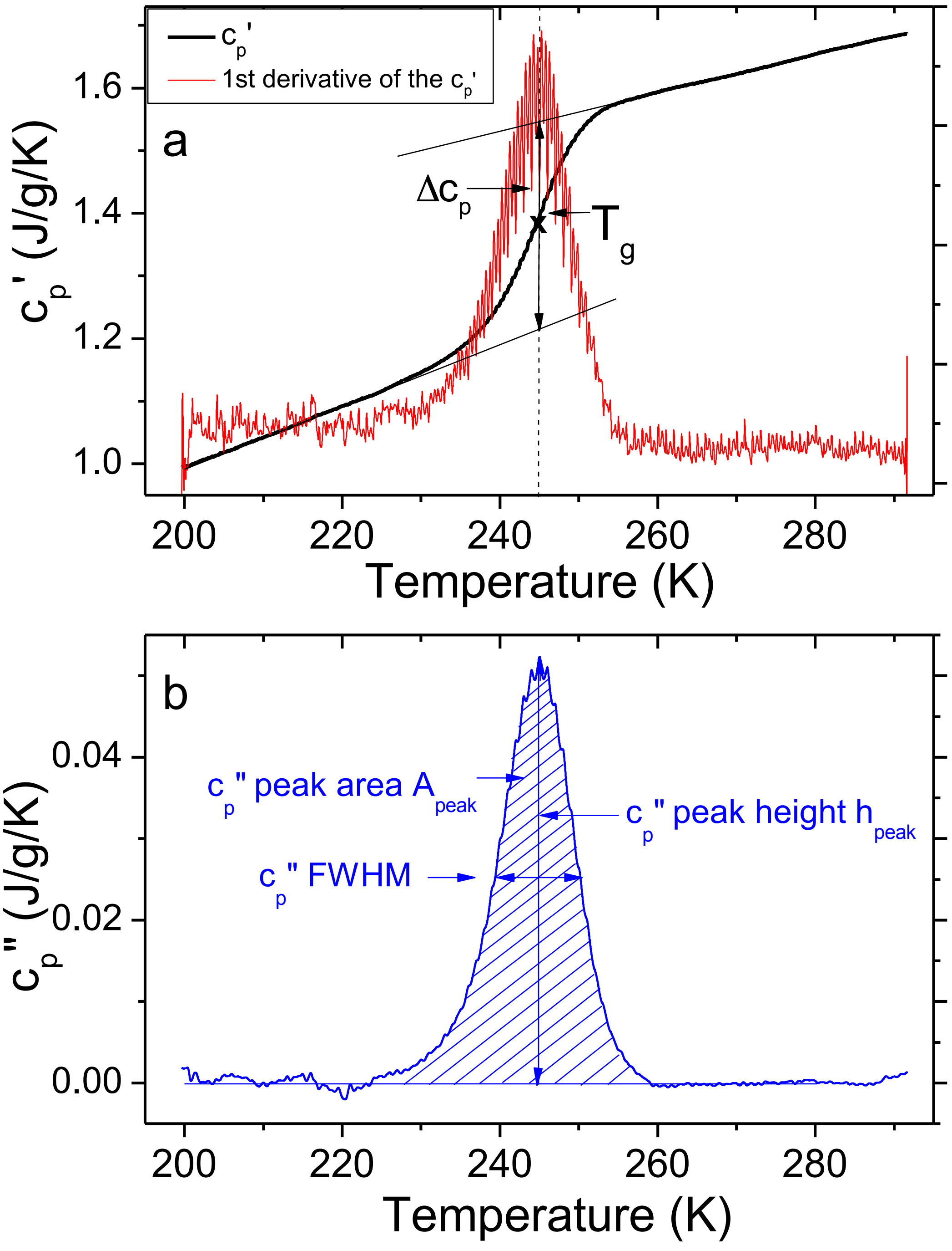

Figure III.5. Schematical illustration on how to determine TMDSC parameters: a) T_g and Δc_p from c_p'; b) A_{peak}, h_{peak} and FWHM from c_p''.

III.4.2. DMA investigations

In this work, all of the DMA measurements were performed in a linear response regime. The results of linearity tests you can find in Annex IV. The force of 1N and the displacement of 5μm were selected as parameters for further experiments.

Fig. III.6 shows master curves of the storage modulus *G'* and the loss modulus *G"* of neat SBR at the reference temperature T_0=273 K.

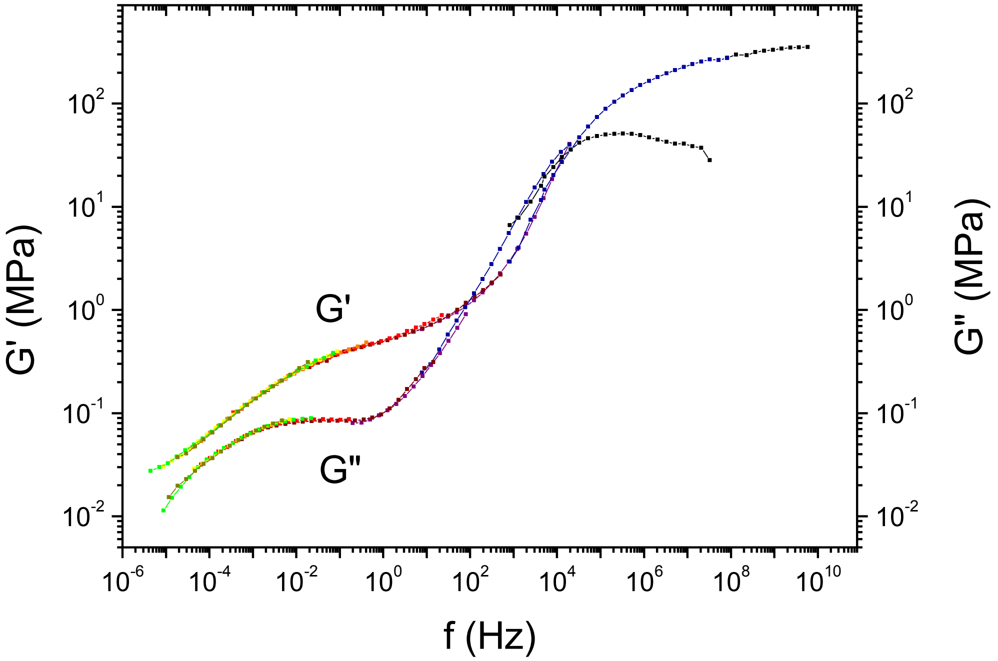

Figure III.6.DMA master curves of the real (G') and imaginary (G") parts of the complex shear modulus G for neat SBR.*

Four different regions which are characteristic for the viscoelastic behavior of a rubber-like material can be distinguished:

1) the glassy region in the high frequency range where the polymer molecules are dynamically frozen;

2) the transition zone between rubber and glass where the mechanic properties are dominated by the structural relaxation processes connected to the dynamic freezing;

3) the rubbery plateau where the slope of the master curve is reduced due to physical cross-links by entanglement of SBR molecules;

4) the "terminal flow range" at low frequencies.

Only in the transition zone 2) the loss modulus of SBR is larger than the storage modulus. In all the other regions the behavior of neat SBR is rather solid-like (*G'>G"*). Obviously, at very low frequencies where one would expect terminal flow in an ideal liquid polymer, the storage and loss shear moduli do not obey to the expected power-law behaviors $G' \propto f^2$ and $G" \propto f$. We rather find, at f<10^{-3} Hz

$$G' \propto f^{0.32}$$
$$G" \propto f^{0.29}$$

From the fact that *G'>G* (unusual for polymer liquids) and $\tan\delta = \frac{G"}{G'} \approx c^{te}$ we conclude that in the low-frequency range SBR behaves like a physical gel [8-9]. Physical interactions between the SBR molecules prevent ideal flow at very low frequencies.

The horizontal shift factors a_T used for the construction of the master curve are depicted in Fig. III.7 and show the classical dependence. No vertical shift was necessary ($b_T = 1$).

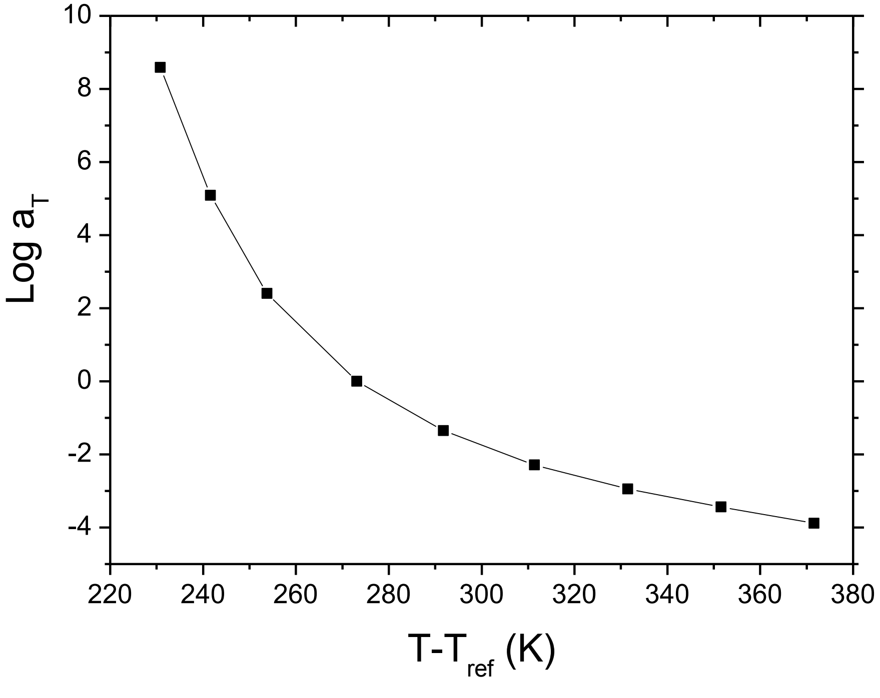

Figure III.7. Shift factors log a_T as a function of temperature for neat SBR. Solid line is just a guide for the eyes.

The similar behaviour presents rheological investigation (Fig. III.8). In the Annex IV you can find the comparison of the *G'* and *G"* master curves obtained using these two methods.

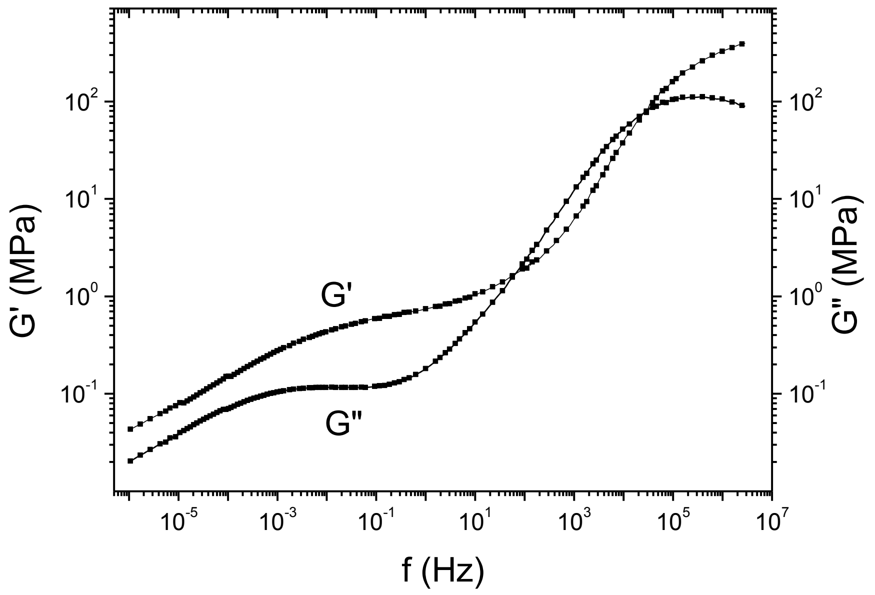

Figure III.8.Rheology master curves of the real (G') and imaginary (G") parts of the complex shear modulus G for neat SBR.*

Fig. III.9. shows the dependence of *tan δ* on the frequency *f.*

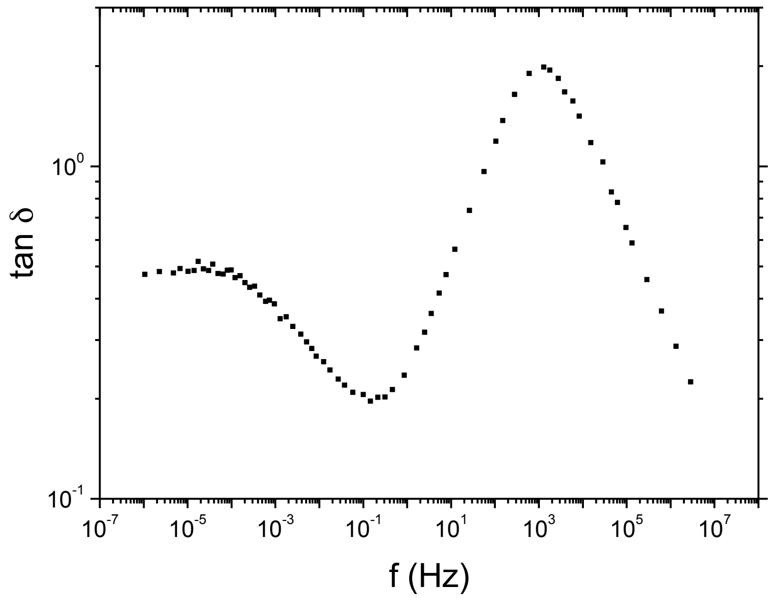

Figure III.9. Rheology master curve of the loss factor tg δ for neat SBR.

The literature research showed that SBR containing 45% styrene is not well studied: the most popular investigated systems are so called "SBR 1502" (which contains 23.5% styrene), "Duradene 715" (23.5% styrene) and "Buna VSL 5025-2 HM"(25% styrene) [10-18]. Due to that, we are unable to compare our experimental values (e.g. shear moduli, glass transition temperature) with the values found in literature. But it is well known that the ratio of styrene to butadiene controls the relative T_g of the SBR: the higher the styrene content, the stiffer is the copolymer resulting in a higher T_g [19].

III.5. Investigations of the SBR/Alu C nanocomposites

III.5.1. TMDSC investigations

Figure III.21 illustrates how the specific storage heat capacity c_p' of the investigated SBR – x wt% Al_2O_3 (x = 0; 1; 1.5; 2; 3; 4; 10; 20; 30) varies as a function of temperature. The dashed line in Fig. III.21 represents the c_p' evolution as a function of temperature of neat Alu C (an Alu C pellet has been prepared from powder using the laboratory press). The TMDSC experiments reveal that all of the nanocomposites undergo a single glass transition in the temperature 210-290 K. This means that up to a filler concentration of 30 wt% our experiments do not yield any evidence for the existence of interphases manifesting themselves by an additional glass transition (unless it is hidden by the one of the matrix). Such interphases could emerge at the filler' surfaces as layers formed by immobilized SBR molecules or matrix molecules with strongly reduced mobility [20-21]. However the formation of such layers would request strong interactions between the matrix molecules and the nanoparticles. The occurrence of such interactions is unlikely if we take into account the polar character of the alumina and non-polar character of the SBR molecules.

In nanocomposites three phases can envisaged to contribute to the specific heat capacity [22]: the polymer matrix ($c^*_p{}^{polymer}$), the fillers ($c^*_p{}^{filler}$) and a possible interphase emerging between both phases. The specific heat capacities of the neat polymer (SBR) and the fillers (Alu C) are known. Assuming the validity of a simple mixing rule for the real parts of the specific heat capacities of the nanocomposites, we can evaluate the real part of the heat capacity per gram matrix:

(Eq. III.1)
$$c_p'^{SBR} = \frac{|c_p^*|\cos\varphi - x c_p^{Alu\ C}}{(1-x)} = \frac{c_p' - x c_p^{Alu\ C}}{(1-x)} .$$

The imaginary part cp" of the specific heat capacity is only related to the relaxation process of the polymer molecules during the glass transition; thus the contribution of the filler particles to cp" is zero, and the imaginary part of the specific heat capacity of the polymer component can be calculated using the following equation:

(Eq. III.2)
$$c_p''^{SBR} = \frac{|c_p^*|\sin\varphi}{(1-x)} = \frac{c_p''}{(1-x)} .$$

The calculation of $c_p{}'^{\,SBR}$ and $c_p{}''^{\,SBR}$ using a simple mixing rule is useful: in case of all of the $c_p{}'^{\,SBR}$ and $c_p{}''^{\,SBR}$ values obtained for the various nanocomposites coinciding, we can conclude that the fillers do not have any influence on the dynamic behavior of the matrix molecules. In such a case the matrix molecules behave identically to those of unfilled SBR. Thus, deviations from the results provided by the mixing rule allow us to highlight the existence of an influence of the nanoparticles on the matrix.

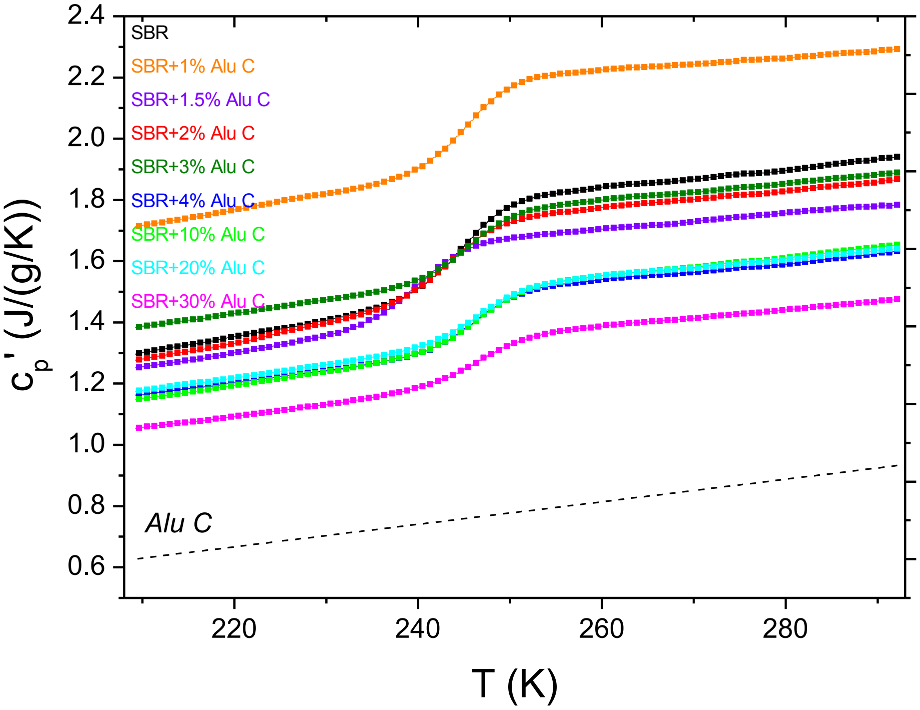

Figure III.21. Temperature dependence of the specific storage heat capacity c_p' for SBR-x wt% AluC nanocomposites. Measurements were realized upon cooling (cooling rate:-0.5K/min). Temperature modulation: amplitude 0.5K, period 2min.

Fig. III.22 and III.23 correspondingly show the evolutions of $c_p{}^{'\,SBR}$ and $c_p{}^{''\,SBR}$ as a function of temperature for the SBR/Alu C nanocomposites.

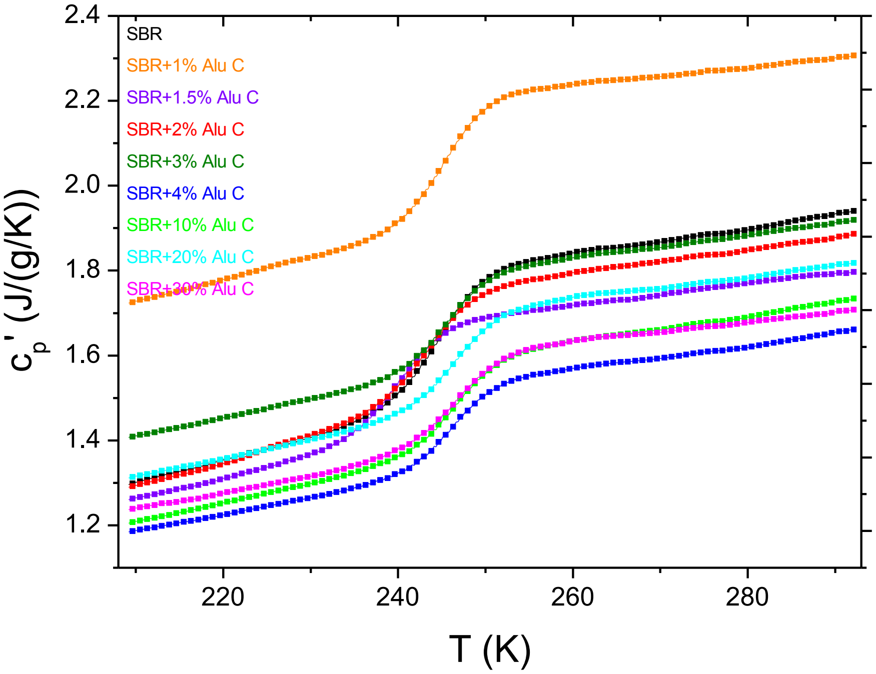

Figure III.22. Real part $c_p{}'^{SBR}$ of the complex heat capacity c_p for SBR/Alu C nanocomposites.*

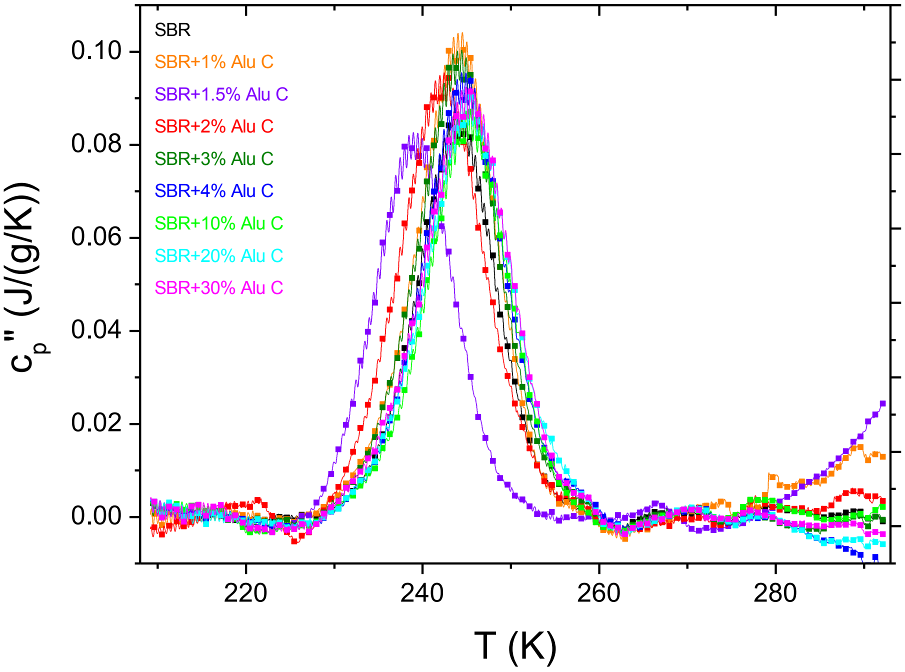

Figure III.23. Imaginary part $c_p{}''^{SBR}$ of the complex heat capacity c_p for SBR/Alu C nanocomposites.*

Obviously in Fig. III.23 it is impossible to observe a general trend for the absolute values of $c_p{}'^{SBR}$ when the filler concentration is changed. The data scatter is a well-known problem emerging when DSC or TMDSC experiments are carried out (e.g. accuracy is limited by hardly reproducible boundary conditions for heat conduction upon changing from one sample to another).

To be able to better judge the influence of the fillers on the thermal behaviour of the investigated nanocomposites we follow Sargsysan et al. [23]: the authors assume that in the glassy state, the specific heat capacities of SBR and potential interphases are similar and that, consequently, the $c_p{}'^{SBR}(T)$ curve of the various nanocomposites can be aligned to the one of neat SBR.

Fig. III.24 shows the $c_p{}'^{SBRcorr}(T)$ curves for the various investigated systems. The symbol $c_p{}'^{SBRcorr}$ is used to make clear that the curves represent specific heat capacity data which have been corrected to the nanocomposite's SBR fraction, and which in addition have been adjusted in such a way that they coincide with the specific storage heat capacity of the SBR matrix in the glassy state (at the lowest temperature achieved in the measurements).

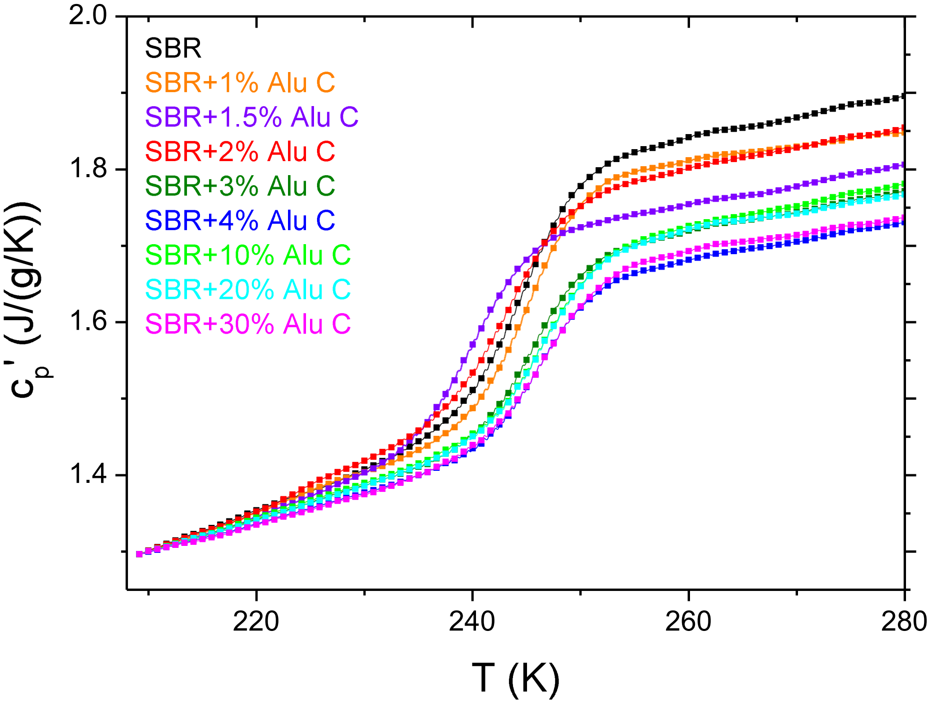

Figure III.24. $c_p{}'^{SBRcorr}(T)$ dependence for SBR/Alu C nanocomposites. The curves are shifted to the $c_p{}'$ of the neat SBR value below the glass transition.

The most prominent feature observed in Fig. III.23 and III.24 regards the complex dependence of the glass transition temperature T_g on the filler concentration. While at high Alu C loadings T_g seems to slightly shift to larger values (compared to the glass transition temperature of neat SBR), it clearly exhibits a minimum at $w_{Alu\ C} \approx 1.5\text{-}2\%$. Fig.III.25 illustrates how the glass transition temperature evolves as a function of the filler content. The transition temperature has been determined as explained in chapter III.4.1.

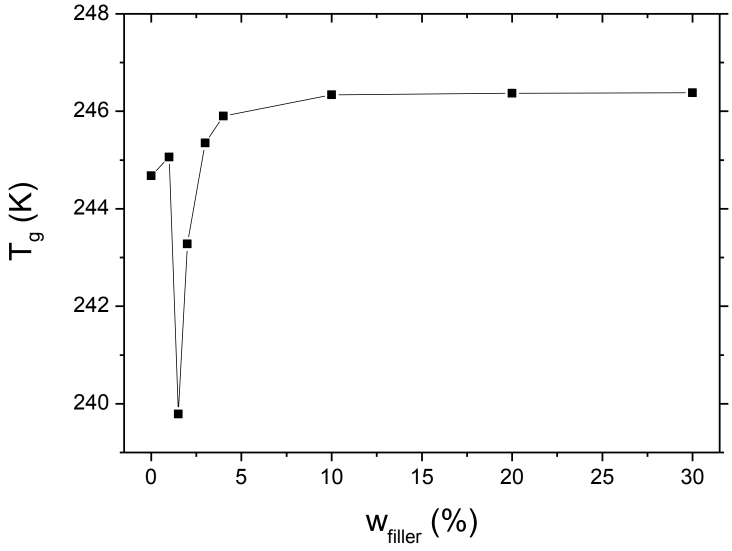

Figure III.25. Glass transition temperature T_g dependence upon filler (Alu C) concentration.

While the slopes of the $c_p'^{\,SBRcorr}(T)$ curves of the investigated systems fairly coincide in the rubbery phase, in the glassy regime they only superimpose at the lowest temperatures (Fig III.24). Interestingly at low temperatures, in the glassy state, the slopes of the the $c_p'^{\,SBRcorr}(T)$ curves depend on the filler concentration. More precisely, at concentrations $w_{filler} \geq 10\%$, the increase of the specific storage per Kelvin is practically independent of the filler concentration and lower than the slopes of the $c_p'^{\,SBRcorr}(T)$ curves at low Alu C contents. Knowledge of the variation of the inner energy U of a system with temperature is essential to quantitatively evaluate the temperature dependence of the specific heat capacity and thus to get information on the slope of a $c_p(T)$ curve. However, for complete evaluation of U one needs to know the distribution of the molecules over the different energy levels, something that is rarely available [24]. Moreover, Fig.III.24 suggests that the step height $\Delta c_p'^{\,SBRcorr}$ depends on the filler concentration. In Fig. III.26, *a* and *b* we have represented $\Delta c_p'^{\,SBRcorr}$ and the loss peak height h^{SBR} respectively as a function of the Alu C concentration (for the evaluations see chapter III.4.1). While h^{SBR} is practically independent of the filler content, $\Delta c_p'^{\,SBRcorr}$ exhibits an interesting behavior: at low concentrations ($0 \leq w_{filler} \leq 4\%$), the step height decreases upon increasing w_{filler}; however, at higher alumina contents ($w_{filler} > 4\%$), $\Delta c_p'^{\,SBRcorr}$ is nearly constant. It is well known that for an ideal Debye relaxation process the loss peak height and the step height of the storage modulus rigorously obey to [25]

(Eq. III.3) $$h^{Debye} = \frac{\Delta c_p^{Debye}}{2}.$$

To test whether the investigated systems respect Debye-like behaviour we compare in Fig. III.26a the concentration dependence of the double loss peak height $2h^{SBR}$ to the relaxator strength $\Delta c_p{}^{'\,SBRcorr}$. Obviously, in the concentration interval $0 \leq w_{filler} \leq 4\%$, $2h^{SBR}$ does not reflect the evolution of $c_p{}^{'\,SBRcorr}$ as a function of filler content. In contrast, for $w_{filler} > 4\%$, the double loss peak height fairly mimics the behavior of the relaxator strength (although, as for many other systems different from SBR, the values of both quantities are not equal). Why at low Alu C concentrations $w_{filler} \leq 4\%$, the relaxator strength decreases while the loss peak height remains constant is an interesting but still open question. Currently we hypothesise that the decrease of $\Delta c_p{}^{'\,SBRcorr}$ with increasing filler concentration is related to the slope changes of the $c_p{}^{'\,SBRcorr}*(T)$ curves in the glassy regime.

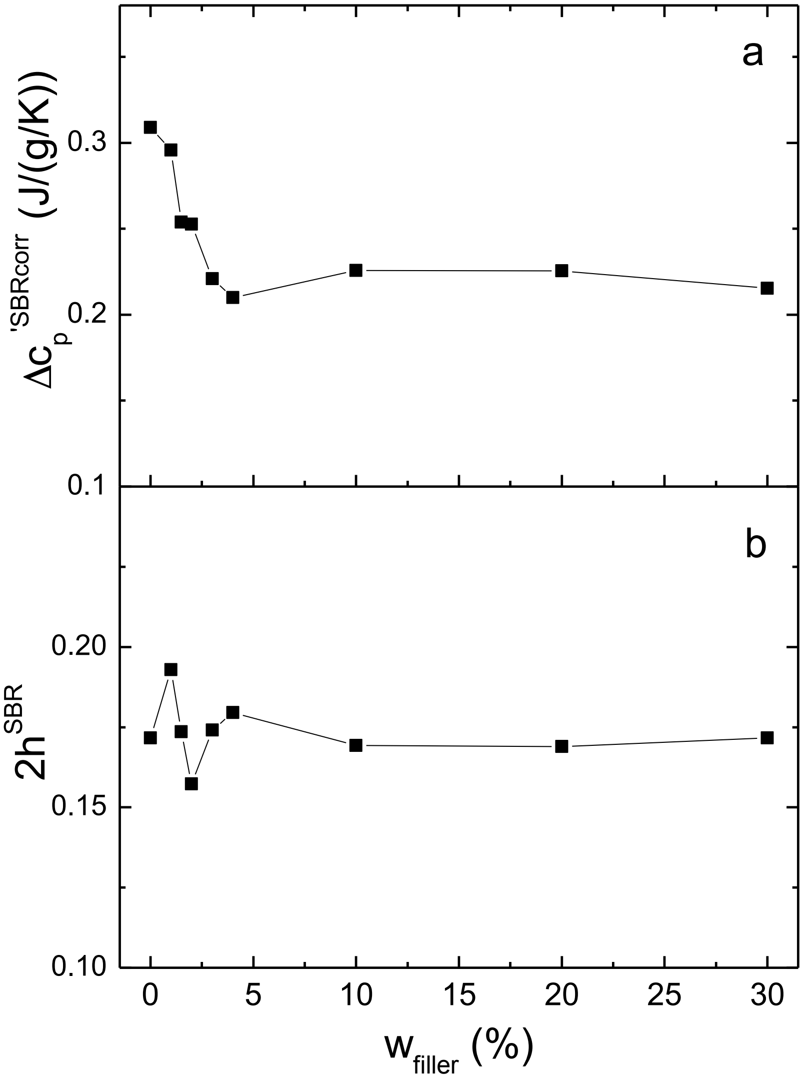

Figure III.26. $\Delta c_p{}^{'\,SBRcorr}$ and the double loss peak height $2h^{SBR}$ as a function of the filler content.The solid line is just a guide for the eyes.

III.5.2. DMA and rheology investigations

Figures III.27 and III.28 show master curves of the storage modulus *G'(f)* and loss modulus *G"(f)* at the reference temperature T_0=273K for composites with different concentrations of untreated alumina nanoparticles. The horizontal shift factors $log\ a_T(T)$ used for the construction of the master curves of the investigated samples are shown in Figure III.29. No vertical shift was necessary (b_T=1). It has to be mentioned that the shape of the $log\ a_T$ curves does not vary much with the nanoparticle content, which means that the temperature dependences of the intrinsic relaxation processes are qualitatively the same for all nanoparticle concentrations.

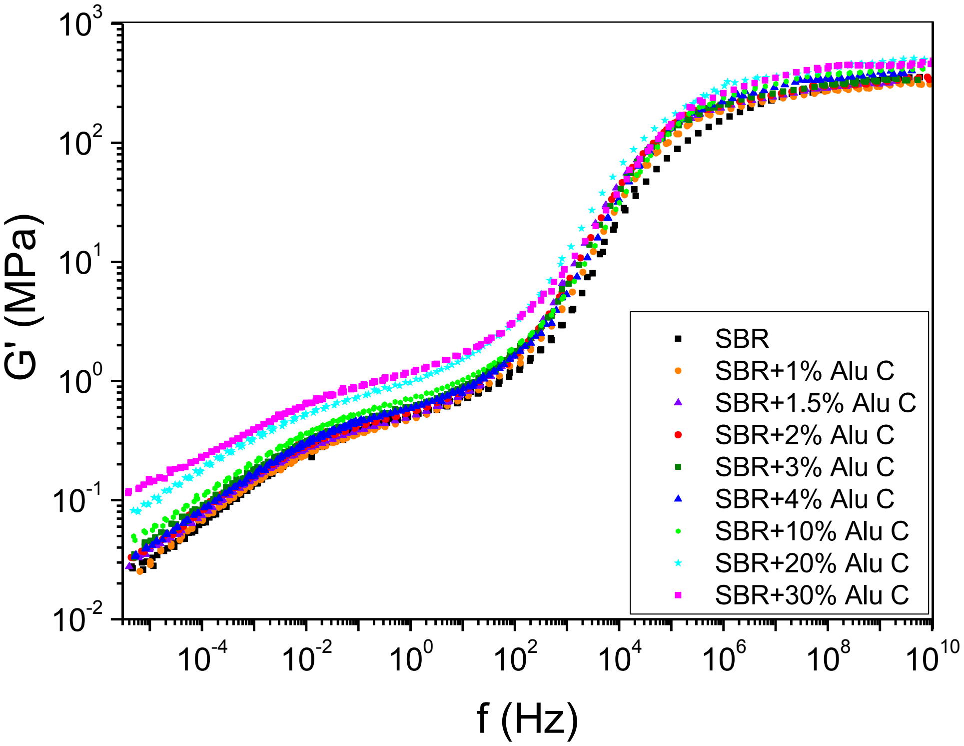

Figure III.27. DMA master curves of the real (G') part of the complex shear modulus G for neat SBR/Alu C nanocomposites. Reference temperature 273K.*

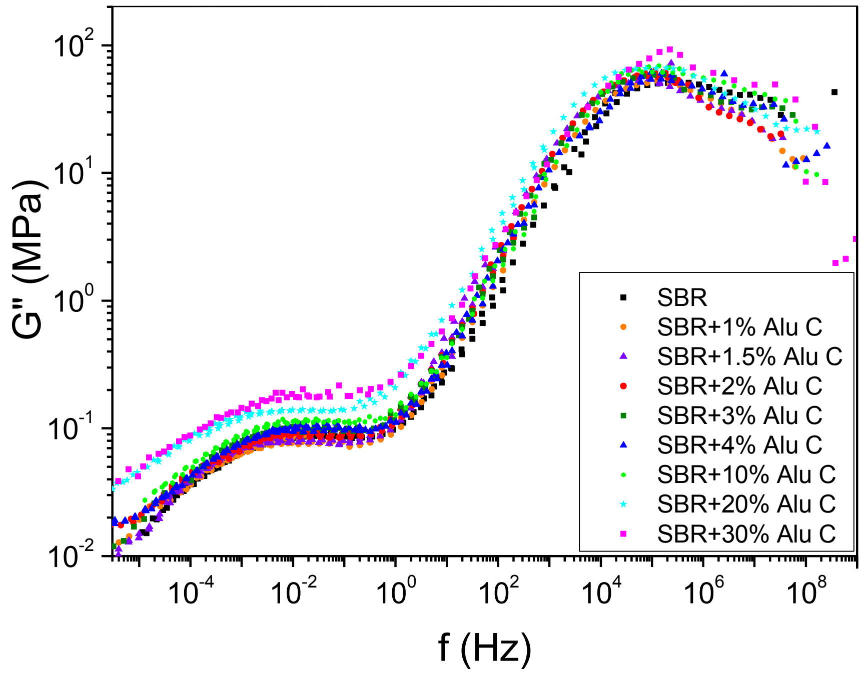

Figure III.28. DMA master curves of the imaginary (G'') part of the complex shear modulus G for SBR/Alu C nanocomposites. Reference temperature 273K.*

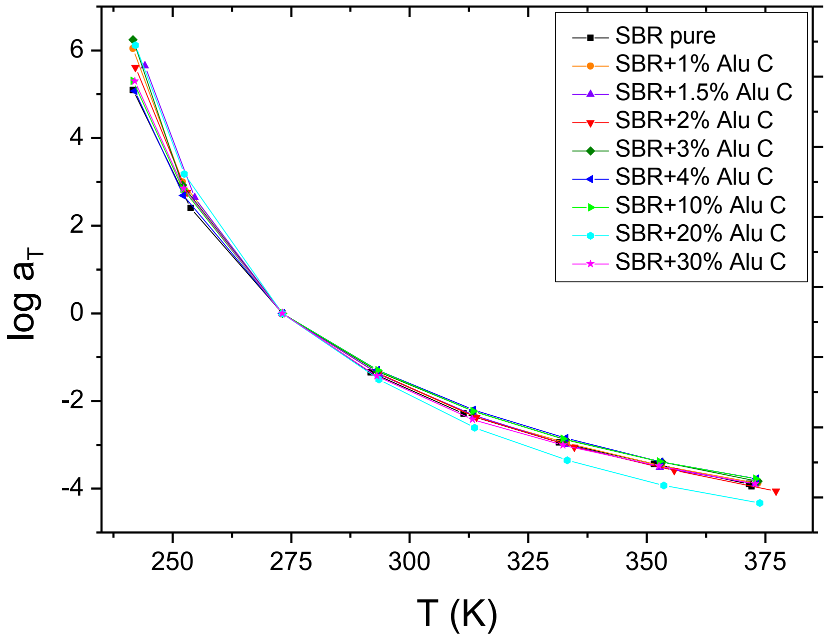

Figure III.29. Shift factor a_T (logarithmic) dependence upon temperature for SBR/Alu C nanocomposites.

Similar to neat SBR, the master curves of the nanocomposites display the four characteristic regions already discussed in the subchapter III.4.2: glassy regime, glass-rubber transition, rubbery plateau and “terminal“ low frequency regime. In the glassy regime, the effect of the nanoparticles is less pronounced than in the other regions. This is due to the fact that the stiffness modulus of the SBR matrix approaches the high modulus of the alumina nanoparticles at high frequencies. In all other regions, the influence of the nanoparticles can clearly be seen in the frequency dependence of both master curves. Obviously, as can be observed in Figure III.30 the systems with filler concentrations $w_{filler} \geq 10\%$ present noticeable reinforcement effect in the rubbery plateau and low-frequency (“terminal”) regimes.

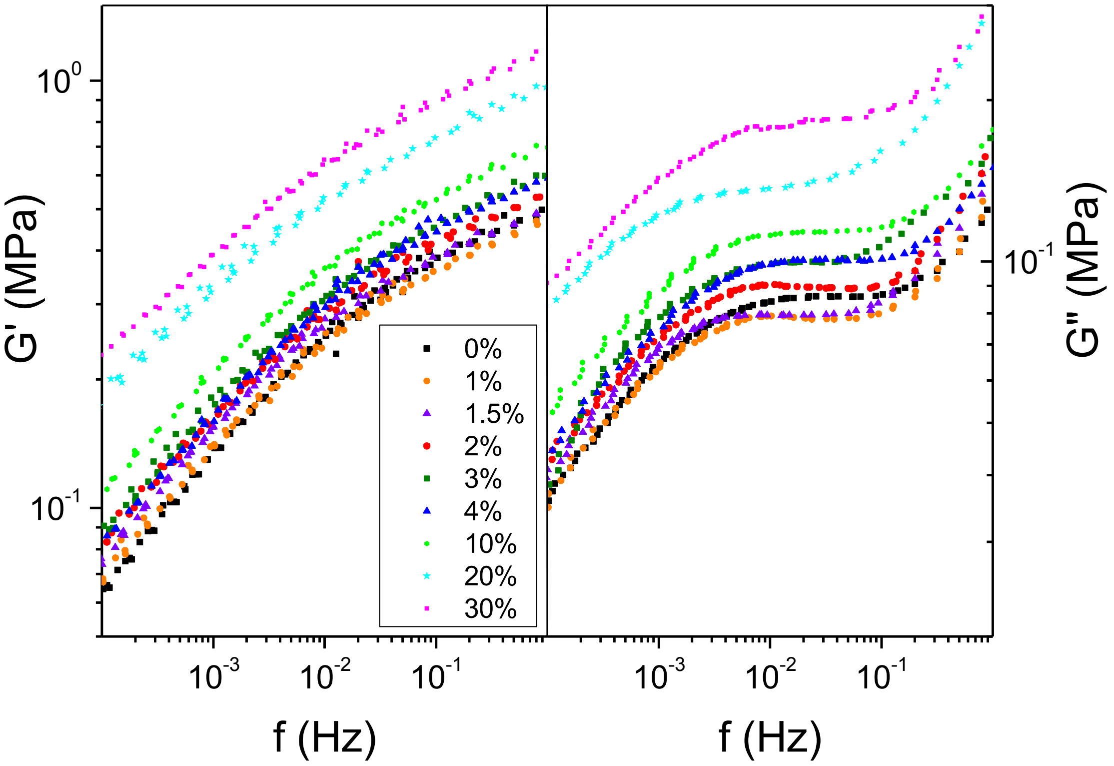

Figure III.30. DMA master curves of the elastic moduli for SBR/Alu C nanocomposites in a frequency region around the rubbery plateau.

Reinforcement is also found for small nanoparticle concentrations ($w_{filler} <10\%$). Figure III.30 suggests that this effect is frequency-dependent. Figures III.31 and III.32 illustrate this dependence for the real *G’* and the imaginary *G”* parts of the complex shear modulus correspondingly. The $G'(w_{filler})$ curve for 10^{-4} Hz obviously shows a reinforcement effect which increases with the concentration of nanoparticles. This general trend is observed up to a frequency of about 10 Hz. For higher frequencies approaching the dynamic glass transition, the reinforcement is increasing rapidly at low concentrations - almost showing a local maximum at about w_{filler}=1.5%. The same behavior is observed for the *G"*(w_{filler}) curves (Fig.III.32). The local *G"* maximum at about w_{filler}=1.5% is even more pronounced than for *G'*.

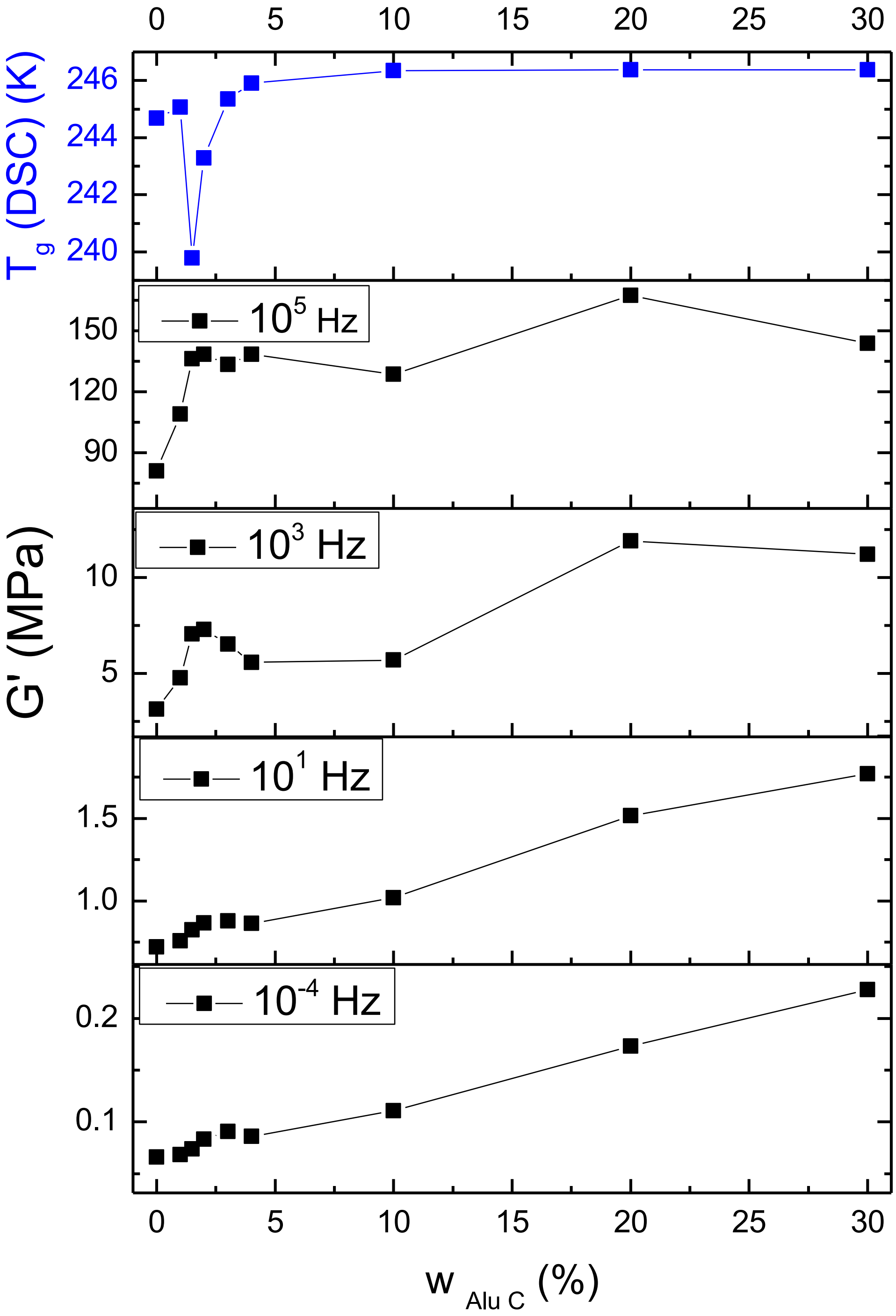

Figure III.31. Storage modulus G' values at different frequencies (DMA data) and the glass transition temperature T_g (TMDSC data).

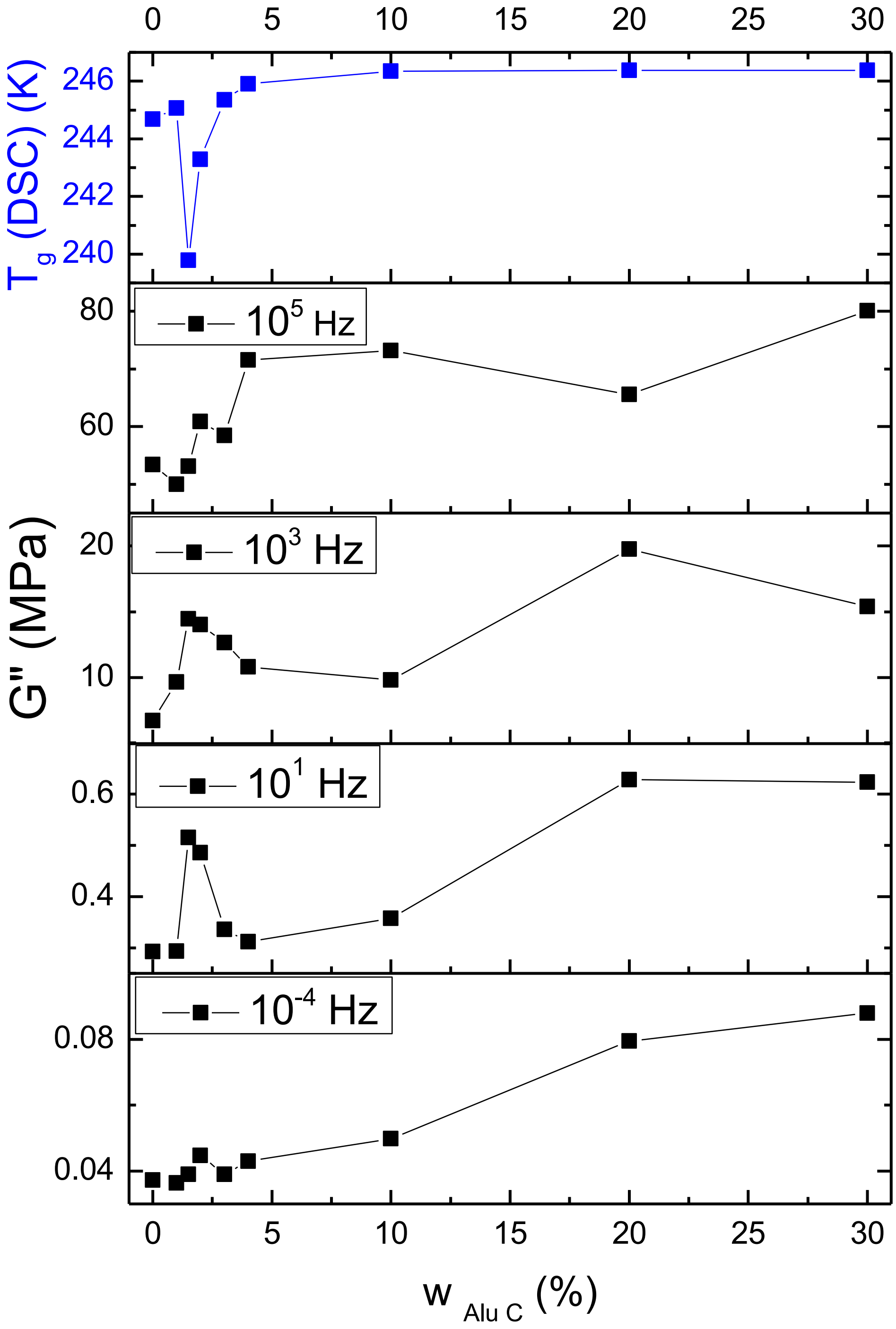

Figure III.32. Loss modulus G" values at different frequencies (DMA data) and the glass transition temperature T_g (TMDSC data).

The uppermost curves in Figures III.31 and III.32 reproduce the dependence of the glass transition temperature T_g on the filler content as revealed by TMDSC measurements (see chapter

III.5.1). Comparing the concentration dependences of both shear moduli and of the glass transition temperature respectively, it is obvious that the maximum in the moduli appears at the same nanoparticle concentration as the minimum in T_g.

It turned out that the examination of the dynamic glass transition behavior of the nanocomposites is difficult to realize with DMA since this requires performing frequency sweeps very close to and below the thermal glass transition temperature. Due to the volume shrink of the rubber nanocomposite, a measuring geometry where the thickness of the sample can only be adapted with big difficulties (opening the instruments at low temperatures, formation of ice etc.) is not well suited. Therefore I include results from rheological measurements in the thesis. Here it is easily possible to define the normal force of the geometry, i.e. the thickness of the sample is adapted to thermal expansion/shrink. The *tan δ* data from rheometry are much clearer than those obtained from DMA measurements especially at high frequencies (low temperatures). In Annex IV (Fig.A.15-A.16) we document for an SBR sample that shear data obtained from DMA and rheometry evolve in a fairly similar way as a function of frequency.

In the upper part of Fig.III.33 the frequency dependence of the loss factor *tan δ* is shown at the reference temperature T_0=273K for all of the investigated nanocomposites. As justified here above, the *tan δ* values have been calculated from shear storage and loss data obtained from rheometry. The corresponding master curves are shown in Annex IV.

Identifying the loss factor peak maximum with dynamical freezing of the investigated system, we can state that the glass transitions of the samples filled with 1% and 1.5% of nanoparticles occur at higher frequencies than those of the other investigated samples. Thus, measurements of the loss factor *tan δ* suggest increased molecular mobility at about 1.5-2% of Alu C nanoparticles and slowed mobility at $w_{filler} > 4\%$. The lower part of Fig.III.34 shows the same curves scaled vertically by a factor such that all curves have the same height at the maximum. There are three important results:

1) The shift of a single *tan δ* curve corresponding to a specific filler concentration with regard to the curve of neat SBR is the same at all frequencies shown in Fig. III.33. This means that the influence of the nanoparticles on the dynamics of the rubber molecules is the same at low frequencies where flow plays a role and at high frequencies around the dynamic glass transition where segmental mobility dominates. This holds true for the curves which are shifted to higher frequencies as well as for curves shifted to lower frequencies.

2) The shift of the *tan δ* maximum with the filler concentration, i.e. the shift of the dynamic glass transition at the reference temperature of 273 K, reflects the results obtained from TMDSC. In the lower part of Fig.III.34 the frequencies of the loss factor maximum are plotted as a function of w_{filler}. At the filler concentrations where the glass transition temperatures T_g (measured by TMDSC) show a minimum, the data related to *tan δ* show a maximum.

3) At very low frequencies, irrespective of the AluC content, *tan δ (f)* tends to turn towards a constant when $f \rightarrow 0$. Thus the gel-like behavior observed on neat SBR (see chapter III.4.2) seems to be conserved in the presence of the nanoparticles.

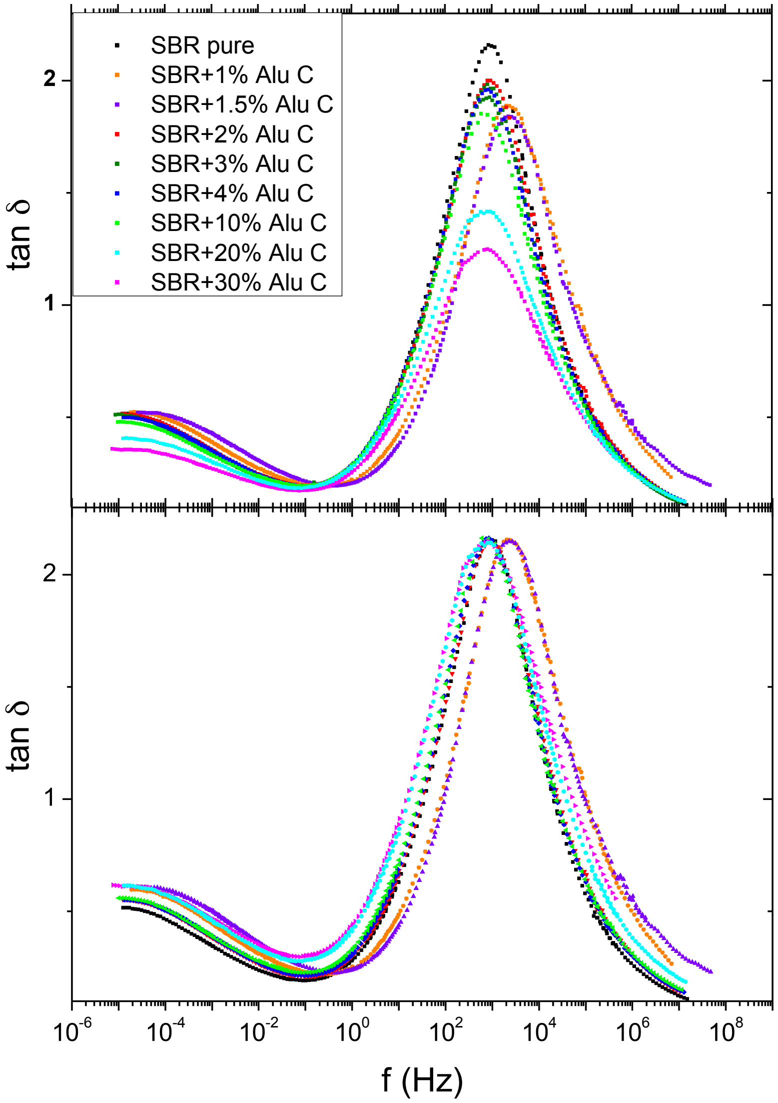

Figure III.33. Rheology loss factor tan δ frequency dependence for SBR/Alu C nanocomposites.

Regarding 3), Fig. III.35 exemplarily shows the "terminal", the rubbery plateau and the rubber-glass transition regimes of the master curves *G'(f)* and *G"(f)* for neat SBR and the nanocomposite with the highest filler load (SBR/30 wt% Alu C) at the reference temperature $T_0=273K$. Reinforcement is obvious. Similar to neat SBR, the behavior of the nanocomposite is solid-like at low frequencies ("terminal regime"): *G'(f)>G"(f)*. Moreover, in the mentioned frequency regime, the slopes of both master curves *G'(f)* and *G"(f)* fairly coincide and are smaller than the one observed for the respective master curves obtained for neat SBR (see Fig.III.35).

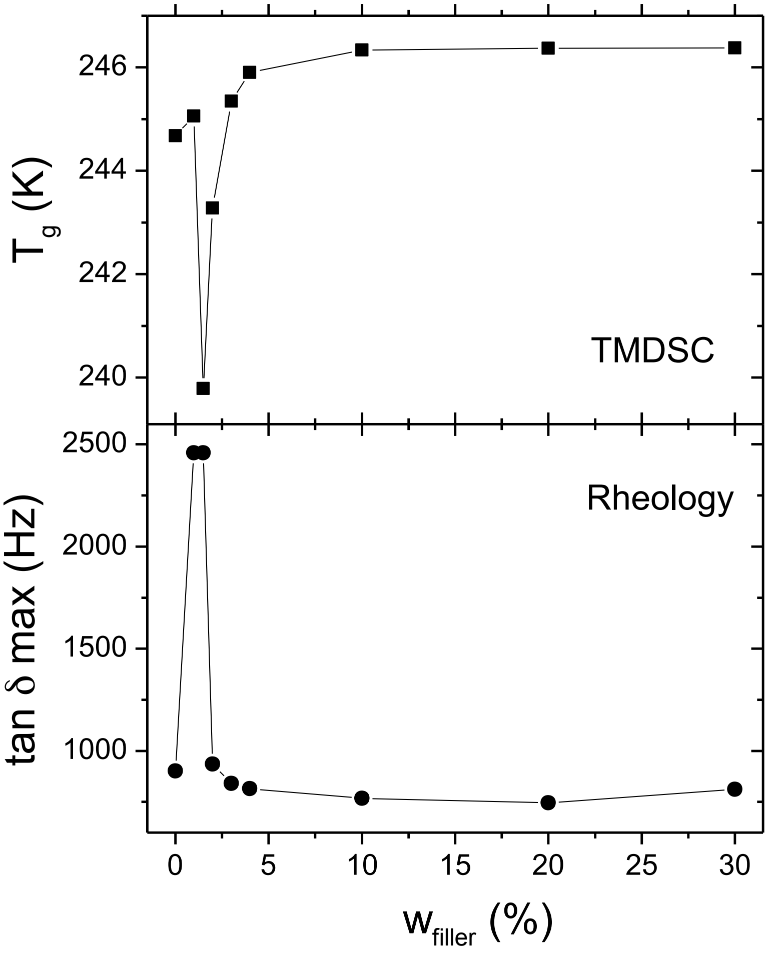

Figure III.34. T_g values measured by TMDSC and tan δ peak position (determined from rheological frequency measurements) as a function of filler concentration.

In Fig. III.36 the "terminal" regime behavior of the storage shear moduli is represented for the investigated SBR/AluC systems at the reference temperature $T_0=273K$.

Irrespective of the filler concentration, at low enough frequencies, the behaviour of the respective storage shear moduli (and loss modulus) obey to power laws $G' \propto f^{\nu}$. Fig.III.37 shows the evolution of the exponent ν (slope of $G'(f)$ in the double-logarithmic representation) as a function of the filler content w_{filler}.

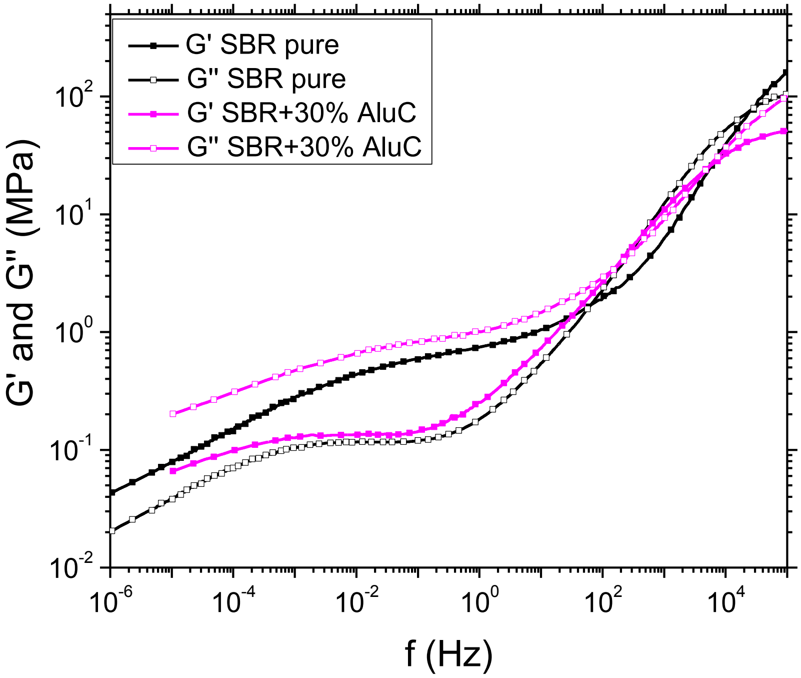

Figure III.35. G'(f) and G"(f) values from rheometry for neat SBR and SBR/30% Alu C.

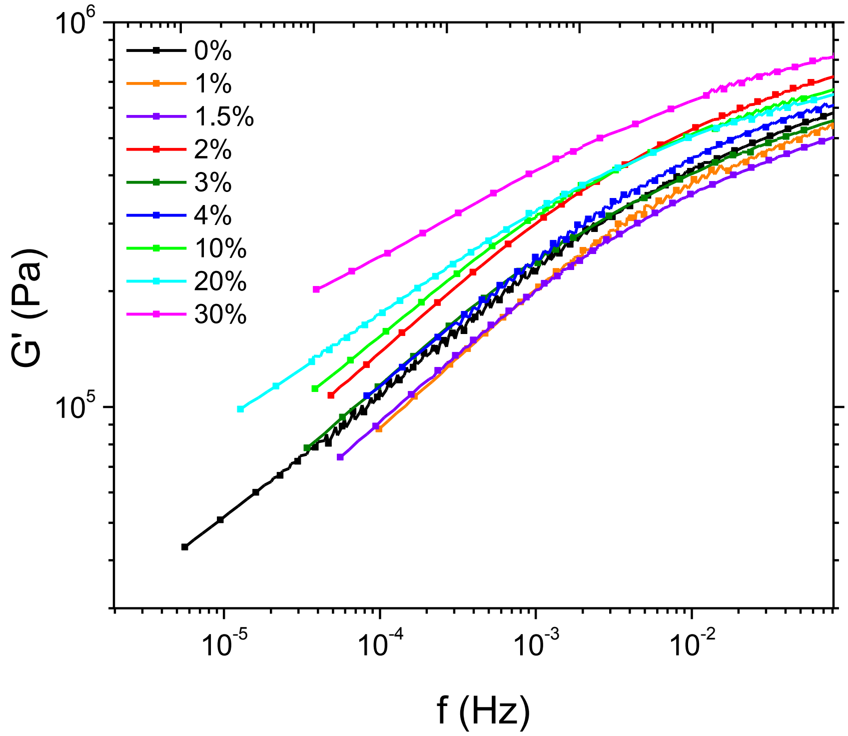

Figure III.36. "Terminal" regime behavior of the G'(f) for the SBR/AluC nanocomposites.

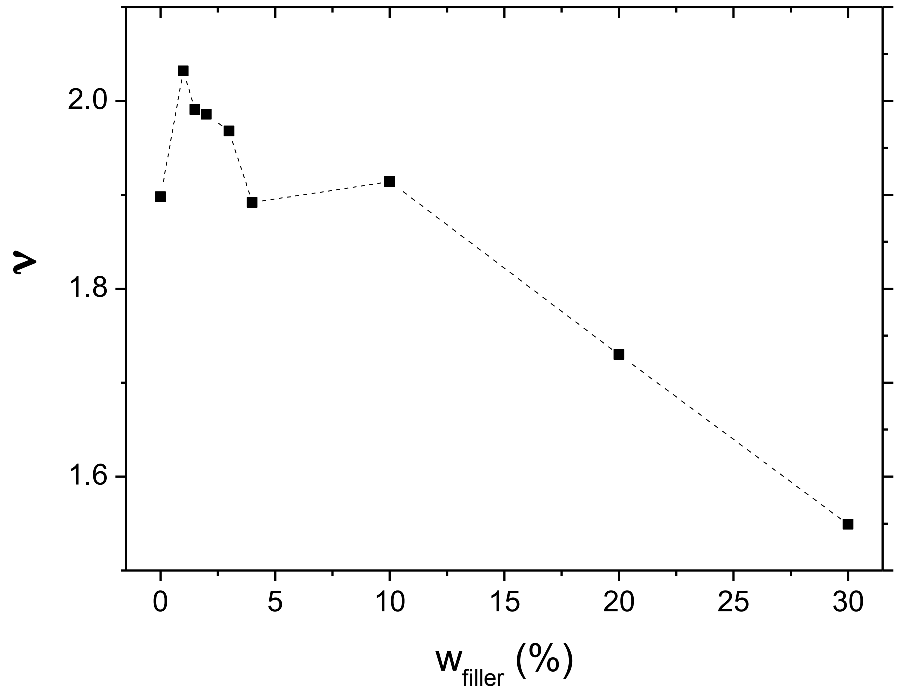

Fig.III.37. Slope v of G'(f) in the double-logarithmic representation as a function of the filler content w_{filler}.

Interestingly, in the filler concentration window 0< w_{filler} < 4%, we again observe an evolution of $v(w_{filler})$ which significantly differs from the general trend manifesting itself by a decrease of the slope of *G'(f)* with increasing AluC content. As a matter of fact, the power law exponent exhibits a weak maximum within the concentration interval [0; 4%] around w_{filler}=1-1.5%. The lower the slope of *G'(f)*, the more solid-like is the behavior of the nanocomposite in the low-frequency regime. Thus, increasing the AluC concentration enhances the solid-like behavior of the nanocomposite at low frequencies excepted in the concentration interval [0; 4%] where the fillers seem to keep the respective nanocomposites more "fluid" in comparison to neat SBR.

To test to which extent the filled systems behave like a gel in the low-frequency regime, we use Table III.3 to compare the slopes *v* and *v'* of the *G'(f)* and the *G"(f)* curves respectively (double-logarithmic representation) in the corresponding "terminal" regimes. While at high concentrations (w_{filler} ≥4%) *v* and *v'* as in case of neat SBR, *v'* systematically deviates a little more from *v* at low filler contents.

Table III.3. The slopes v and v' of the G'(f) and the G"(f) curves respectively (in double-logarithmic representation) in the "terminal" regimes.

$w_{filler, wt.\%}$	v	v'
0	0.28	*0.28*
1	0.31	*0.27*
1.5	0.3	*0.26*
2	0.3	*0.26*
3	0.29	*0.26*
4	0.28	*0.26*
10	0.28	*0.26*
20	0.24	*0.24*
30	0.19	*0.18*

III.5.3. Discussion of the results obtained from TMDSC and DMA/rheometry

Parts of this paragraph have been published in [28].

As already mentioned in chapter III.5.1, the most prominent feature of the results obtained from TMDSC is the minimum in the glass transition temperature T_g of the nanocomposites for low filler concentrations. This minimum is accompanied by a general trend to increasing T_g values with increasing Alu C concentration. Results obtained from DMA/rheometry confirm the trend observed by calorimetry. The minimum in T_g or the maximum of the α-relaxation frequency (=frequency at which the maximum of the loss factor occurs) can only be explained by a mechanism or process which accelerates the dynamics of the rubber molecules for filler concentrations up to about 2 wt%. This would be the opposite of what is known as "bound rubber" [26]. Since the untreated alumina nanoparticles have a hydrophilic character, it could be argued that the hydrophobic SBR molecules show only weak interactions with the nanoparticles' surfaces leading to accelerated dynamics of rubber molecules near the rubber-filler interfaces. This should however also be the case for higher filler concentrations leading to a general trend to lower glass transition temperatures (higher relaxation frequencies) which appears to be in contradiction to the experimental findings. However, Bindu et al [27] argue for natural rubber/ZnO nanocomposites that starting at concentrations of about 2 vol%, aggregation of nanoparticles takes place leading to a preference of filler/filler interactions over nanoparticle/rubber interactions. At low filler contents, our TEM data (Fig.III.2) shows the AluC nanoparticles clusters, but this tendency can be found for all of the samples investigated by TEM (1%, 2% and 4%). The sample with 2% of filler does not show structural peculiarities. Furthermore, experiments with SBR nanocomposites with various surface-treated alumina particles show a similar T_g minimum at low filler concentrations (see next chapter). This leads us to the conclusion that aggregation of nanoparticles cannot be the reason for the observed behavior. Moreover we claim that the reduction of the number of physical cross-links (e.g. entanglements) between polymer chains by small amounts of nanoparticles is responsible for the accelerated local dynamics at small filler concentrations. During the preparation of the nanocomposites from solution (see chapter II.3), the nanoparticles seem to hinder the formation of physical cross-links. The structural relaxation (α-process) of the SBR molecules becomes faster which explains the decrease of T_g (increase of the frequency at which freezing occurs while performing dynamical DMA/rheometry tests) for these small concentrations. This interpretation is not in contradiction to the low-frequency behavior of the nanocomposites observed in the filler concentration interval [0; 4%] by mechanical spectroscopy (see subchapter III.5.2): the modest trend of the filled systems towards more fluid-like behavior, the slight deviation from gel-like behavior can be related to a reduction of the number of physical cross-links [28].

Intuitively one would expect that by introducing an increasing number of nanoparticles into the SBR matrix (i.e. by opting for higher filler concentrations) the number of physical cross-links continues to grow. We however observe a minimum of the glass transition temperature at a filler concentration of only 1.5%. At concentrations w_{filler}>1.5% the Alu C start to slow down the molecular dynamics involved in the α-process. A possible explanation for the limit of the molecular acceleration could be the existence of only a limited number of entanglements in unfilled SBR. Another hypothesis for the limit for the molecular acceleration bases on the observation of structural changes undergone by the nanoparticles when the filler concentration increases. As can be seen in Fig.III.2, the size of the nanoparticles slightly increases due to agglomeration when the AluC content grows. Hence by increasing the filler concentration one does not necessarily increase the number of particles with the potential to hinder the formation of physical cross-links in the SBR matrix. Moreover the fractal character of the agglomerates of nanoparticles favors mechanical coupling between matrix molecules and the filler surfaces.

In any case the accelerated dynamics at low concentrations is superimposed by a general trend to slower local dynamics with increasing filler concentration. This could be due to the fact that weak physical interactions (amongst others e.g. mechanical filler/SBR coupling leading to additional cross-links) at the fillers' surfaces have a small retardation effect on the glass-forming dynamics of the SBR molecules. This effect seems to be far too small to talk of "bound rubber": the increase of T_g from unfilled to 30 wt% is only about 1.7K and TMDSC measurements do not deliver evidence for the existence of a rigid amorphous phase ($\Delta c_p{}^{'SBRcorr}=c^{te}$ when $w_{filler}\geq 4\%$; see Fig. III.26). In addition to possible attractive interactions between rubber molecules and nanoparticle surfaces, confinement of the rubber molecules by the nanoparticles could also be the reason for the slight overall increase of the glass transition temperature [28].

We have already discussed (see subchapter III.5.2) that measurements of the loss factor *tan δ* by rheometry support the idea of increased and slowed molecular mobility. Using the activation plot of the α-process measured by dielectric spectroscopy for the pure SBR system, it can be calculated that a frequency of 8.3 mHz (modulation period of 2 minutes) at T_g from the TMDSC measurements corresponds to about 300 Hz at the reference temperature of 273 K used for the master curves of the *tan δ* data. From the fact, that the concentration dependent shift of the *tan δ* curves is independent of frequency (see subchapter III.5.2), it can be expected that the minimum of T_g from TMDSC measurements can be found at the same filler content as the maximum of the *tan δ* curves (see Fig.III.34 in subchapter III.5.2).

To summarize, acceleration due to reduction of physical cross-links on one hand and retardation due to nanoparticle/rubber interactions and confinement on the other hand could be made responsible for the unexpected behavior of the glass transition from TMDSC and the loss maximum frequency from rheology [28].

The effect of disentanglement can be seen in the evolution of the shear storage and loss moduli as a function of filler concentration (see Fig.III.31-III.32 in subchapter III.5.2): there is a step at filler contents, where the influence of disentanglement is expected to end.

III.6. Investigations of the SBR/Alu C-Mercapto and SBR/Alu C-Mercapto-grafted nanocomposites

"SBR/Alu C-Mercapto" designate nanocomposites filled with Alu C nanoparticles silanized with γ-mercaptotrimethoxysilane (see subchapters II.2.2 and II.3). In case of the "SBR/Alu C-Mercapto grafted" systems SBR molecules are chemically attached to the layer of γ-mercaptotrimethoxysilane at the surface of the Alu C nanoparticles (see subchapter II.4). For each family of materials, samples with the same nanoparticle concentrations as in case of the SBR/Alu C systems were prepared (TGA degradation measurements on silanized Alu C nanoparticles (see Annex I) showed that the weight of silane layer is negligible, therefore it was not accounted during sample preparation).

III.6.1. TMDSC investigations of SBR/Alu C-Mercapto nanocomposites

In Fig. III.38 and III.39 we have represented the temperature dependences of the specific storage and loss heat capacities normalized to the respective SBR contents of the various SBR/Alu C-Mercapto nanocomposites. Eq.III.1 and Eq. III.2 were used to calculate the $c_p^{'SBR}$ and $c_p^{''SBR}$ values. To be able to better evaluate the influence of the surface-treated alumina on the evolution of the normalized specific storage heat capacity data, we applied the same procedure as in III.5. yyyy: the calculated $c_p^{'SBR}$ values were vertically shifted in such a way that, irrespective of the filler content, they coincide at the lowest temperatures achieved in the glassy state. The final data are named $c_p^{'SBRcorr}$.

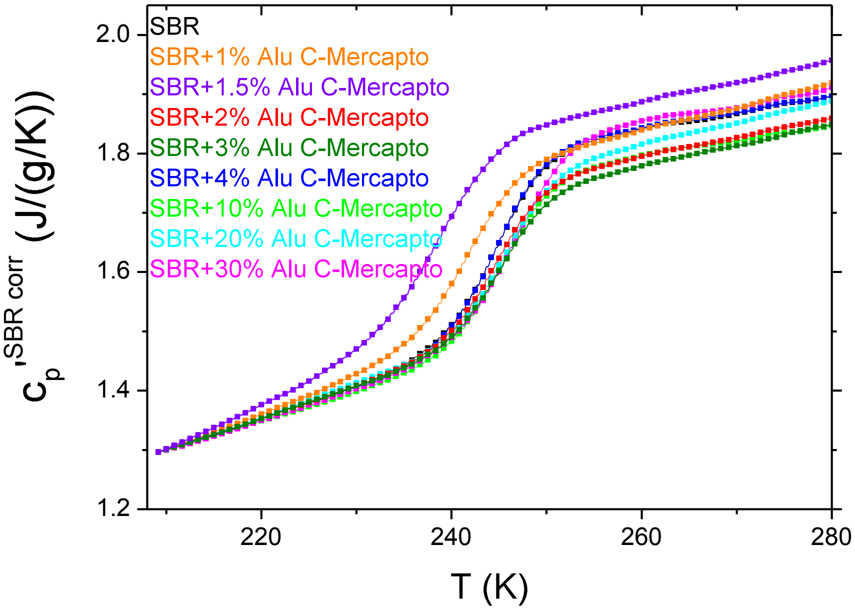

Figure III.38 Real part c_p' of the complex heat capacity c_p for SBR/Alu C-Mercapto nanocomposites. The curves are shifted to the c_p' of the neat SBR value below the glass transition. Measurements were realized upon cooling (cooling rate:-0.5K/min). Temperature modulation: amplitude 0.5K, period 2min.*

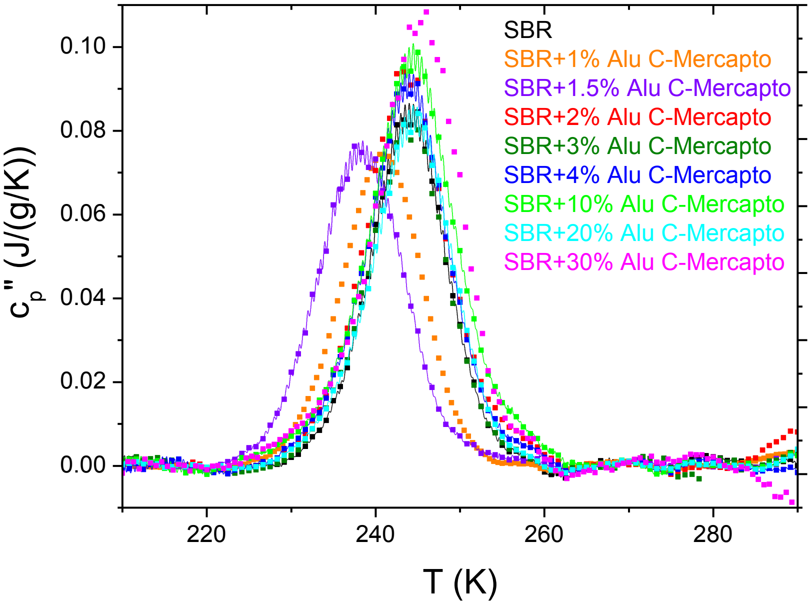

Figure III.39. Imaginary part c_p" of the complex heat capacity c_p for SBR/Alu C-Mercapto nanocomposites. Measurements were realized upon cooling (cooling rate:-0.5K/min). Temperature modulation: amplitude 0.5K, period 2min.*

As in case of the SBR/Alu C nanocomposites, the TMDSC experiments confirmed the existence of a single glass transition for all of the investigated systems. This means that the surface modification of the alumina fillers does not manifest itself by the emergence of an additional glass transition process in the investigated temperature range. We cannot exclude that an additional structural relaxation process associated to the Mercapto surface layers is too feeble to be detected or hidden by the α-process of the SBR matrix.

Most interestingly, the complex evolution of the glass transition temperature as a function of the filler content observed on SBR/AluC nanocomposites is also found for the systems filled with surface treated alumina. Low concentrations of AluC fillers accelerate the structural α-process of the SBR matrix whereas, at higher filler contents, the AluC particles practically do not influence the molecular dynamics of the matrix (Fig. III.38-III.39)

Fig. III.40 allows for a direct comparison of the evolutions of the glass transition temperature T_g of the SBR/AluC and SBR/AluC-Mercapto systems when the filler content changes.

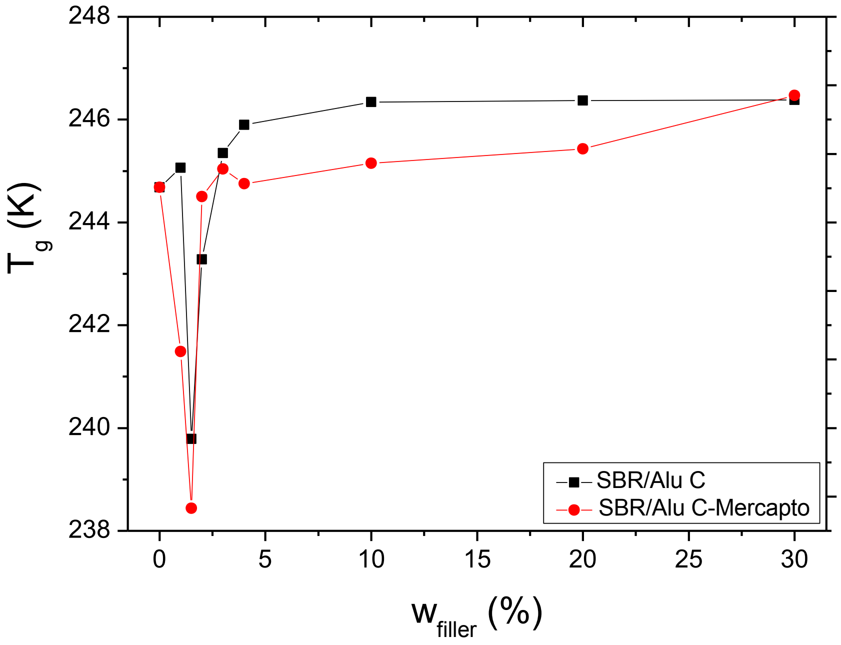

Figure III.40. Glass transition temperature dependence upon filler concentration for all of the nanocomposites.

Obviously, as already announced in chapter III.5, the T_g minimum at 1.5-2% filler does not depend on the surface treatment of the alumina. Thus interactions between SBR molecules and the particles' surfaces cannot be made responsible for the appearance of the phenomenon. This observation is in favour of the interpretation of the existence of the T_g minimum suggested in subchapter III.5.3. Generally, within the filler concentration interval under consideration, the glass transition temperatures of the nanocomposites containing silanized nanoparticles are lower than those of the SBR/Alu C systems. At filler contents $w_{filler} \geq 4\%$ the glass transition temperatures of the systems with surface treated fillers stays at the same level as T_g of neat SBR. We assume that this behavior can be explained by the presence of the silane molecules at the surfaces of the nanoparticles, which have the potential to reduce the interfacial adhesion strength in comparison to the interactions taking place between the untreated alumina and SBR molecules (for a similar behavior see [29]).

While, at high temperatures, i.e. in the rubbery state of the SBR matrix, the slopes of the $c_p^{'SBRcorr}$ curves fairly coincide, in the glassy state the increase of $c_p^{'SBRcorr}$ per Kelvin depends on the filler concentration. As in case of SBR/Alu C systems, the behavior of the SBR/1wt% AluC-Mercapto and SBR/1.5wt% AluC-Mercapto nanocomposites stands out: he respective slopes of the corresponding $c_p^{'SBRcorr}(T)$ are clearly larger than those of the other investigated systems.

In Fig.III.41 we have represented $\Delta c_p^{'SBRcorr}$ and the double loss peak height $2h^{SBR}$ as a function of the AluC-Mercapto concentration.

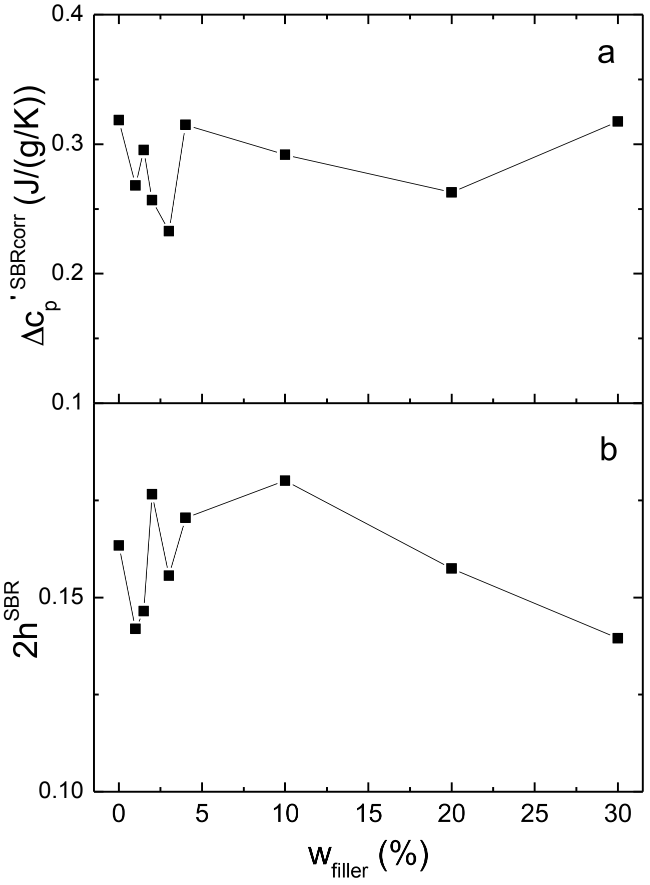

Figure III.41. $\Delta c_p^{'SBRcorr}$ and the double loss peak height $2h^{SBR}$ as a function of the filler content. The solid line is just a guide for the eyes.

Similarly to the results obtained for the SBR/AluC nanocomposites (see Fig.III.26), $2h^{SBR}$ is practically independent of the filler content. Again, at low concentrations ($0 \leq w_{filler} \leq 4\%$), the step height $\Delta c_p^{'SBRcorr}$ decreases when w_{filler} grows. At filler contents $w_{filler} > 4\%$, $\Delta c_p^{'SBRcorr}$ is nearly constant and in good approximation equal to the step height $\Delta c_p^{'SBRcorr}$ measured for neat SBR. Thus, at high enough concentrations, the silanized AluC nanoparticles practically do not influence the thermal glass transition of the SBR matrix. To explain this behavior, we discreetly surmise that the interaction between the hydrophilic silane layers at the fillers' surfaces and the hydrophobic SBR molecules are less pronounced than in case of untreated AluC. In any case, as we investigated SBR/AluC-Mercapto nanocomposites with the same filler concentrations as those used for the SBR/AluC systems, we expect that the confinement effects generated by the AluC-Mercapto particles are at least comparable to those produced by the untreated AluC.

III.6.2. TMDSC investigations of SBR/Alu C-Mercapto grafted nanocomposites

In Fig.III.42 and III.43 we have represented the temperature dependences of the specific storage and loss heat capacities normalized to the respective SBR contents of the SBR/Alu C- Mercapto grafted nanocomposites. Again Eq.III.1 and Eq. III.2 were used to calculate the $c_p^{'SBR}$ and $c_p^{''SBR}$ values. To be able to better evaluate the influence of grafting on the evolution of the normalized specific storage heat capacity data, we applied the same procedure as in III.5.1 (Fig. III.24): the calculated $c_p^{'SBR}$ values were vertically shifted in such a way that, irrespective of the filler content, they coincide at the lowest temperatures achieved in the glassy state. As usual, the final data are named $c_p^{'SBRcorr}$.

Figures III.42 and III.43 give an impression on the thermal glass transition behavior of the nanocomposites when SBR molecules are grafted to the alumina nanoparticles using γ-mercaptopropyltrimethoxysilane layers at the surfaces of the fillers. Several features are worthwhile to be mentioned:

i) The the $c_p^{'SBR}$ and $c_p^{''SBR}$ curves do not deliver hints to the existence of a second glass transition which e.g. could be associated to the presence of SBR layers chemically linked to the nanoparticles [23] or to the emergence of regions of SBR molecules with reduced mobility [20]. The increase of $c_p^{'SBR}$ at low temperatures ($T \leq 220K$) especially in case of the sample filled with 4 wt.% is considered as an artefact of measurement.

ii) As in case of the SBR/AluC and SBR/AluC-Mercapto systems the glass transition temperature T_g shows a minimum at a filler concentration of about 2 wt.% (see Fig. III.44). At high nanoparticle contents ($w_{filler} \geq 4\%$) the glass transition occurs at temperatures which are about 4 K higher than those measured for the respective SBR/AluC-Mercapto systems. Thus, grafting of SBR molecules to the AluC-Mercapto particles yields a pronounced deceleration of the molecular dynamics taking influence on the α-process of the polymer matrix. Obviously AluC nanoparticles with grafted SBR molecules have the same disentanglement effect on the SBR matrix than AluC or AluC-Mercapto fillers.

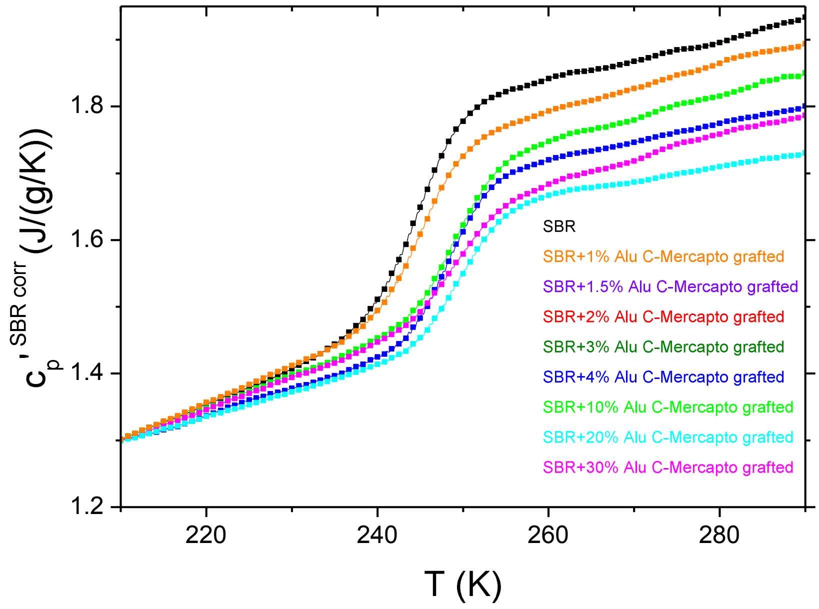

Figure III.42. Real part c_p' of the complex heat capacity c_p for SBR/Alu C-Mercapto grafted nanocomposites. The curves are shifted to the c_p' of the neat SBR value below the glass transition. Measurements were realized upon cooling (cooling rate:-0.5K/min). Temperature modulation: amplitude 0.5K, period 2min.*

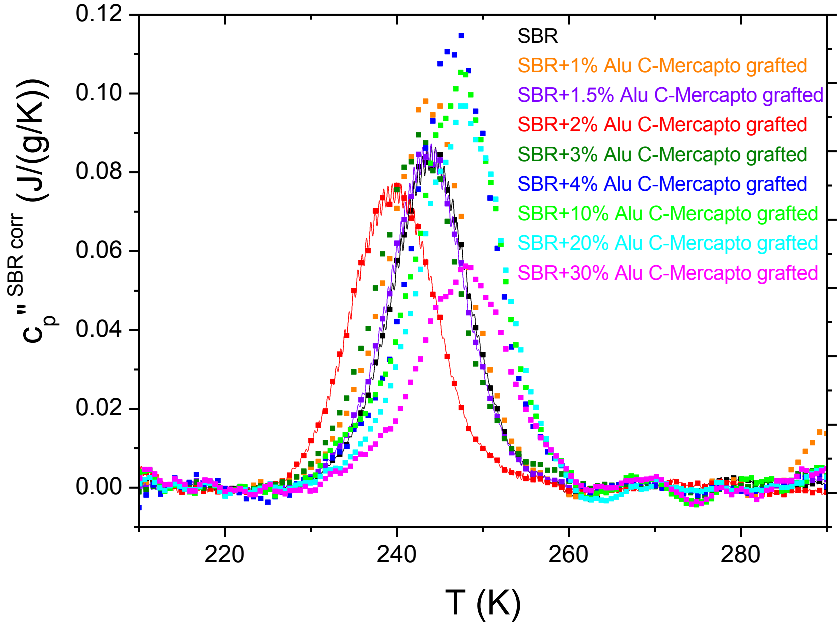

Figure III.43. Imaginary part c_p" of the complex heat capacity c_p for SBR/Alu C-Mercapto grafted nanocomposites. Measurements were realized upon cooling (cooling rate:-0.5K/min). Temperature modulation: amplitude 0.5K, period 2min.*

iii) In Fig.III.45 we compare the evolutions of the relaxation strength $\Delta c_p{}^{'SBRcorr}$ as a function of the filler content for the three investigated families of nanocomposites. While for the SBR/AluC and SBR/AluC-mercapto systems $\Delta c_p{}^{'SBRcorr}$ stays constant at higher filler concentrations (whereby $\Delta c_p{}^{'SBRcorr}$*(AluC-Mercapto)*≈$\Delta c_p{}^{'SBRcorr}$*(SBR)*>$\Delta c_p{}^{'SBRcorr}$*(AluC)*), the relaxation strength decreases when the nanoparticle content inside the SBR/AluC-Mercapto grafted systems grows.

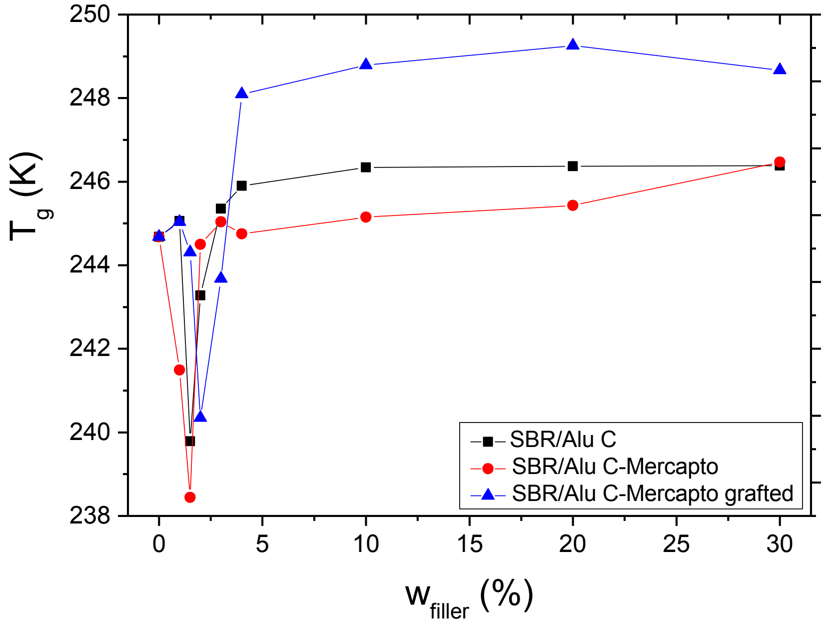

Figure III.44. Evolution of the thermal glass transition temperature T_g *as a function of filler content for SBR/AluC, SBR/AluC-Mercapto and SBR/AluC-Mercapto grafted nanocomposites.*

iv) As can be seen in Fig.III.46, at least at high concentrations the double height of the loss peak $2h^{SBR}$ of the SBR/AluC-Mercapto grafted systems shows the similar behavior as $\Delta c_p{}^{'SBRcorr}$.

The observation that the minimum of the glass transition temperature practically occurs at the same filler concentration irrespective of the investigated family of nanocomposites supports our hypothesis that the acceleration of α-process at low filler contents results from a reduction of physical cross-links between SBR molecules by the nanoparticles rather than from characteristic interfacial interactions between the fillers' surface and the matrix molecules.

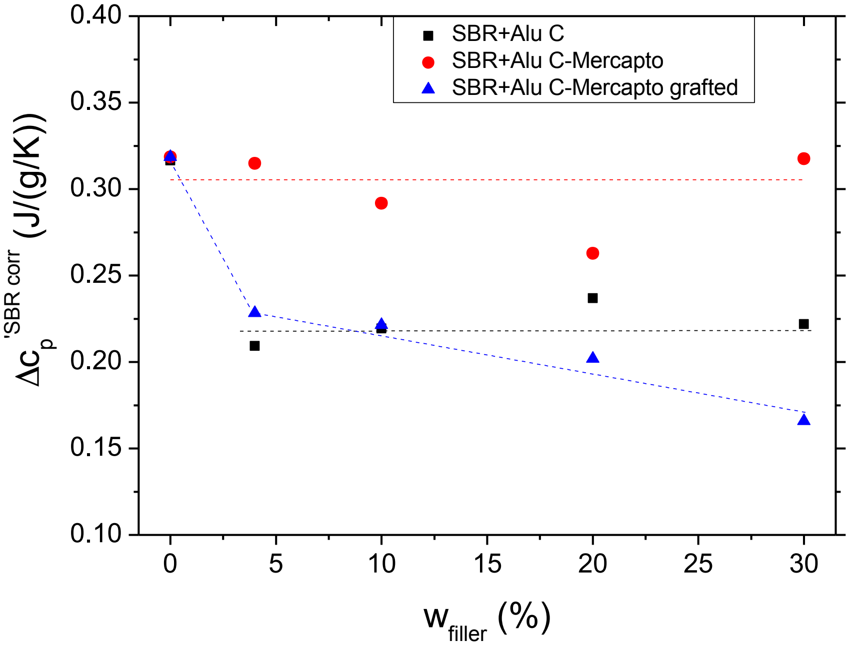

Figure III.45. $\Delta c_p{}^{'\,SBRcorr}$ *as a function of the filler content for SBR/AluC, SBR/AluC-Mercapto and SBR/AluC-Mercapto grafted nanocomposites. The dashed lines are just guides for the eyes.*

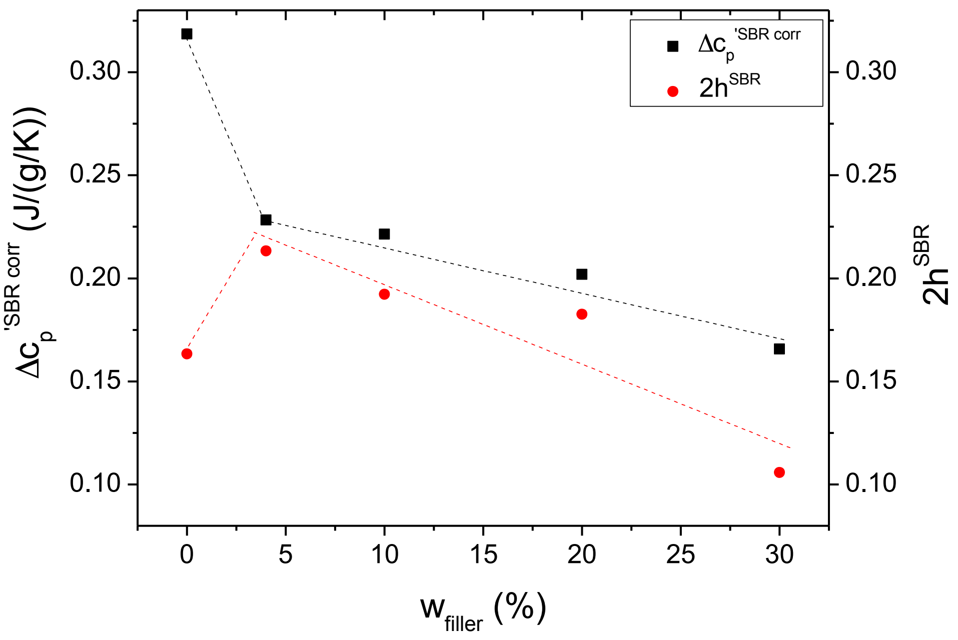

Figure III.46. The double loss peak height $2h^{SBR}$ *as a function of the filler content. The dashed lines are just guides for the eyes.*

Obviously, grafted Alu C-Mercapto nanoparticles have a significant influence on the $\Delta c_p^{'\,SBRcorr}$ and $2h^{SBR}$ values at high filler content. The increase of T_g by 4 K goes along with a decrease of the relaxation strength $\Delta c_p^{'\,SBRcorr}$ and the height $2h^{SBR}$ of the specific loss heat capacity peak. First of all both features prove that the silanization/grafting process that we have operated has been successful. Secondly, both experimental results point to the existence of bound rubber at the surfaces of the AluC-Mercapto fillers. The question whether the bound rubber layers are formed by totally or only partially immobilized SBR molecules can currently not been answered. In any case our specific heat capacity data do not provide evidence for the existence of a second glass transition in the investigated temperature range. Moreover our data do not allow for drawing conclusions regarding the existence of regions formed by "free" molecules with reduced mobility [20].

Thus we have been successful in creating interphases. However, information on possible gradients of mobility across the interphases is currently missing. In the following we want to address the question which is the influence of surface treatment of the nanoparticles on the rheological behaviour of the nanocomposites.

III.6.3. DMA/Rheometry investigations

Which are the effects of silanization (hydrophilic Mercapto layers at the surfaces of the AluC) and grafting of SBR molecules to the AluC-Mercapto fillers respectively on the mechanical behavior of the investigated nanocomposites? This interesting question will be addressed in the present chapter.

From TMDSC measurements we know that the three families of nanocomposites investigated in this project show three different evolutions of the glass transition temperature when the filler concentration is changed (Fig.III.44). SBR/AluC, SBR/AluC-Mercapto and SBR/AluC-Mercapto grafted systems have in common that T_g shows a minimum at $w_{filler}\approx1.5$-2%. At higher filler concentrations (generally $w_{filler}\geq4\%$), the variation of the glass transition temperature with respect to neat SBR is maximal for the grafted systems ($\Delta T_g\approx4$K) and practically zero for the SBR-Mercapto systems. In case of the nanocomposites filled with untreated AluC, we observe a rather weak variation $\Delta T_g\approx1.5$K.

In the discussion related to the SBR/AluC systems (see chapter III.5.3) we argued that a competition between impeding crosslink formation (during sample preparation) and rubber/filler interactions seems to be responsible for the complex evolution of the glass transition temperature as a function of the AluC content. The experimental results suggest that at low filler concentrations the number of crosslinks in the SBR matrix decreases. At higher filler contents interactions between the hydrophilic nanoparticles and hydrophobic SBR molecules seem to become dominant. We have also discussed the possible role played by structure formation in the nanocomposites when the filler concentration increases. As a matter of fact, increasing the filler concentration yields the formation of AluC agglomerates with fractal structure. It can be assumed that the corrugated surfaces of the agglomerates favor mechanical interactions between the fillers and the SBR molecules. The existence of other types of interaction cannot be excluded. Confinement was also evoked to take influence on the deceleration of molecular dynamics (α-process) at higher filler concentrations. Results obtained from DMA/rheometry support our model: the gel-like character of neat SBR under "terminal regime" conditions tends to slightly weaken at the lowest filler concentrations. In contrast, still under "terminal regime" conditions, the nanocomposites' answer to shear strains becomes more elastic when the filler concentration increases

III.6.3.1 SBR/AluC-Mercapto nanocomposites

Figures III.47 and III.48 show the master curves of the storage shear modulus *G'(f)* and loss modulus *G"(f)* for SBR/AluC-Mercapto nanocomposites with filler contents w_{filler}*=0; 4; 10; 20; 30%*. The data shown corresponds to results obtained by DMA.

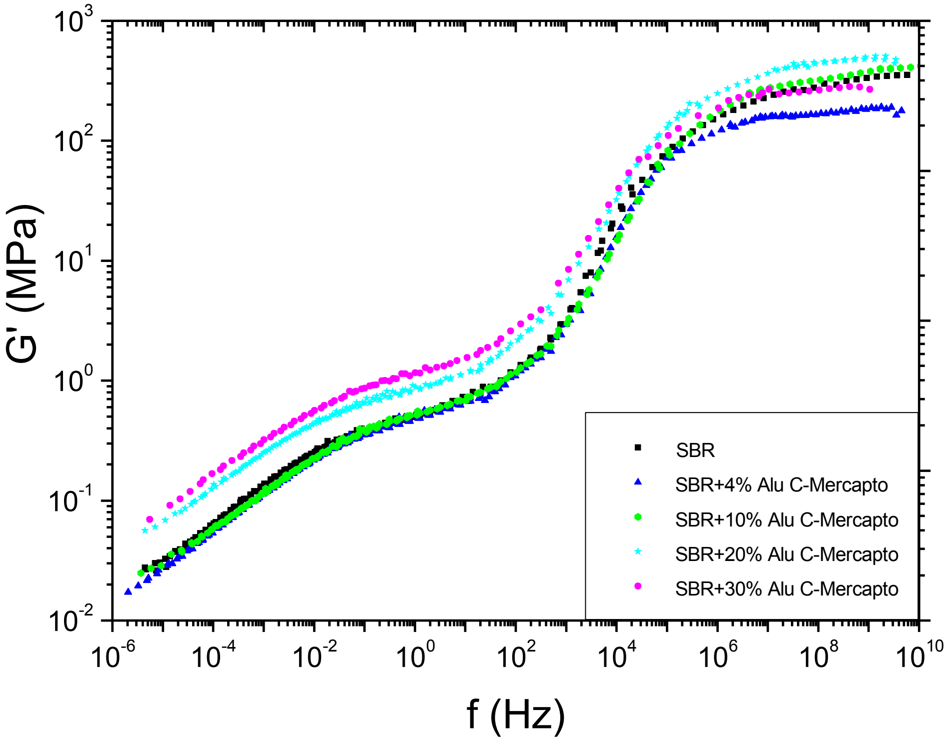

Figure III.47. DMA master curves of the real (G') part of the complex shear modulus G for neat SBR/Alu C-Mercapto nanocomposites. Reference temperature: 273K.*

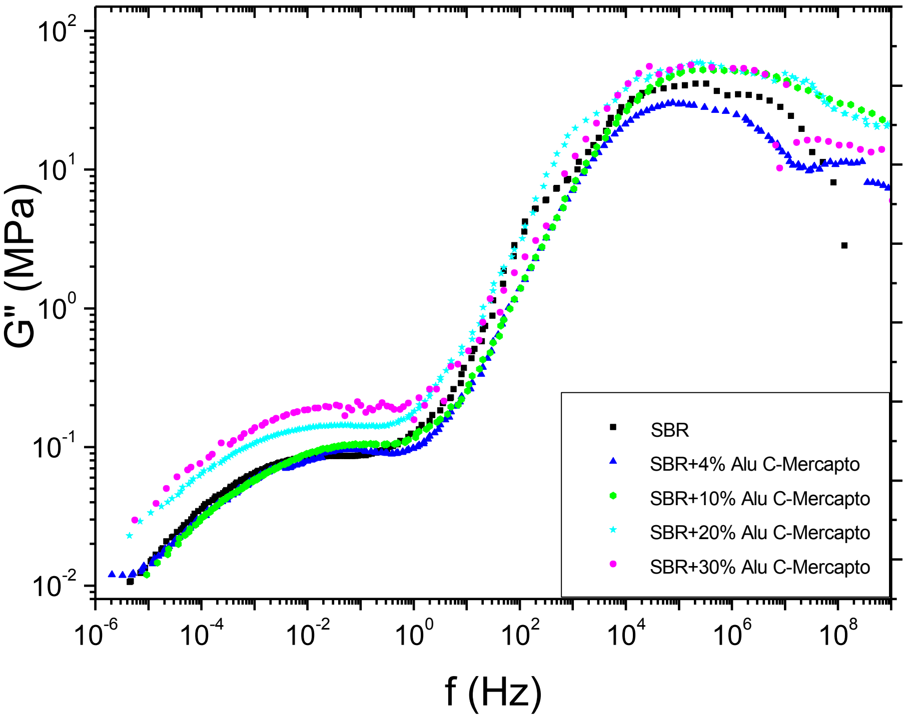

Figure III.48. DMA master curves of the imaginary (G") part of the complex shear modulus G for SBR/Alu C-Mercapto nanocomposites. Reference temperature: 273K.*

Obviously, the fillers do not substantially take influence on the rubber-glass transition. However for experimental reasons already discussed in chapter III.5.2 we observe severe data scattering while carrying out isothermal frequency sweeps with DMA at low temperatures. We therefore used the same samples to repeat the measurements in the critical temperature range by means of rheometry. Fig. III.49 shows the evolution of the loss factor *tan δ* as a function of frequency in vicinity of the dynamic glass transition. We observe that the frequency at which the loss peak maximum is in good approximation independent of the filler concentration and corresponds to the dynamic glass transition of neat SBR (only the vitrification of the 4% sample seems to be slightly shifted to higher frequencies). This experimental finding fairly corresponds to the results obtained by TMDSC (Fig.III.44 e.g.)

Most interestingly at frequencies corresponding to rubbery plateau and "terminal" regimes, the storage and loss shear moduli measured for the 4% and 10 % samples practically coincide with the respective values obtained for neat SBR. Only at the highest filler concentrations (w_{filler}= 20; 30%) the values of *G'(f)* and *G"(f)* exceed the corresponding results obtained for the polymer matrix. Moreover, as can be observed in Fig. III.50, the storage shear moduli of the SBR/AluC-Mercapto nanocomposites with filler contents of 20% and 30% are smaller than those obtained for the corresponding SBR/AluC systems.

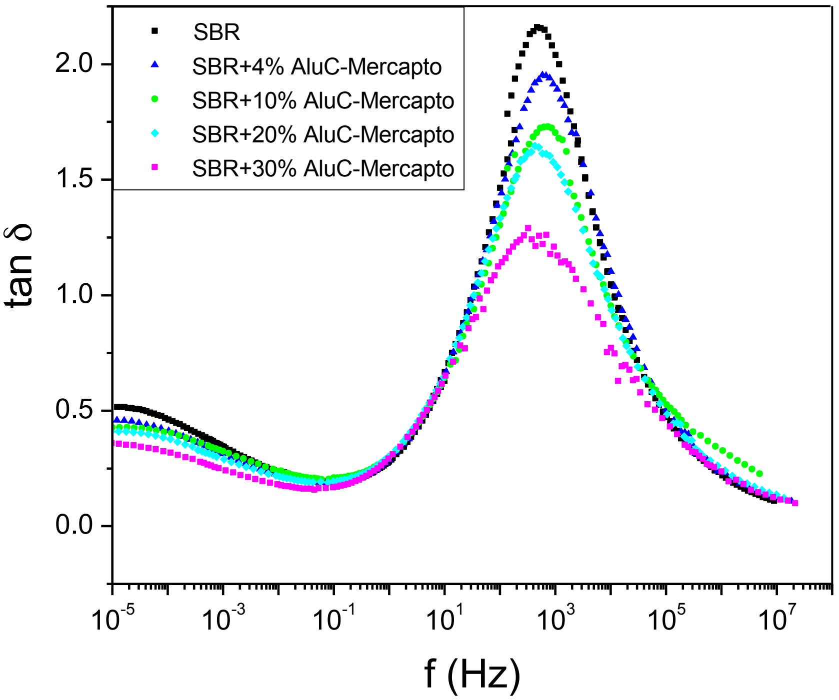

Figure III.49. Rheology loss factor tan δ frequency dependence for SBR/Alu C-Mercapto nanocomposites with filler contents 0; 4; 10; 20; 30%.

Fig.III.51 exemplarily shows the rubbery plateau and "terminal" regime parts of the master curves *G'(f)* and *G''(f)* of the SBR/AluC-Mercapto sample with a filler weight fraction of 20%. Clearly, as in case of the SBR/AluC systems, *G'*>G*''* in the frequency range corresponding to the "terminal"regime. This means that the behavior of the nanocomposite is solid-like at the lowest frequencies. Moreover, in the same frequency range, the slopes of the *G'(f)* and *G''(f)* curves practically coincide. It follows that, similar to the SBR/AluC nanocomposites, the SBR- 20 wt%AluC-Mercapto sample behaves like a gel in the terminal frequency range.

Relying on the results obtained from TMDSC (see chapter III.6.1) and our rheological investigations we come to the following conclusion regarding the influence of the surface-treated AluC-Mercapto nanoparticles on the SBR matrix.

The mechanism leading to the minimum of $T_g(w_{filler})$ at a filler weight fraction of about 1.5% is the same as the one described for the SBR/AluC nanocomposites: AluC-Mercapto fillers seem to hinder the formation of physical crosslinks between SBR molecules. Apparently, surface-treatment is not relevant for this mechanism.

γ-mercaptopropyltrimethoxysilane molecules at the nanoparticles' surface reduce the surface hydrophilicity due to the presence of the alkyl fragment (-CH_2-CH_2-CH_2-). Studies of the water contact angle on similar systems showed that surfaces treated with γ-mercaptopropyltrimethoxysilane exhibit “super hydrophobicity” compared to the initial untreated surfaces [30-31].

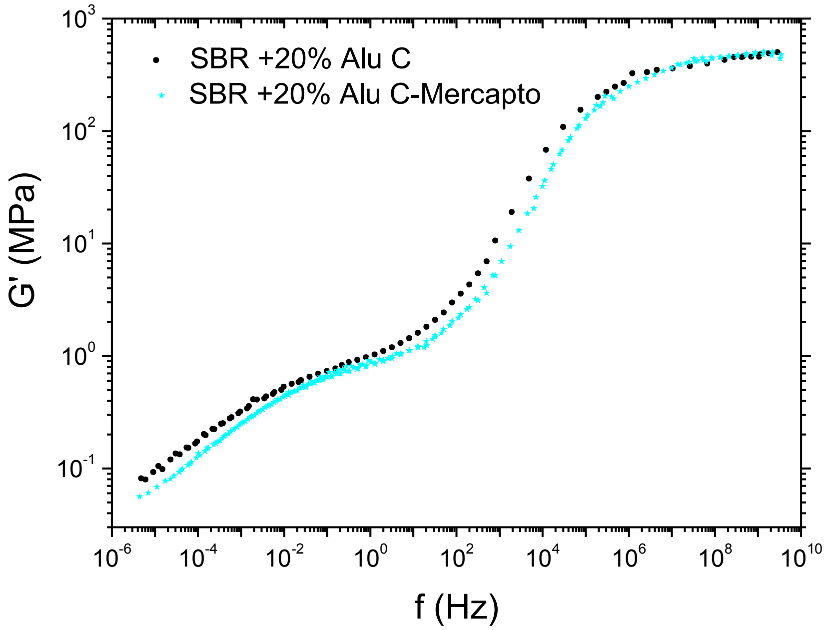

a)

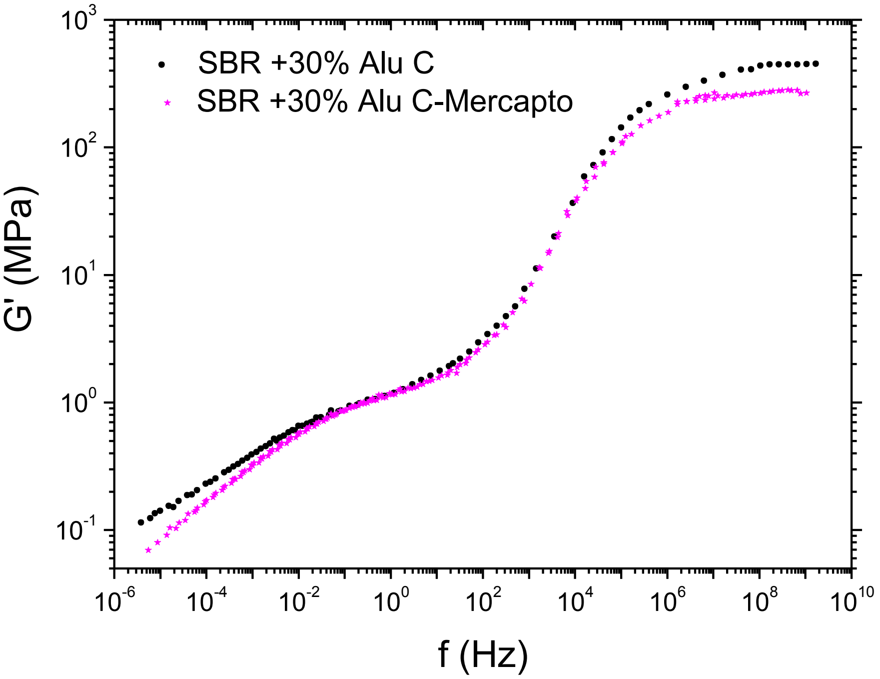

b)

Figure III.50. Storage G’ and loss G” shear moduli of the SBR/Alu C-Mercapto nanocomposites containing a) 20 and b) 30% of the nanoparticles.

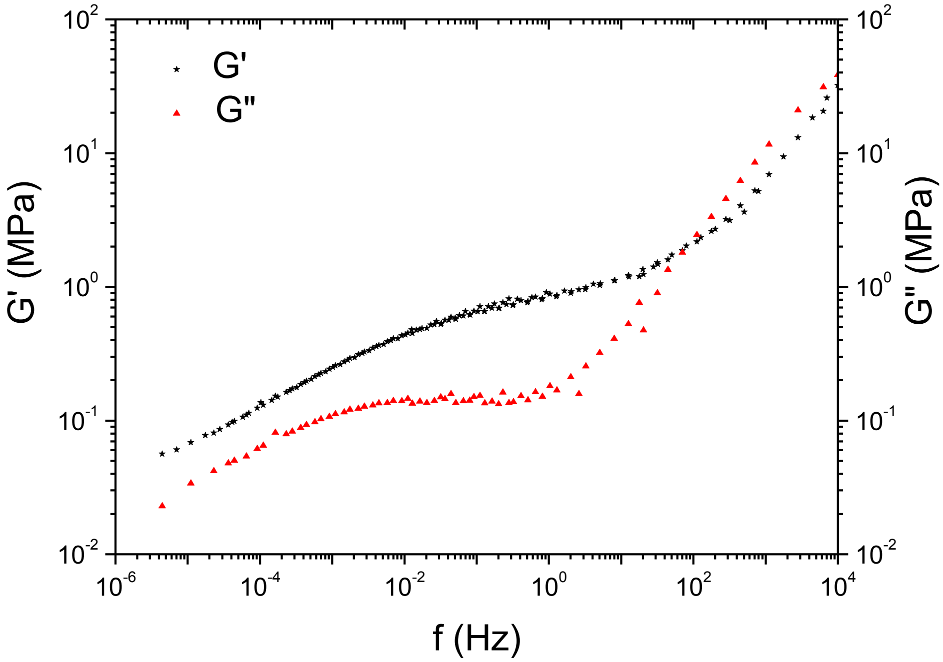

Figure III.51. Storage G' and loss G" shear moduli of the SBR/20% Alu C-Mercapto nanocomposite.

Having established that the Mercapto layers at the fillers' surfaces are less hydrophilic than the surfaces of the neat AluC, we assume that interactions between nanoparticles and hydrophobic matrix molecules gain in importance. If we assume that the particles are perfectly dispersed in the rubber matrix (or at least that the dispersion quality is comparable to the one achieved for the corresponding SBR/AluC samples), we expect a stronger influence of the fillers on the glass transition as the one observed in case of the SBR/AluC systems.

This would mean that, at higher filler concentrations, the T_g's of the SBR/AluC-Mercapto nanocomposites are expected to become larger than the glass transition temperatures of the corresponding. However, our finding, confirmed by TMDSC measurements and rheometric tests, is that at high enough filler concentrations the glass transition temperatures are lower than those of the corresponding SBR/AluC systems. As a possible explanation of the discrepancy we suggest that, due to the surface treatment with Mercapto-molecules, the surface corrugation of the alumina agglomerates changes. If we surmise that silanization flattens the surfaces of the agglomerates (reduction of corrugation) then simple mechanical coupling of SBR molecules to the filler's surfaces could be hindered. As a consequence the number of SBR molecules with reduced mobility (due to "mechanical" entanglement with the fillers surfaces) decreases. Our experimental results (e.g. $T_g($SBR/AluC-Mercapto$)\approx T_g($SBR$)$ and $\Delta c_p{'}^{SBRcorr}\approx\Delta c_p{'}$ (SBR) at $w_{filler}\geq 4\%$ (see Fig.III.40 and Fig.III.41)) suggest that the latter mechanism is dominant if we deal with SBR/AluC-Mercapto nanocomposites. In general, mechanical sticking of SBR molecules to nanoparticles can lead to the creation of additional crosslinks in the SBR matrix. The number of nodes in the SBR matrix determines the elasticity of the rubbery plateau and the strength of the gel-like structure under “terminal” regime conditions. We observe that the shear moduli measured on SBR/AluC-Mercapto systems in the rubbery plateau and “terminal” regimes (see Fig.III.47-III.48, Fig.III.50) are lower than those obtained for the corresponding SBR/AluC systems. This observation supports the assumption that due to the modification of the alumina’s surface corrugation by the γ-mercaptopropyltrimethoxysilane layers the number of “mechanical” links between SBR molecules and AluC-Mercapto fillers is reduced.

III.6.3.2 SBR/AluC-Mercapto grafted nanocomposites

Figures III.52 and III.53 show the rubbery plateau and “terminal” regime parts of the master curves constructed for the storage shear modulus G'(f) and loss shear modulus G"(f) of SBR/AluC-Mercapto grafted nanocomposites with filler contents w_{filler}=0; 4; 10; 20; 30%. The data shown corresponds to results obtained by DMA.

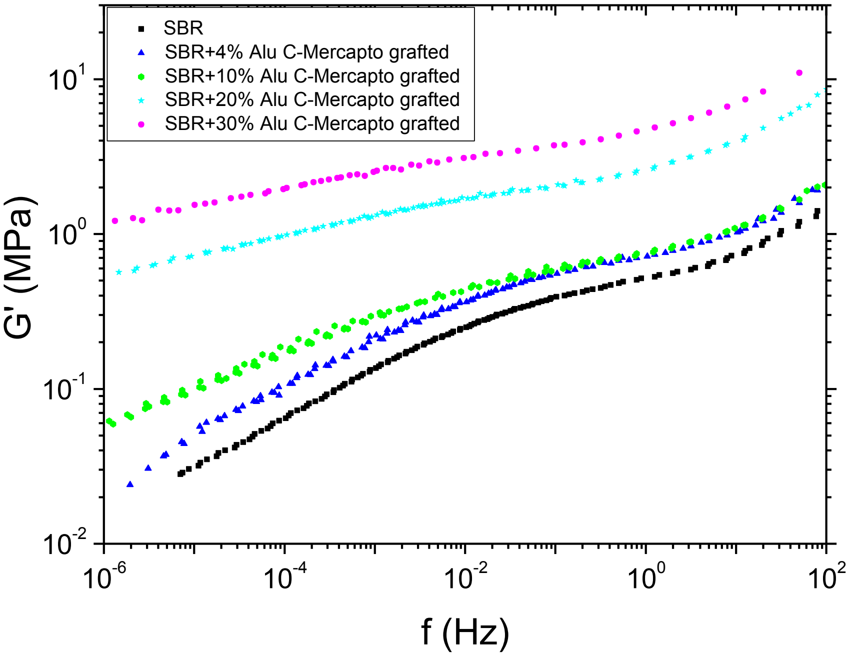

Figure III.52. Rubbery plateau and “terminal” regime parts of the DMA master curves G’(f) for SBR/Alu C-Mercapto grafted nanocomposites. Reference temperature T_0=273K.

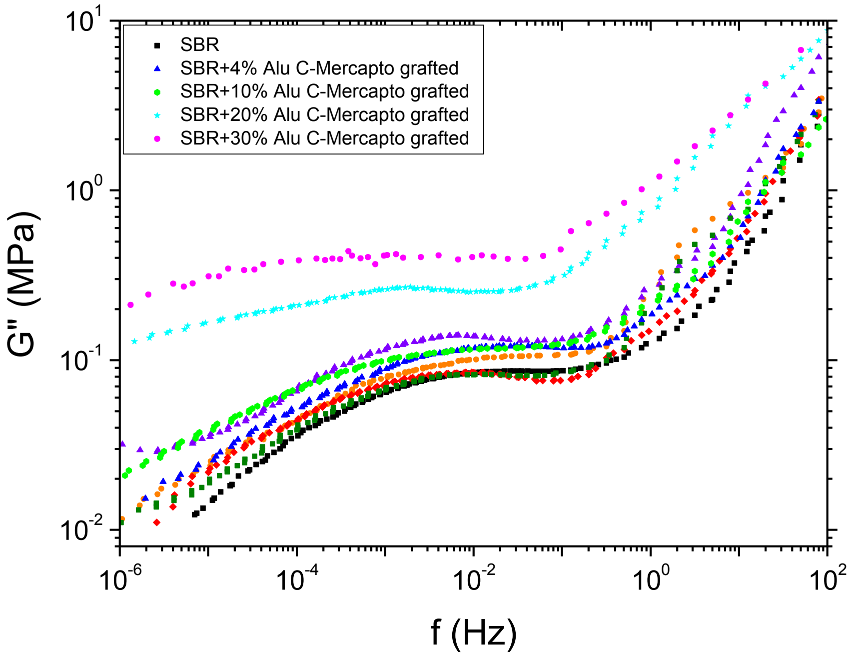

Figure III.53. Rubbery plateau and "terminal" regime parts of the DMA master curves G"(f) for SBR/Alu C-Mercapto grafted nanocomposites. Reference temperature T_0=273K.

In Fig.III.54 we exemplarily compare the low-frequency evolutions of the storage and loss shear moduli of the SBR/AluC-Mercapto grafted sample with a filler weight fraction of 20 %. As well in the rubbery plateau regime as in the "terminal" regime the behavior of the sample is solid-like: *G'>G''*. Again the slopes of *G'(f)* and *G"(f)* practically coincide under terminal regime conditions. The latter observation suggests gel-like behaviour of the sample at the lowest probe frequencies.

Fig. III.55 allows comparing the frequency dependences of the storage shear moduli of neat SBR and the 20 wt% representatives of the three families of nanocomposites. Clearly, in the rubbery plateau regime, the largest reinforcement is achieved by the SBR/AluC-Mercapto grafted sample. At a frequency *f*=0.1 Hz the reinforcements for the three samples with a filler fraction of 20% are:

$$\frac{G'(SBR\,/\,AluC)}{G'(SBR)} = 1.9$$

$$\frac{G'(SBR\,/\,AluC - Mercapto)}{G'(SBR)} = 1.7$$

$$\frac{G'(SBR\,/\,AluC - Mercapto\ grafted)}{G'(SBR)} = 5.3$$

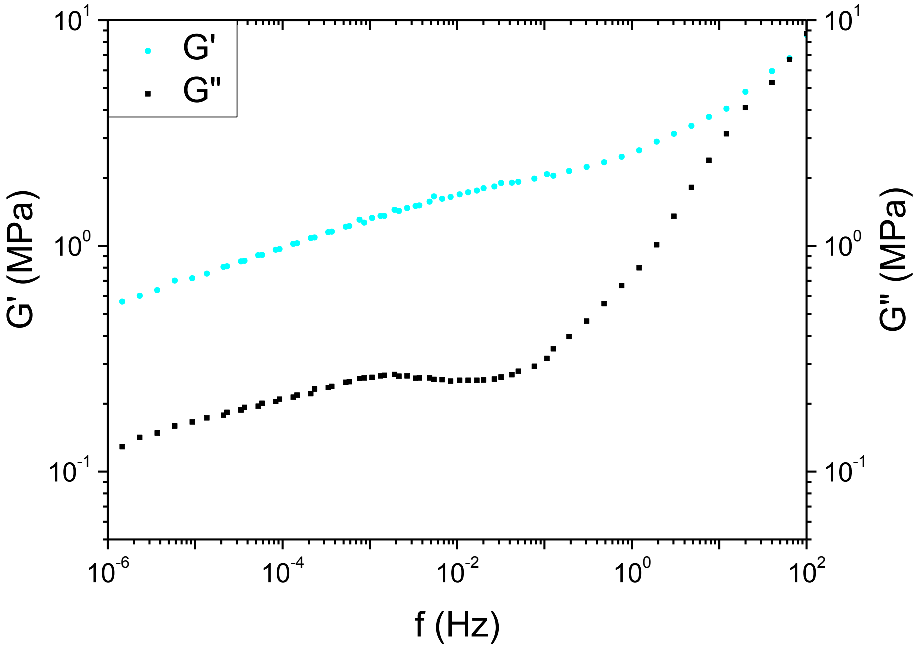

Figure III.54. Rubbery plateau and "terminal" regime parts of the DMA master curves G'(f) and G"(f) for SBR/20% Alu C-Mercapto grafted nanocomposite. Reference temperature T_0=273K.

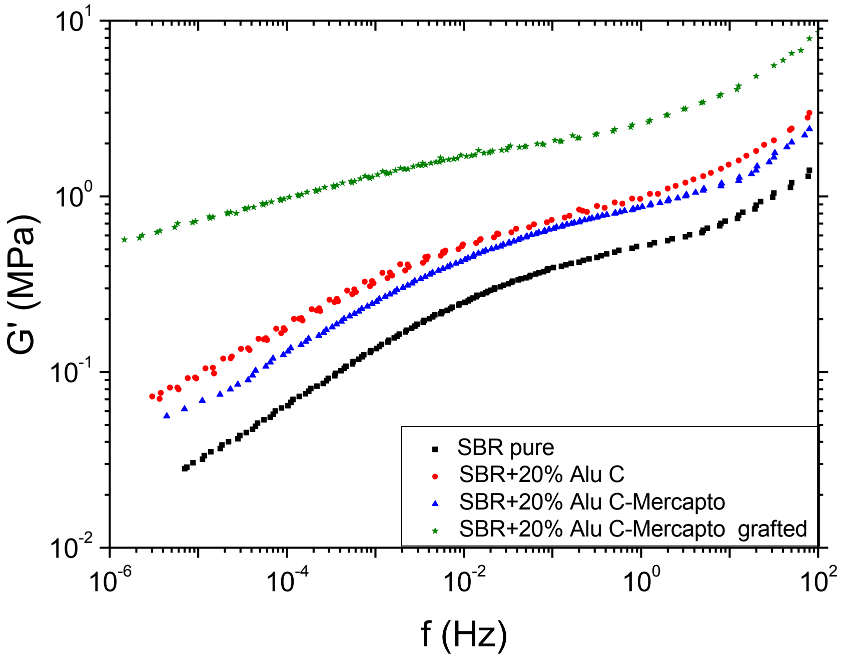

Figure III.55. Comparison of the frequency dependences of the storage shear moduli of neat SBR and the 20 wt% representatives of the three families of nanocomposites. Data is shown for the rubbery plateau and the "terminal regime.

At the lowest frequencies, i.e. under "terminal" regime conditions, the most striking effect consists in the important change of slope of the *G'(f)* curves. For sake of clarity we have represented in Fig.III.56 the slopes of the "terminal" regime tails of the storage modulus master curves for neat SBR and the 20 wt% representatives of the three families of investigated nanocomposites. Obviously the slope for the SBR/AluC-Mercapto grafted system is twice as low as the one calculated for the SBR/Alu C system and nearly three times smaller than the one obtained for the neat SBR system. Solid-like behavior is even slightly more pronounced for the 30 wt% sample of the SBR/AluC-Mercapto grafted nanocomposites (Fig.III.52).

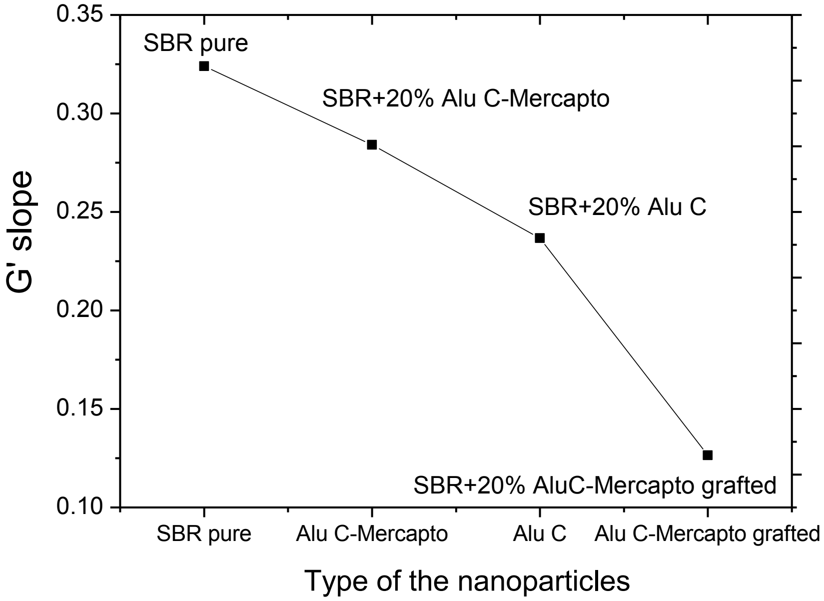

Figure III.56. Comparison of the slopes of the "terminal" regime tails of the G'(f) master curves for neat SBR and the 20 wt % representatives of the three families of investigated nanocomposites. The lines are just guides for the eyes.

The pronounced solid-like low-frequency behavior ("terminal" regime) of the SBR/AluC-Mercapto grafted samples with the two highest filler loads suggests the appearance of a second network in the nanocomposites at high enough concentrations. The formation of the first network, which manifests itself by gel-like behavior shown by all of the investigated samples (even neat SBR), at the lowest frequencies is a result of physical crosslinks between SBR molecules and SBR/nanoparticle interactions. From TMDSC measurements (see subchapter III.6.2) we know about the existence of layers of bound rubber at the surfaces of the fillers in the SBR/AluC-Mercapto grafted samples. SBR molecules are chemically bound to the nanoparticles.

We tend to assume that grafting of SBR molecules to AluC-Mercapto nanoparticles leads to:

(i) An enhancement of the SBR/nanoparticle interactions, which at low filler contents, results in a modest increase of reinforcement compared to the SBR/AluC nanocomposites.

Comparing e.g. the storage moduli of the 4 wt% and 10 wt % samples of the SBR/AluC and SBR/AluC –Mercapto grafted nanocomposites we find the following values (see Fig.III.27 and Fig.III.52):

	$SBR\,/\,AluC$	$SBR\,/\,AluC - Mercapto\ grafted$
$4\ wt\%\ sample$	$G' = 0{,}08\ MPa$	$G' = 0{,}105\ MPa$
$10\ wt\%\ sample$	$G' = 0{,}111\ MPa$	$G' = 0{,}174\ MPa$

While in case of the SBR/AluC and SBR/AluC-Mercapto systems only those particles interacting with SBR molecules (e.g. via mechanical entanglement) are possible "candidates" for additional network nodes, in case of the systems with grafted SBR molecules all of the fillers have to be considered as possible nodes. An enhancement of the SBR/nanoparticle interactions, which at low filler contents results in a modest increase of reinforcement compared to the SBR/Alu C nanocomposites.

(ii) Interactions between fillers mediated by SBR molecules chemically attached to the particles' surfaces (and possibly also molecules entangling with latter) when the concentration of the nanoparticles becomes so high that the average distance between the Alu C allows for establishing links. We surmise that this kind of specific interactions generates a second network in the SBR matrix, which is supposed to be responsible for the elasticity of the samples with the highest filler loads.

References:

[1] K.S. Chen, R.Y. Yen and Y.-M. Chou, On the Thermal Decomposition Kinetics of Styrene-Butadiene Rubber in Nitrogen Atmosphere, *Environmental Engineering Science*, 1997, 14 (3), p.175-181.

[2] P. Mélé, S. Marceau, D. Brown, Y. de Puydt, N.D. Albérola, Reinforcement effects in fractal-structure-filled rubber, *Polymer*, 2002, 43, p.5577-5586.

[3] B. Wetzel, P. Rosso, F. Haupert and K. Friedrich, Epoxy nanocomposites - fracture and toughening mechanisms, *Engineering Fracture Mechanics*, 2006 , 73, p.2375-2398.

[4] J. Baller, M. Thomassey, M. Ziehmer and R. Sanctuary, Thermoplastic and thermosetting polymers and composites, ed L.D. Tsai and M.R. Hwang (Hauppauge: Nova Science Publishers), 2011, p.197-211.

[5] Roy J., Bandyopadhyay N., Das S., Maitra S. Studies of the formation of mullite from diphasic Al2O3-SiO2 gel by Fourier Transform Infrared Spectroscopy, *Iranian Journal of Chemistry and Chemical Engineering*, 2011, 30 (1), 2011, p.65-71.

[6] Shukla D.K., Kasisomayajula S.V., Parameswaran V. Epoxy composites using functionalized alumina platelets as reinforcements, *Composites Science and Technology*, 2008, 68, 14, p.3055–3063.

[7] Schawe J. E. K. A comparison of different evaluation methods in modulated temperature DSC, *Thermochimica Acta*, 1995, 260, p.1-16.

[8] N. Jouault, P. Vallat, F. Dalmas, S. Said, J. Jestin and F. Boué, Well-Dispersed Fractal Aggregates as Filler in Polymer− Silica Nanocomposites: Long-Range Effects in Rheology, *Macromolecules*, 2009, 42 (6), p.2031–2040.

[9] H.H. Winter and F. Chambon, Analysis of linear viscoelasticity of a crosslinking polymer at the gel point, *Journal of Rheology*, 1986, 30 (2), p.367-382.

[10] Robertson C.G., Lin C.J., Rackaitis M., Roland C.M., Influence of particle size and polymer-filler coupling on viscoelastic glass transition of particle-reinforced polymers, *Macromolecules*, 2008, 41, p.2727-2731.

[11] Zhang A., Wang L., Zhou Y., A study on rheological properties of carbon black extended powdered SBR using a torque rheometer, *Polymer Testing*, 2003, 22, p.133-141.

[12] Gauthier C., Reynaud E., Vassoille R., Ladouce-Stelandre L. Analysis of the non-linear viscoelastic behaviour of silica filled styrene butadiene rubber, *Polymer*, 2004, 45, p.2761-2771.

[13] Xiang K., Wang X., Huang G., Zheng J., Huang J., Li G. Thermal ageing behavior of styreneebutadiene random copolymer: A study on the ageing mechanism and relaxation properties, *Polymer Degradation and Stability*, 2017, 97, p.1704-1715.

[14] Hassan H.H., Ateia E., Darwish N.A., Halim S.F., Abd El-Aziz A.K. Effect of filler concentration on the physico-mechanical properties of super abrasion furnace black and silica loaded styrene butadiene rubber, *Materials and Design*, 2012, 34, p. 533–540.

[15] Cerveny S., Ghilarducci A., Salva H., Marzocca A.J. Glass-transition and secondary relaxation in SBR-1502 from dynamic mechanical data, *Polymer*, 2000, 41, p.2227–2230.

[16] Kummali M.M., Miccio L.A., Schwartz G.A., Alegría A., Colmenero J., Otegui J., Petzold A., Westermann S., Local mechanical and dielectric behavior of the interacting polymer layer in silica nano-particles filled SBR by means of AFM-based methods, *Polymer*, 2013, 54, p.4980-4986.

[17] Guo B., Lei Y., Chen F., Liu X., Du M., Jia D., Styrene–butadiene rubber/halloysite nanotubes nanocomposites modified by methacrylic acid, *Applied Surface Science*, 2008, 255, p.2715–2722 .

[18] Huth H., Beiner M., Donth E., Temperature dependence of glass-transition cooperativity from heat-capacity spectroscopy: Two post-Adam-Gibbs variants, *Physical review B*, 2000, 61 (22), p.15092-15101.

[19] T.E. Rolando, Solvent-Free Adhesives, *Rapra Review Reports*, 1998, V.9, 5, p.10.

[20] Tsagaropoulos G, Eisenberg A. Dynamic mechanical study of the factors affecting the two glass transition behavior of filled polymers. Similarities and differences with random ionomers, *Macromolecules*, 1995, 28 (18), p.6067–6077.

[21] Arrighi V, McEwen I J, Qian H and Prieto M B S The glass transition and interfacial layer in styrene-butadiene rubber containing silica nanofiller, *Polymer*, 2003, 44, 6259-66.

[22] J. Baller, M. Thomassey, M. Ziehmer and R. Sanctuary, Thermal and chemical glass transition of thermosets in the presence of two types of inorganic nanoparticles, In: Thermoplastic and Thermosetting Polymers and Composites, Ed.: Linda D. Tsai and Matthew R. Hwang, Nova Science Publishers, Inc. 2011.

[23] Sargsyan A., Tonoyan A., Davtyan S., Schick C. The amount of immobilized polymer in PMMA SiO_2 nanocomposites determined from calorimetric data, *European Polymer Journal*, 2007, 43, p.3113-3127.

[24] Handbook of Thermal Analysis and Calorimetry, Volume 3: Applications to Polymers and Plastics S. Z. D. Cheng, editor, Chapter 1, Heat capacity of polymers B. Wunderlich, p.1-828 (2002).

[25] G.R. Strobl, The Physics of Polymers, Concepts for Understanding Their Structures and Behavior, 3rd ed. 2007, XIV, 518, 295p.

[26] Heinrich G., Kluppel M. and Vilgis T.A., Reinforcement of elastomers, *Current Opinion in Solid State & Materials Science*, 2002, 6, p. 195-203.

[27] Bindu P. and Thomas S., Viscoelastic Behavior and Reinforcement Mechanism in Rubber Nanocomposites in the Vicinity of Spherical Nanoparticles, *Journal of Physical Chemistry B*, 2013, 117, p.12632-48.

[28] Sushko R., Filimon M., Dannert R., Elens P., Sanctuary R. and Baller J., Anomalous glass transition behavior of SBR–Al_2O_3 nanocomposites at small filler concentrations, *Nanotechnology*, 2014, 25 (42), p.425704-11.

[29] Shi G., Zhang M.Q., Rong M.Z., Wetzel B., Friedrich K., Sliding wear behavior of epoxy containing nano-Al_2O_3 particles with different pretreatments, *Wear*, 2004, 256, p.1072–1081.

[30] Zang D., Paul B., Xu W., Zuan Z., Liu E., Ke X., Wellard R.M., Guo C., Xu Z., Sun Z., Yhu H., Alumina nanofibers grafted with functional groups: A new design in efficient sorbents for removal of toxic contaminants from water, *Water Research*, 2010, 44 (3), p.741-750.

[31] Hu M., Noda S., Okubo T., Yamaguchi Y., Komiyama H., Structure and morphology of self-assembled 3-mercaptopropyltrimethoxysilane layers on silicon oxide, *Applied Surface Science*, 2001, 181 (3–4), p.307–316.

Chapter IV: Conclusions

In the present work styrene-butadiene rubber (SBR) rubber was used as matrix for three types of nanoparticles: untreated alumina (AluC), alumina covered with γ-mercaptopropyltrimethoxysilane (Mercapto) layers and finally fillers with SBR molecules grafted on the surfaces of the AluC-Mercapto nanoparticles.

The aim of the project was to shed light on the influence of surface treatment of a specific type of nanoparticles on the thermal, mechanical and rheological properties of the SBR matrix. Although the matrix is (chemically) uncured, physical crosslinks between SBR molecules impede the development of ideal terminal behavior at the lowest frequencies. In the low-frequency range ("terminal" regime) the matrix behaves solid-like ($G'>G''$). As under "terminal" conditions the loss tangent does practically not change we qualify the corresponding behavior of the SBR matrix as gel-like.

The thermal and mechanical properties of the SBR matrix and of the three families of nanocomposites were investigated by calorimetry and mechanical spectroscopy (DMA and rheometry). Electron microscopy (TEM and ESEM) was exploited for the structural analysis of the filled systems. At low filler concentrations structural analysis reveals that the particles are rather homogeneously dispersed as aggregates throughout the SBR matrix. At higher nanoparticle contents the fractal aggregates tend to cluster and form larger agglomerates.

Most interestingly an unexpected minimum of the glass transition temperature at small filler concentrations could be found for the three families of investigated nanocomposites. Irrespective of the surface treatment of the nanoparticles, $T_g(w_{filler})$ takes its lowest value at about 1.5-2.0 wt.%. Acceleration of molecular dynamics is considered as being a consequence of a reduction of the number of entanglements due to the mere presence of the nanoparticles during sample preparation from solution. The accelerating influence can be limited by the total amount of entanglements present in the neat rubber. Structural changes undergone by the nanoparticles when the filler concentration increases could be another reason for the limitation of the acceleration of the molecular dynamics by the nanoparticles: as a matter of fact with increasing filler content the number of agglomerates present in the SBR matrix grows. Hence the number of particles available as obstacles for physical crosslinking does not necessarily increase to the same degree as w_{filler}. Moreover, there is an underlying trend to higher glass transition temperatures with higher nanoparticle content. The higher the filler content, the more nanoparticle/rubber interactions and possibly also confinement take influence on the molecular dynamics.

By increasing the nanoparticle content of the SBR matrix we were able to observe three different evolutions of the glass transition temperature. For concentrations $w_{filler} \geq 4\%$, the maximal increase of the glass transition temperature with respect to neat SBR is about 1,5 K in case of the SBR/AluC systems and 4 K when we deal with SBR/AluC-Mercapto grafted nanocomposites. T_g does practically not change with respect to the glass transition temperature of neat SBR when the matrix is filled with AluC/Mercapto nanoparticles. The slight increase of T_g observed in case of the SBR/AluC systems is explained by weak interactions between the hydrophobic SBR molecules and the hydrophilic surfaces of the alumina nanoparticles. We assume that surface corrugation of the fractal alumina aggregates and agglomerates favors entanglements (mechanical links) between rubber molecules and the fillers' surfaces. γ-mercaptopropyltrimethoxysilane layers at the surfaces of the fillers possibly "flatten" the surfaces of the nanoparticles and thus render the establishment of mechanical links between matrix molecules and alumina more difficult. This scenario allows for understanding the non-appearance of a deceleration of the structural α-process with respect to the neat SBR in case of the high-loaded SBR/AluC-Mercapto nanocomposites. Mercapto-layers are indeed supposed to reduce the hydrophilic character of the surfaces of the alumina nanoparticles and thus to promote interactions between the fillers and the matrix molecules. Our finding regarding the evolution of the glass transition temperature of the SBR/AluC-Mercapto nanocomposites suggests that the enhancement of rubber/filler interactions seems to be overcompensated by the effect resulting from a possible flattening of the AluC's surfaces by the γ-mercaptopropyltrimethoxysilane layers. Finally, in case of the SBR/AluC-Mercapto grafted systems, where SBR molecules are chemically linked to the surfaces of the AluC-Mercapto nanoparticles, our experimental results point to the existence of layers of bound rubber (layers of SBR molecules with reduced mobility) at the surfaces of the fillers. In contrast to findings reported in literature, there is no experimental evidence for the emergence of an additional glass transition, which might be associated to regions of SBR molecules with reduced mobility. Whatever the investigated system under consideration we only observe a single glass transition. We can only report on an increase of the glass transition temperature by about 4 K with respect to neat SBR. This increase goes along with a systematic decrease of the step height of the specific storage heat capacity - a clear hint at a reduction of the number of configurational degrees of freedom associated to the SBR molecules.

The most substantial reinforcements of the SBR matrix at low frequencies (rubbery plateau and "terminal" regime) could be observed on the SBR/AluC-Mercapto grafted systems with the two highest loads of fillers (20 wt% and 30wt%). At lower nanoparticle contents the reinforcements remain rather comparable to the ones achieved by the corresponding samples of the SBR/AluC family of nanocomposites. We assume that at large enough nanoparticle concentrations, the average distance between the alumina aggregates and agglomerates gets so small that interactions between the nanoparticles can be mediated by SBR molecules which are chemically attached to the fillers' surfaces and possibly also by other matrix molecules entangling with those fixed to the alumina. We thus surmise that besides the original physical network of entangled SBR molecules (already existing in the neat matrix) a second network formed by nanoparticles is created and leads to the enhanced mechanical properties of the highly loaded SBR/AluC-Mercapto nanocomposites (Figure IV.1).

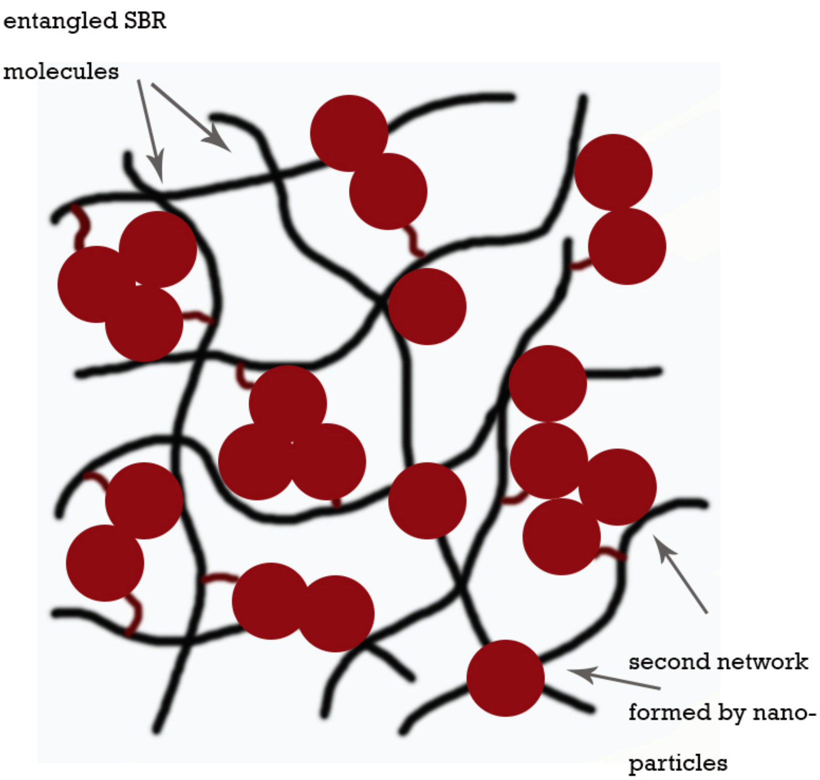

Figure IV.1. Schematic illustration of physical and chemical networks existing in grafted SBR/Al_2O_3 nanocomposites.

We believe that the modest reinforcement measured for the SBR/AluC systems results from an increasing number of nodes reinforcing the network of SBR molecules. Interactions between matrix molecules and nanoparticles possibly lead to additional nodes for SBR molecules. From the observation that in case of the SBR/AluC-Mercapto systems the reinforcement effect is smaller compared to the one measured on the SBR/AluC nanocomposites we discreetly deduce that entanglement of SBR molecules with the corrugated surfaces of the fractal nanoparticles might play an important role in context with reinforcement of the SBR matrix. The surface treatment of the AluC nanoparticles could possibly lead to a certain “flattening” of the corrugated filer surfaces.

Annexes

Annex I. TGA thermograms

As it was mentioned in Chapter III.1, SBR shows initial decomposition at about 330°C and the final decomposition at 500°C. Figure A.1. illustrates the weight loss graphic for neat SBR.

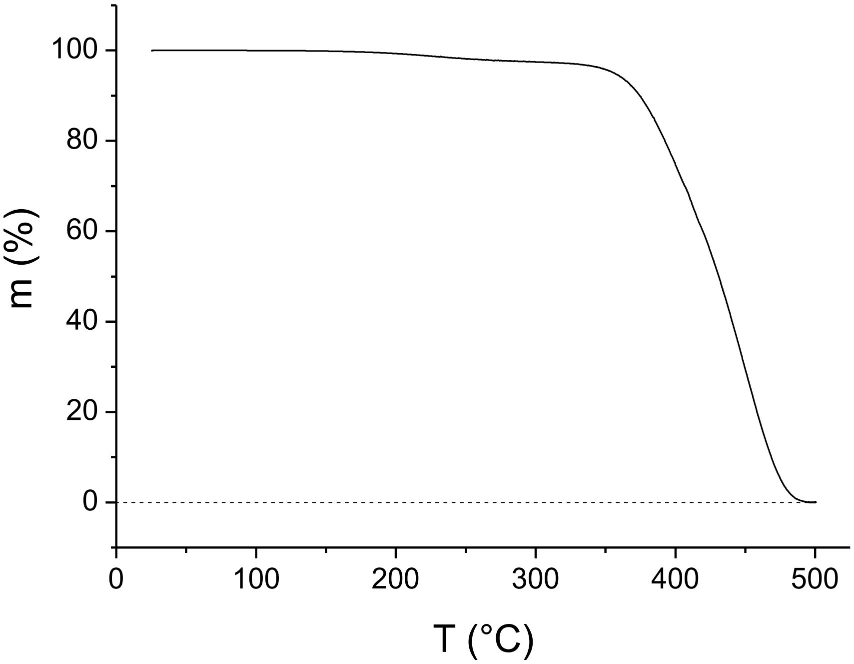

Figure A.1. TGA thermogram of the neat SBR.

Alumina nanoparticles are stable at such temperatures and only loose absorbed water (Fig.A.2). Surface-treated AluC nanoparticles, except water, contain organic part (γ-mercaptopropyltrimethoxysilane) which decomposes at high temperatures. Fig.A.3. shows the thermogram of the silanized AluC nanoparticles.

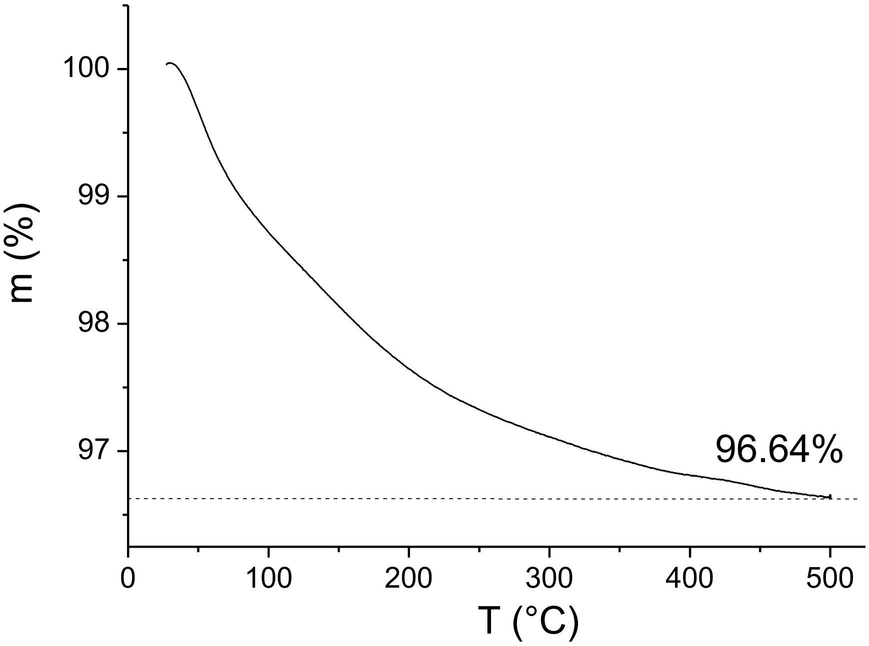

Figure A.2. TGA thermogram of the Alu C nanoparticles.

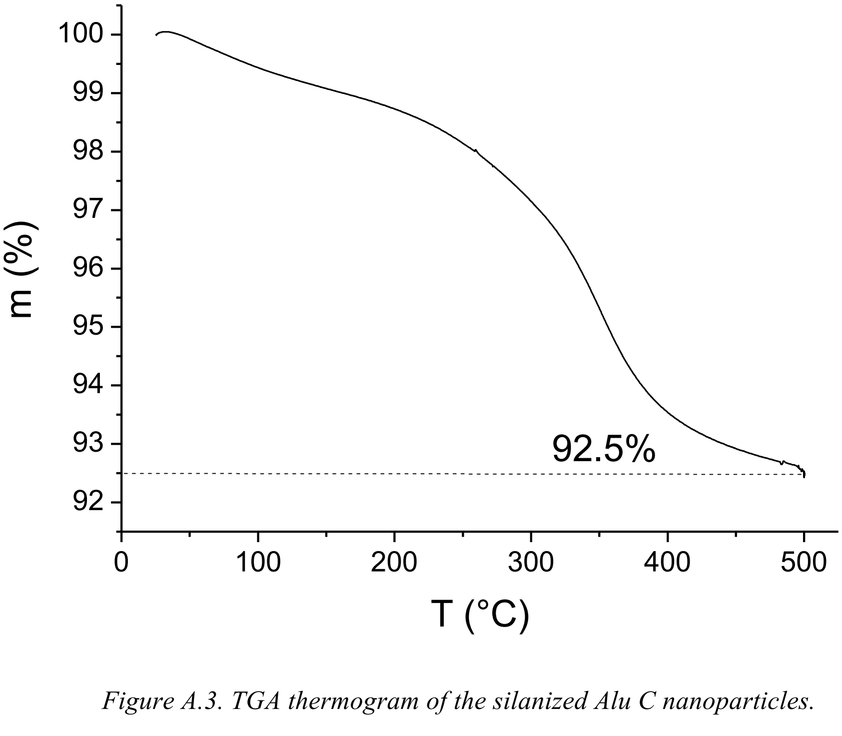

Figure A.3. TGA thermogram of the silanized Alu C nanoparticles.

Annex II. ESEM micrographs of the nanocomposites

The morphology of cross-sectioned areas at the specimen surface was examined by the Environmental Scanning Electron Microscopy (ESEM). The scanning electron microscope (Quanta 400 FEG ESEM) was operated at a high pressure (100Pa) and an accelerated voltage of 5kV.

Examples of dispersion of AluC nanoparticles in the rubber matrix for the SBR/Alu C nanocomposites are presented in Fig. A.4.

The electron microscopy for a large scale (14 µm) was carried out to get an idea regarding the dispersion of AluC nanoparticles. The small white spots presented in the electron micrographs show rather good dispersion of AluC in SBR matrix. In case of high filler contents a tendency towards aggregation of the AluC nanoparticles in rubber matrix is observed (Fig.A.4).

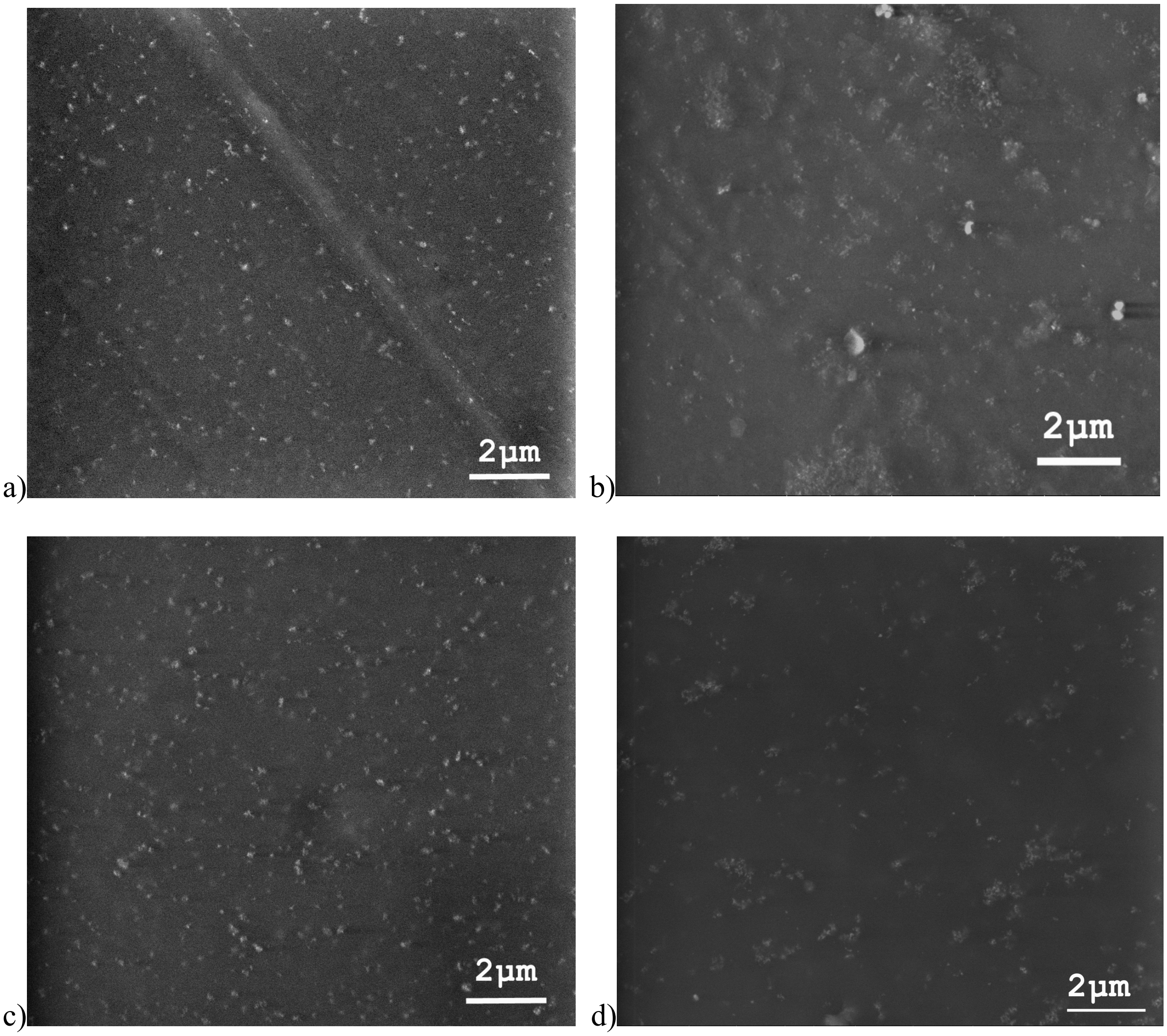

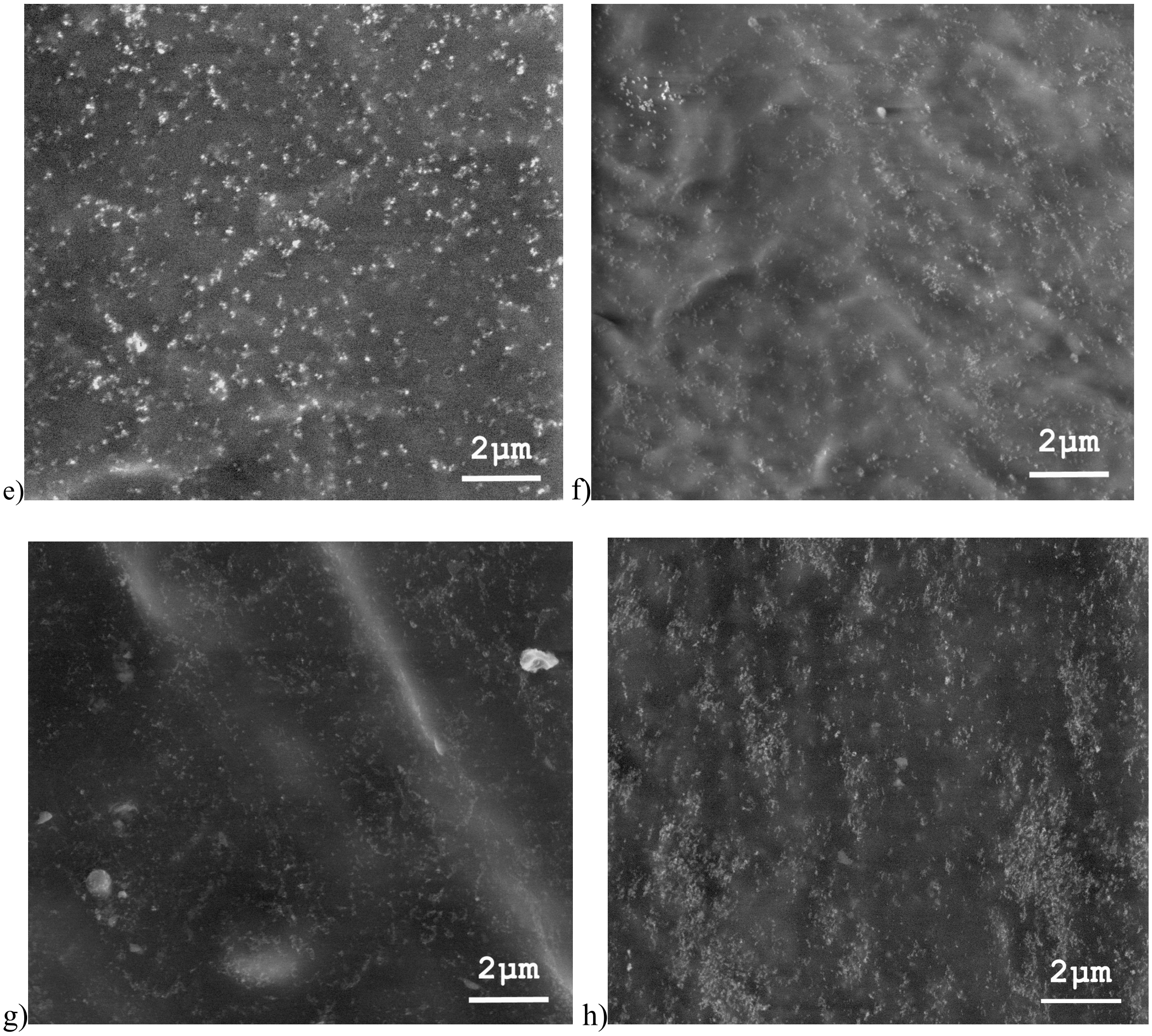

Figure A.4. ESEM micrographs of the SBR/Alu C nanocomposites containing: a) 1% Alu C; b) 1.5% Alu C; c) 2% Alu C; d) 3% Alu C; e) 4% Alu C; f) 10% Alu C; g) 20% Alu C; h) 30% Alu C. Scale: 2μm.

Small scale micrographs were also taken and show good dispersion at that scale the average size of the nanoparticle agglomerates usually less than 500nm (Fig. A.5- A.7).

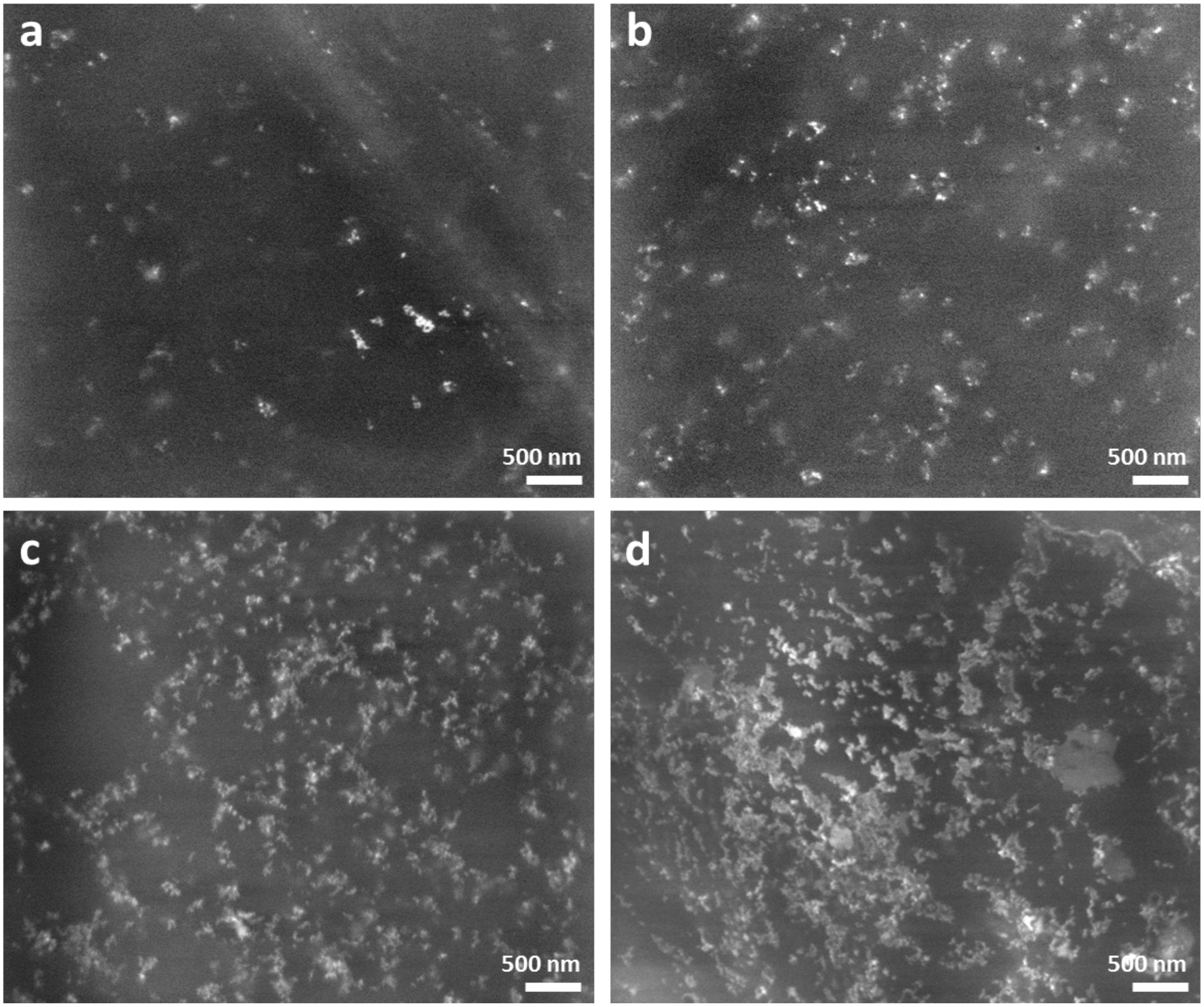

Figure A.5. ESEM micrographs of (a) SBR/1% Alu C, (b) SBR/4% Alu C, (c) SBR/10% Alu C, (d) SBR/20% Alu C. Scale: 500nm.

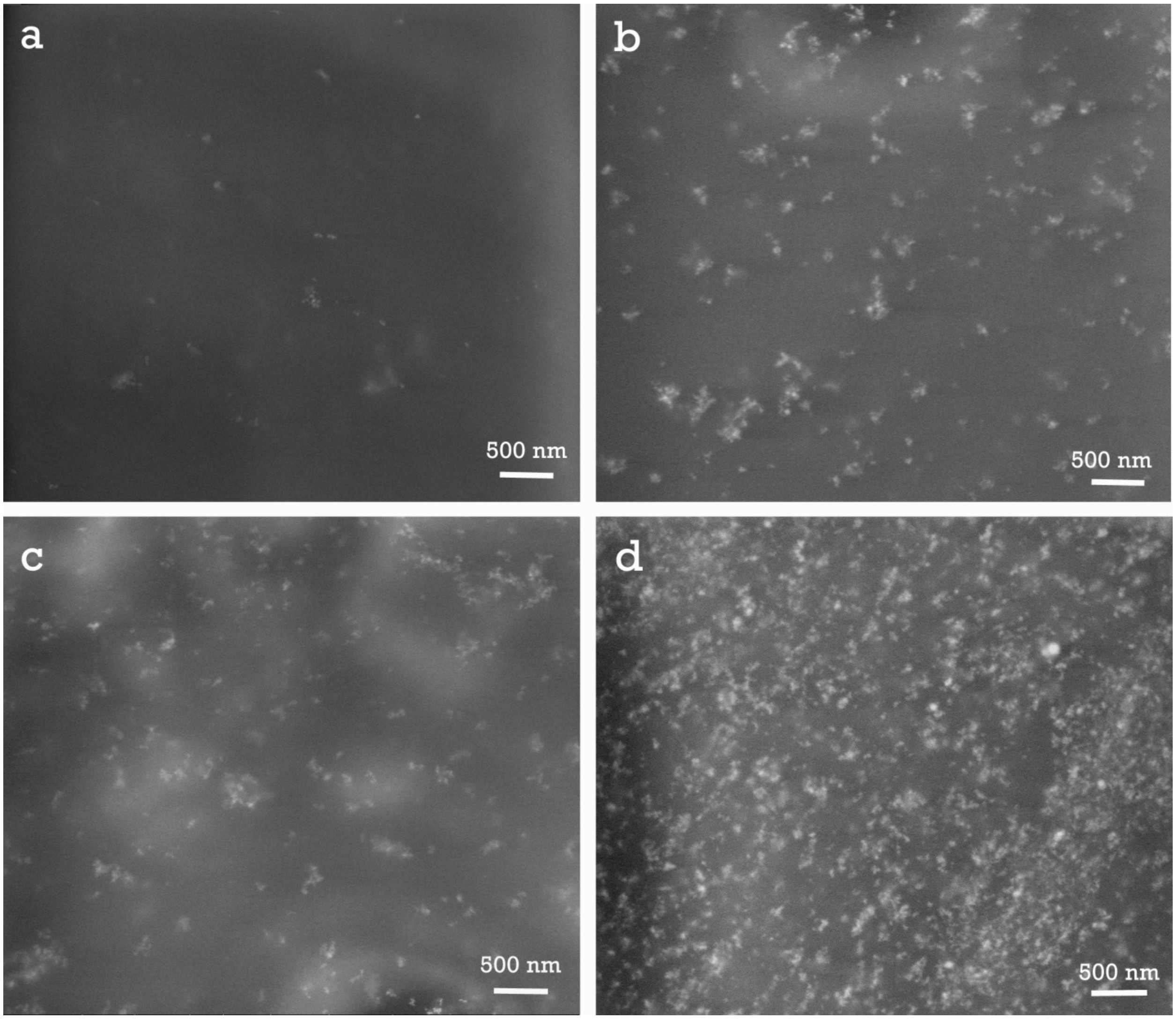

Figure A.6. ESEM micrographs of (a) SBR/1% Alu C-Mercapto, (b) SBR/4% Alu C-Mercapto, (c) SBR/10% Alu C-Mercapto, (d) SBR/20% Alu C-Mercapto. Scale: 500nm.

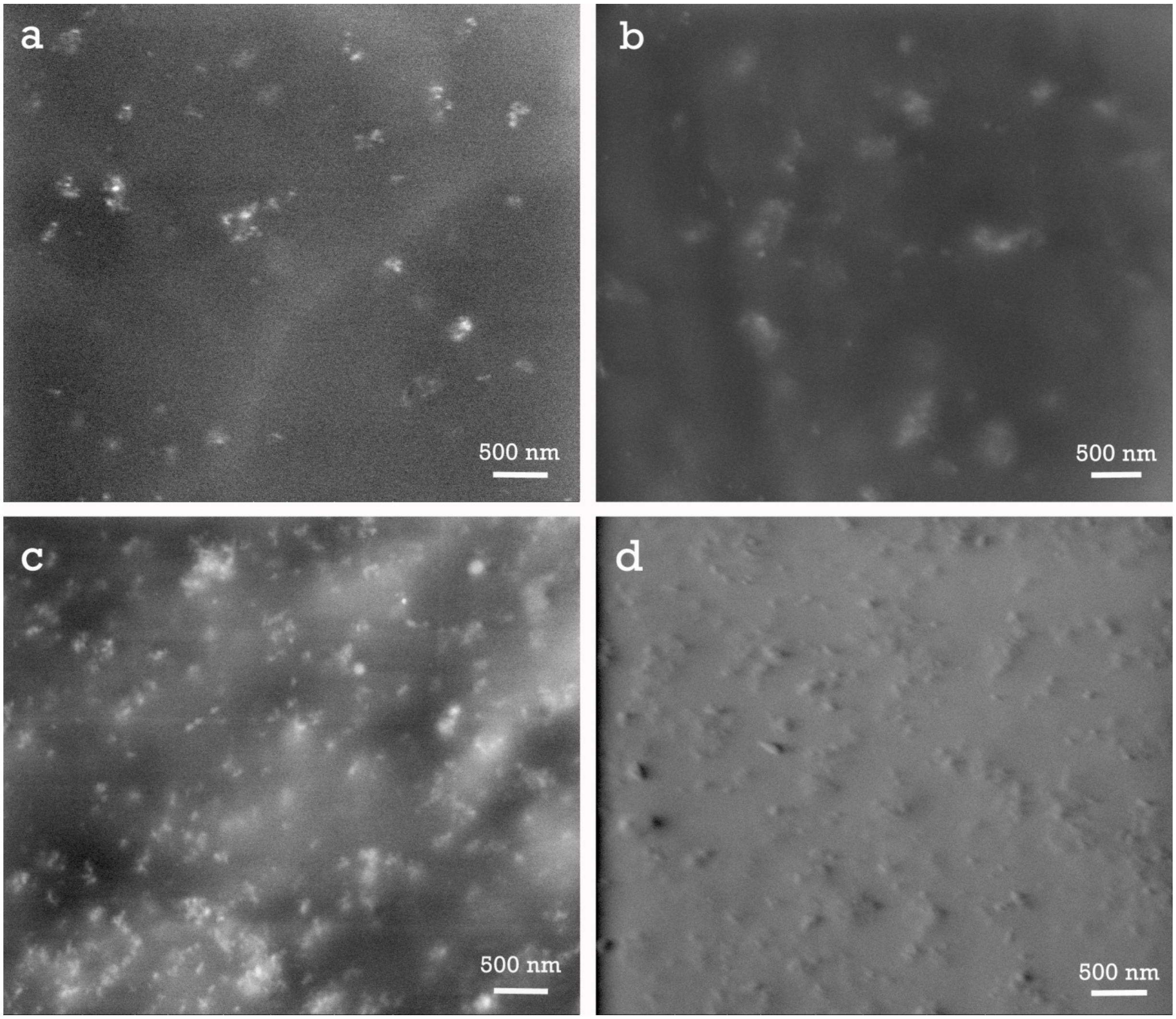

Figure A.7. ESEM micrographs of (a) SBR/1% Alu C-Mercapto grafted, (b) SBR/4% Alu C-Mercapto grafted, (c) SBR/10% Alu C-Mercapto grafted, (d) SBR/20% Alu C-Mercapto grafted. Scale: 500nm.

Annex III. FT-IR spectra of the nanocomposites

FT-IR investigations of the pure SBR, SBR/Alu C and SBR/Alu C-silanized nanocomposites were also carried out. FTIR spectra of the nanocomposites show characteristic peaks of SBR and aluminium oxide (Fig.A.8). The peaks of the silane functional groups are also observed in case of the SBR/Alu C-silanized nanocomposites. It is important to mention that no solvent trace is detected in samples – FT-IR spectra do not show characteristic $CHCl_3$ peaks (intensive peak of the C-Cl bond stretching vibration at 765 cm^{-1} and intensive peak of the C-H bond bending vibration at 1215-1220 cm^{-1}).

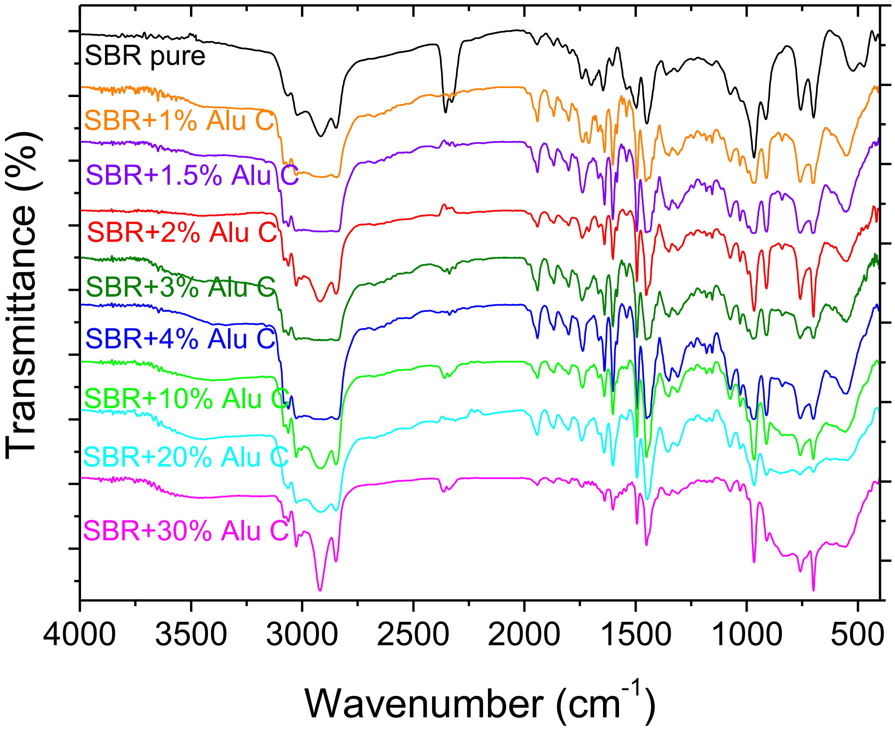

Figure A.8. FTIR spectra of SBR pure and SBR/Alu C nanocomposites.

Figure A.8 illustrates the FT-IR spectra for SBR pure and SBR/Alu C nanocomposites. The common peaks observed in all of the spectra are:

i. 550 cm^{-1} and 842 cm^{-1} corresponds to the PS unit vibrations *.

ii. 700 cm^{-1} and 755 cm^{-1} correspond to out-of-plane bending vibrations in aromatic monosubstituted ring.

iii. 908 cm^{-1} corresponds to the out-of-plane bending vibrations of (=CH_2) in CH_2=CH– group of the 1,2-polybutadiene units *.

iv. 972 cm^{-1} corresponds to the out-of-plane bending vibrations of C-H in -RCH=CHR- group of the 1,4-trans-polybutadiene units.

v. 995 cm^{-1} corresponds to the out-of-plane bending vibrations of (=CH–) in CH_2=CH– group of the 1,2-polybutadiene units.
vi. 1030 cm^{-1} corresponds to the C-H in-plane bending vibrations in aromatic monosubstituted ring.
vii. 1155 cm^{-1} and 1180 cm^{-1} correspond to the in-plane bending vibrations in aromatic monosubstituted ring.
viii. 1237 cm^{-1} corresponds to the C-H in-plane bending vibrations in 1,4-cis-polybutadiene units.
ix. 1310 cm^{-1} corresponds to the =C-H in-plane bending vibrations in -RCH=CHR-group of the 1,4-cis-polybutadiene units.
x. 1350 cm^{-1} corresponds to the C-H in-plane bending vibrations in CH_2 groups of the 1,4-trans and 1,4-cis-polybutadiene units.
xi. 1450 cm^{-1} corresponds to the C-H in-plane bending vibrations in CH_2 groups.
xii. 1496 cm^{-1}, 1583 cm^{-1} and 1600 cm^{-1} correspond to the stretching vibrations of C=C bond in aromatic ring.
xiii. 1640 cm^{-1} correspond to the stretching vibrations of the C=C bond in CH_2=CH-group of the 1,2-polybutadiene units.
xiv. 1745 cm^{-1}, 1800 cm^{-1}, 1865 cm^{-1} and 1941 cm^{-1} are the overtones of the out-of-plane bending vibrations of C-H in monosubstituted aromatic ring.
xv. 2843 cm^{-1} and 2917 cm^{-1} correspond to symmetrical and asymmetrical stretching of CH_2 groups.
xvi. 3006 cm^{-1} corresponds to the stretching vibration of the =CH-H bond in cis-RCH=CHR *.
xvii. 3028 cm^{-1} corresponds to the stretching vibration of the =CH-H bond in trans-RCH=CHR *.
xviii. 3060 cm^{-1} and 3080 cm^{-1} correspond to the stretching vibrations of the C-H bonds in the aromatic ring of the polystyrene units.

The spectra of the nanocomposites show also the peaks of the aluminium oxide:
x. 566 cm^{-1} corresponds to stretching vibration of Al-O in octahedral coordination **.
xi. 756 cm^{-1} corresponds to Al-O-Al stretching vibration in tetrahedral and octahedral coordination **.
xii. 828 cm^{-1} corresponds to stretching vibration of Al-O in tetrahedral coordination **.
xiii. 3451 cm^{-1} corresponds to O-H bond stretching vibration (surface hydroxyl groups of the Alu C nanoparticles and hydroxyl groups of absorbed water molecules).

Unfortunately, due to the difficult sample preparation, the quantitative FT-IR analysis is not possible for these nanocomposites.

The FT-IR spectra of the nanocomposites SBR/Alu C-Mercapto (Fig.A.9) and SBR/Alu C-Mercapto grafted show the characteristic peaks of the SBR component, as well as the peaks of the silanized filler particles described above. It is important to mention that Fig.A.9, comparing to Fig.A.8, doesn't show the broad peak of the OH-group stretching vibration at 3500-3400 cm^{-1} – this is the result of using silanized nanoparticles instead of untreated Alu C. Unfortunately, FT-IR spectra of the grafted nanocomposites cannot provide evidence of grafting and so there is no need to consider them.

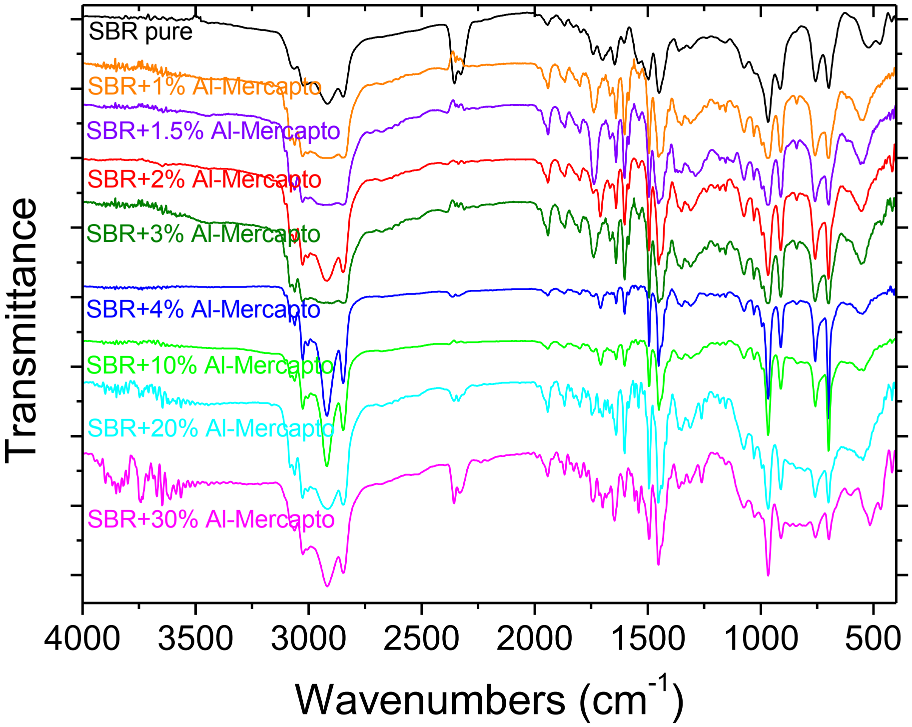

Figure A.9. FTIR spectra of SBR pure and SBR/Alu C-Mercapto nanocomposites.

* Orlov A.S., Kiselev S.A., Kiseleva E.A., Budeeva A.V. and Mashukov V.I. Determination of styrene-butadiene rubber composition by attenuated total internal reflection infrared spectroscopy. J. of Appl. Spectr., 2013, V.80, 1, p. 47-53.

** Roy J., Bandyopadhyay N., Das S., Maitra S. Studies of the formation of mullite from diphasic Al2O3-SiO2 gel by Fourier Transform Infrared Spectroscopy, Iran. J. Chem. Chem. Eng., 2011, 30 (1), 2011, p.65-71.

Annex IV. DMA and rheology

DMA linearity tests

In this work, all of the DMA measurements were performed in a linear response regime. To determine the parameters of this regime, force and displacement linearity tests were performed at different temperatures (25°C, -10°c and -40°C). Fig.A.10 illustrates the result of the force linearity test and Fig.A.11 illustrates the result of the displacement linearity test. The force of 1N and the displacement of 5µm (pointed out with dashed lines in Figures) were selected as parameters for further experiments.

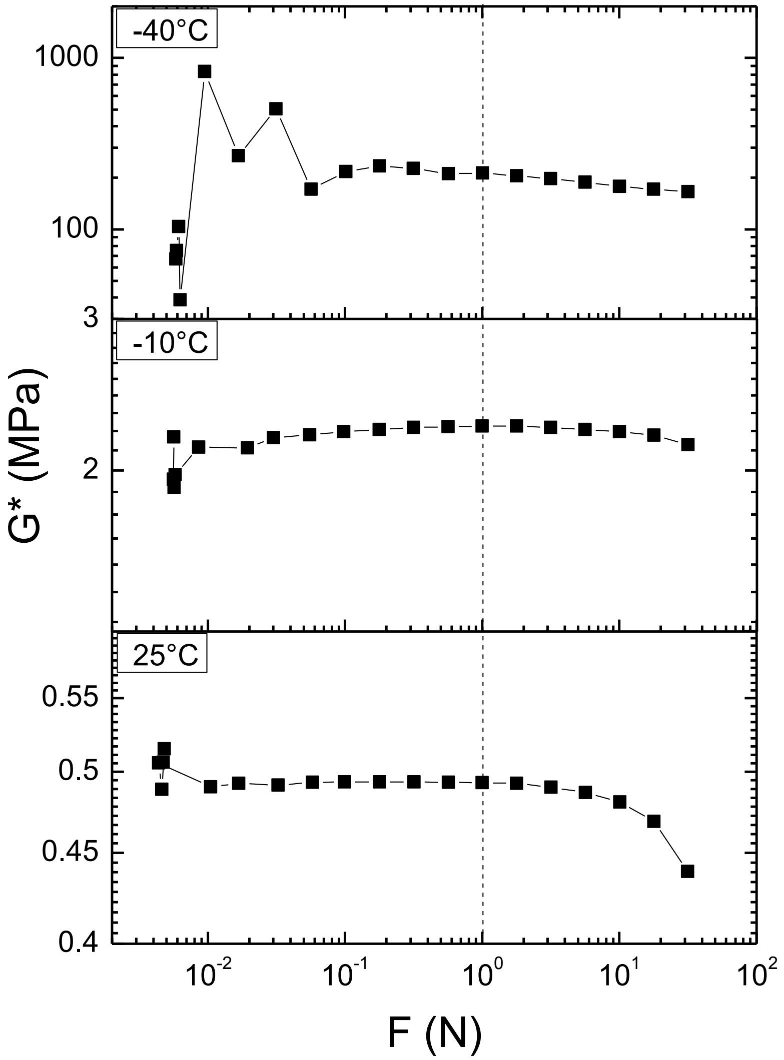

Figure A.10. DMA linearity test: Complex shear modulus G dependence upon force F.*

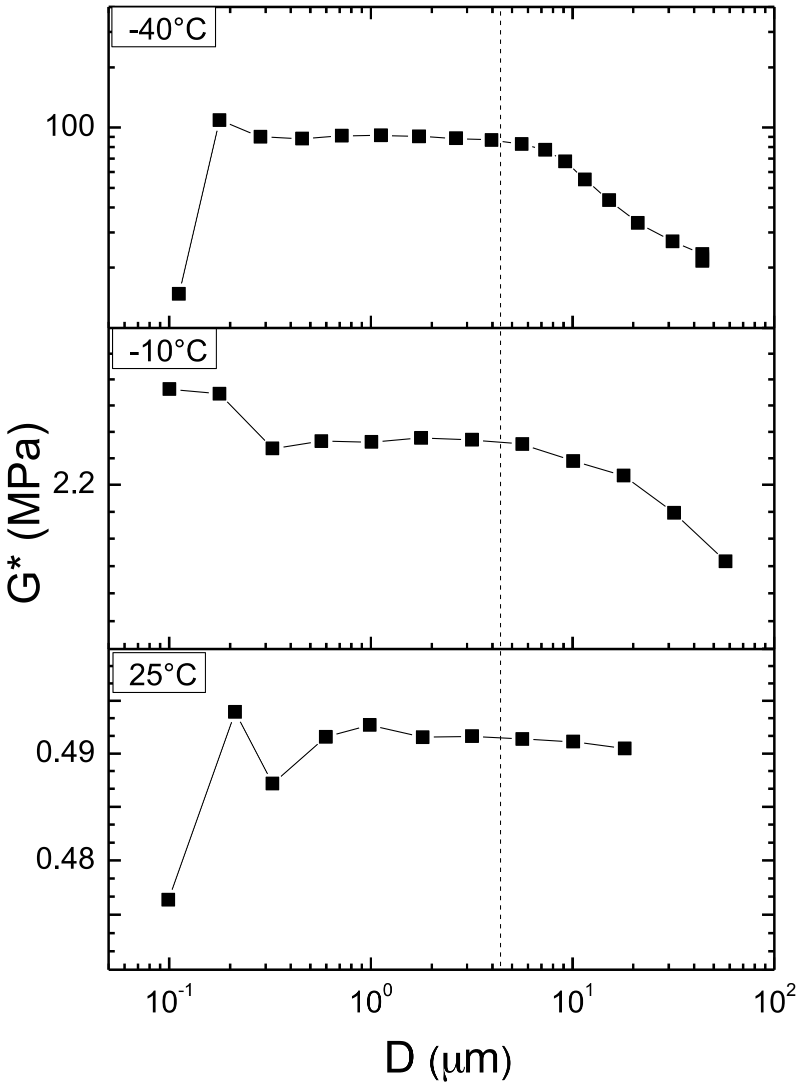

Figure A.11. DMA linearity test: Complex shear modulus G dependence upon displacement D.*

Comparison of the DMA and rheology master curves

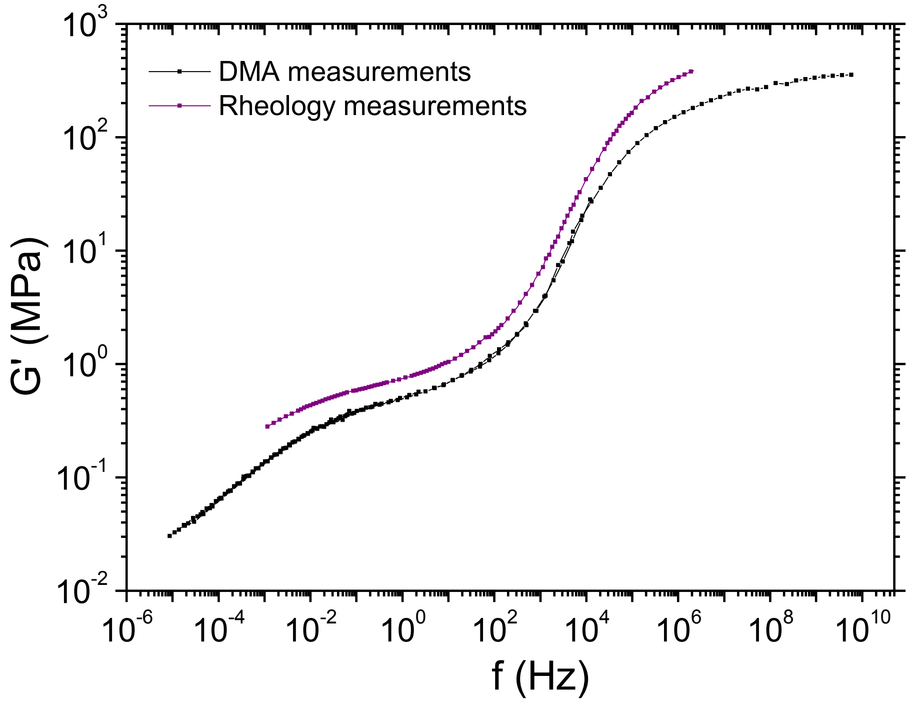

Figure A.12. DMA and Rheology master curves of the real part (G') of the complex shear modulus G for neat SBR.*

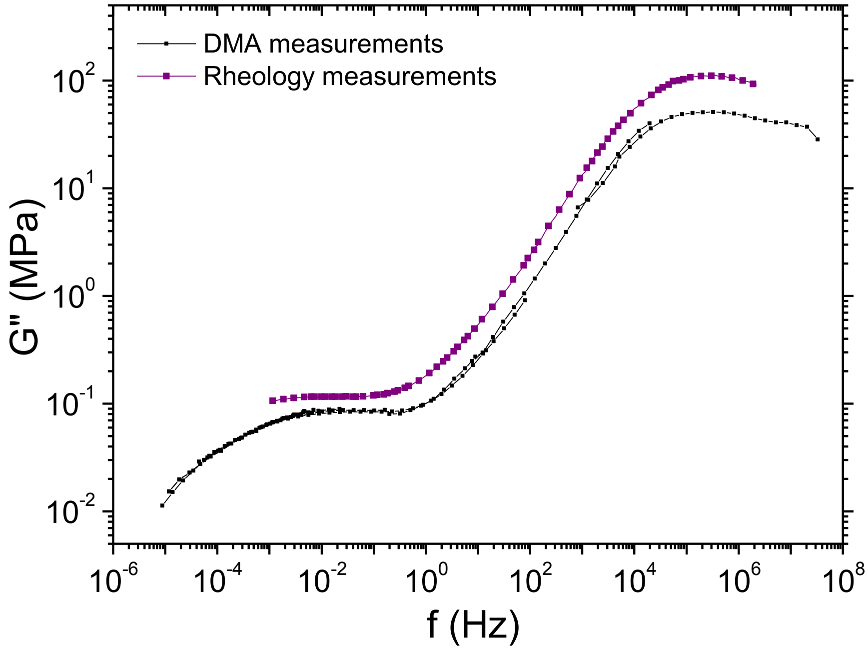

Figure A.13. DMA and Rheology master curves of the imaginary part (G") of the complex shear modulus G for neat SBR.*

Rheology master curves of the SBR/AluC nanocomposites

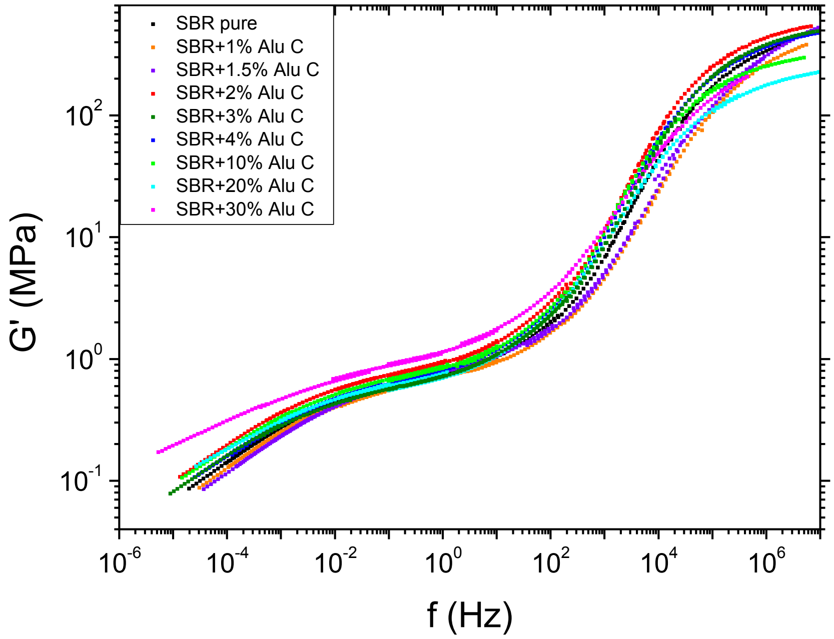

Figure A.14. Rheology master curves of the real part (G') of the complex shear modulus G for SBR/SAlu C nanocomposites.*

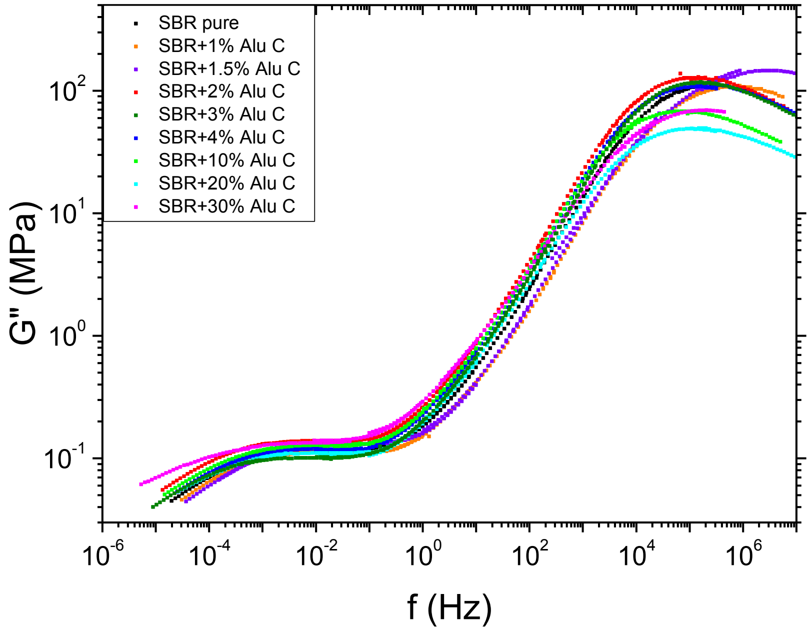

Figure A.15. Rheology master curves of the imaginary part (G") of the complex shear modulus G for SBR/SAlu C nanocomposites.*

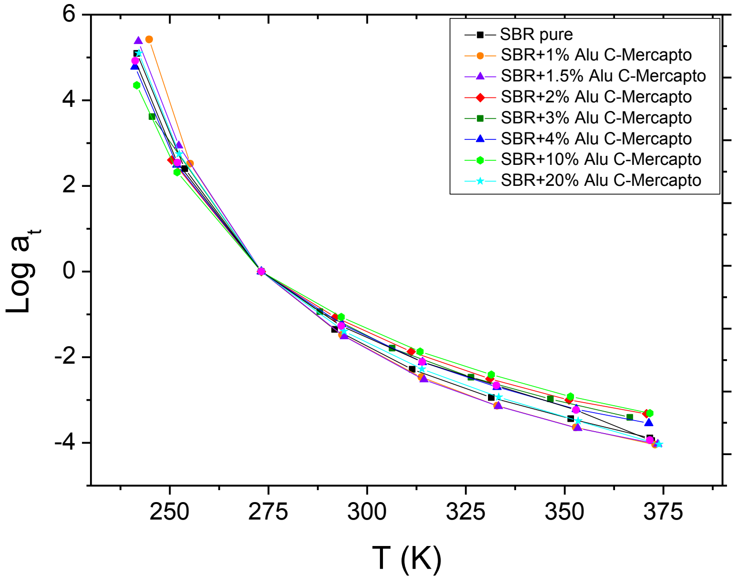

Figure A.16. Shift factor a_T (logarithmic) dependence upon temperature for SBR/Alu C-Mercapto nanocomposites.

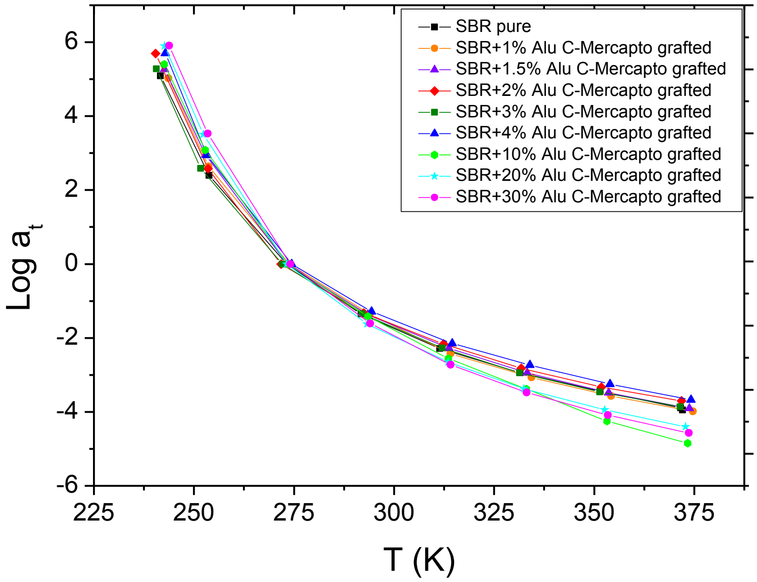

Figure A.17. Shift factor a_T (logarithmic) dependence upon temperature for SBR/Alu C-Mercapto grafted nanocomposites.

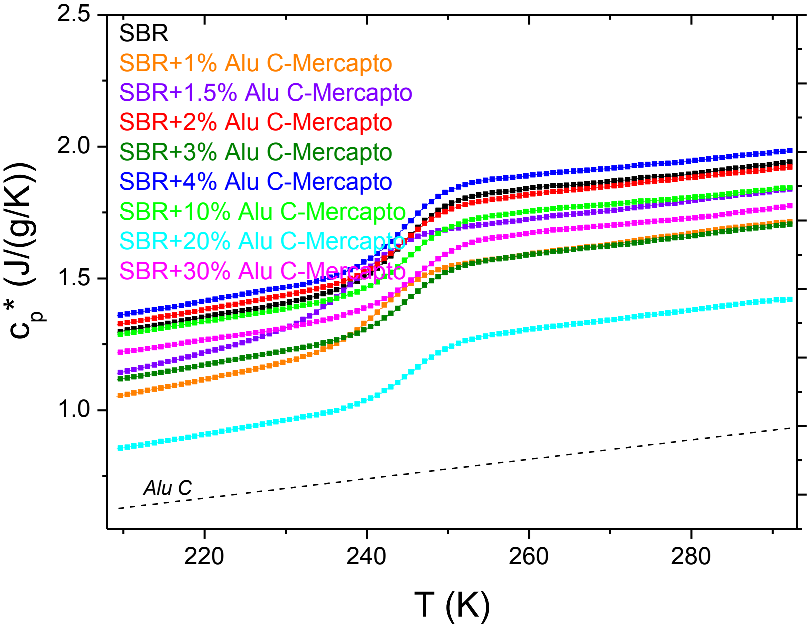

Figure A.18. Complex heat capacity c_p for neat SBR, neat Alu C and SBR/AluC –Mercapto nanocomposites.*

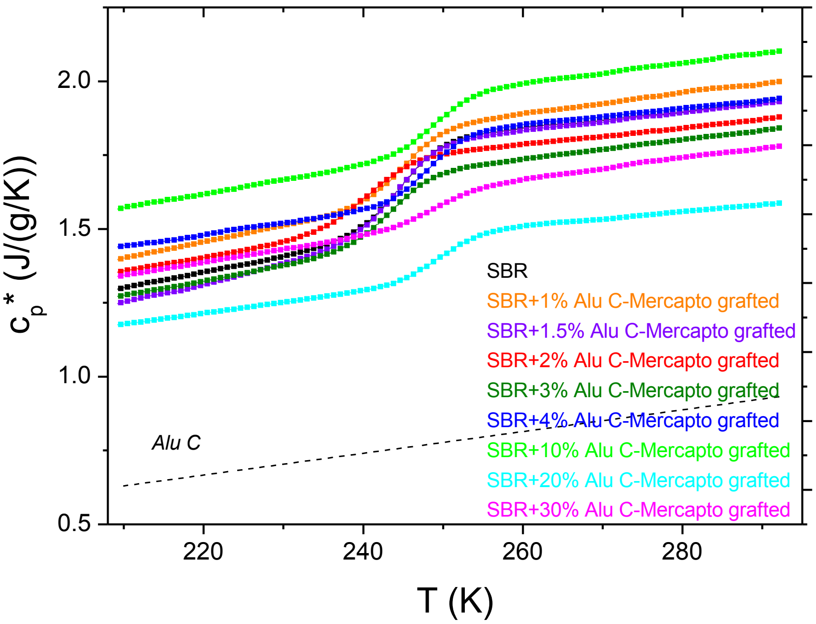

Figure A.19. Complex heat capacity c_p for neat SBR, neat Alu C and SBR/AluC –Mercapto grafted nanocomposites.*

Annex VI. Sample preparation issues

Creation of the polymer nanocomposites (styrene-butadiene rubber (SBR)/Al_2O_3) stood in the center of research activities during the first few months of PhD work. Laboratory of Advanced Materials did not have experience working with rubbers at that time, so I have encountered some problems with sample preparation procedure.

SBR is solid at room temperature, so it was decided to prepare nanocomposites from polymer solution. Appropriate solvents were tested to incorporate the Al_2O_3 filler into the matrix material. The first attempts of using toluene as a solvent resulted in the nanocomposites that contained large amounts of solvent at the end. Numerous unsuccessful attempts were made to evaporate toluene from the samples. The research was made with other solvents (Benzene, n.Hexane, n-Pentane, Chloroform) and Chloroform has been chosen. Fig. A.20 illustrates TGA solvent evaporation experiments for SBR solution in different solvents. Subsequent FTIR investigations showed no Chloroform absorption bands in final samples (Annex III).

During the samples preparation from solution, nanoparticles presented a trend towards agglomeration and sedimentation. Due to that, the nanoparticles dispersion in the final sample was very poor (Fig.A.21, a). To avoid that, nanoparticle agglomerates were broken by sonication before adding polymer solution. After polymer was added, the mixture was processed in a planetary mixer and dried using freeze-dry setup which I assembled myself (Fig. A.22).

Beside the incorporation of nanoparticles, the shaping of samples for DMA or electron microscopy was important. Samples for DMA should have well defined geometry. SBR is a sticky material, and this property is an obstacle for using conventional methods. Molds made out of polyvinylsiloxane were produced to shape the samples (Fig.A.23). This reduced sticking of polymer to the molds.

For the electron microscopy, cross-section samples were needed. Because of low T_g and stickiness of the systems, it was difficult to cut good cross-section samples at normal conditions. To solve this problem, disk-like samples were cooled down to temperatures below T_g using liquid nitrogen and then cross-sections were cut.

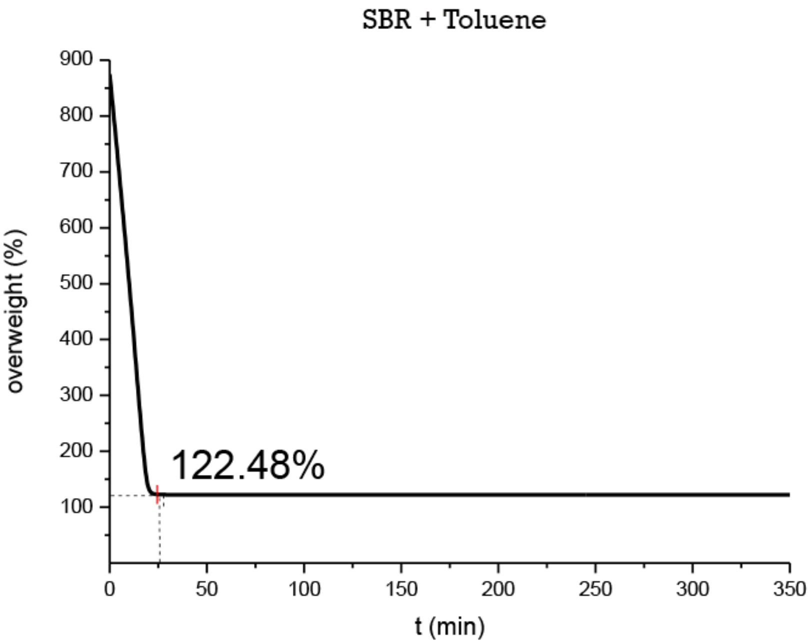
SBR + Toluene
overweight (%)
900
800
700
600
500
400
300
200
100
122.48%
0
50
100
150
200
250
300
350
t (min)

a)

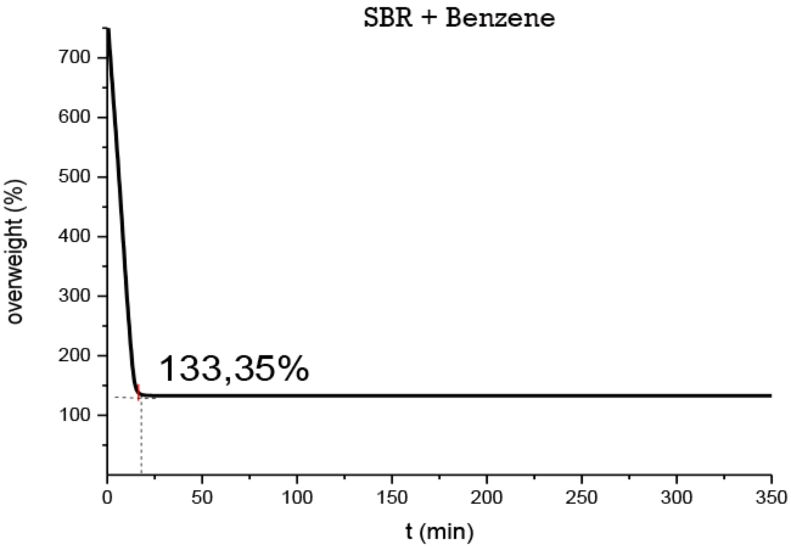
SBR + Benzene
overweight (%)
700
600
500
400
300
200
100
133,35%
0
50
100
150
200
250
300
350
t (min)

b)

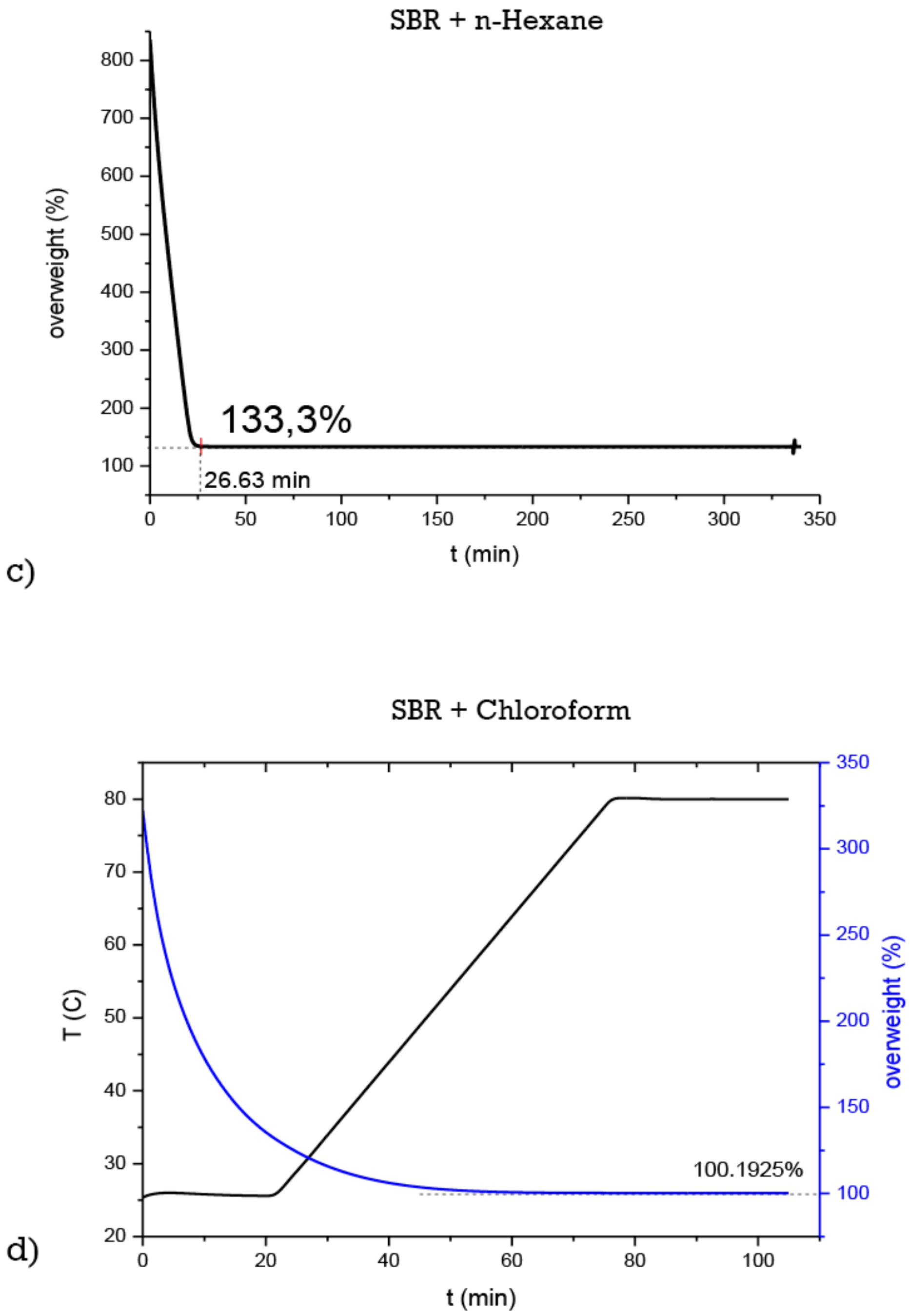

Figure A.20. Solvent evaporation as measured by TGA.

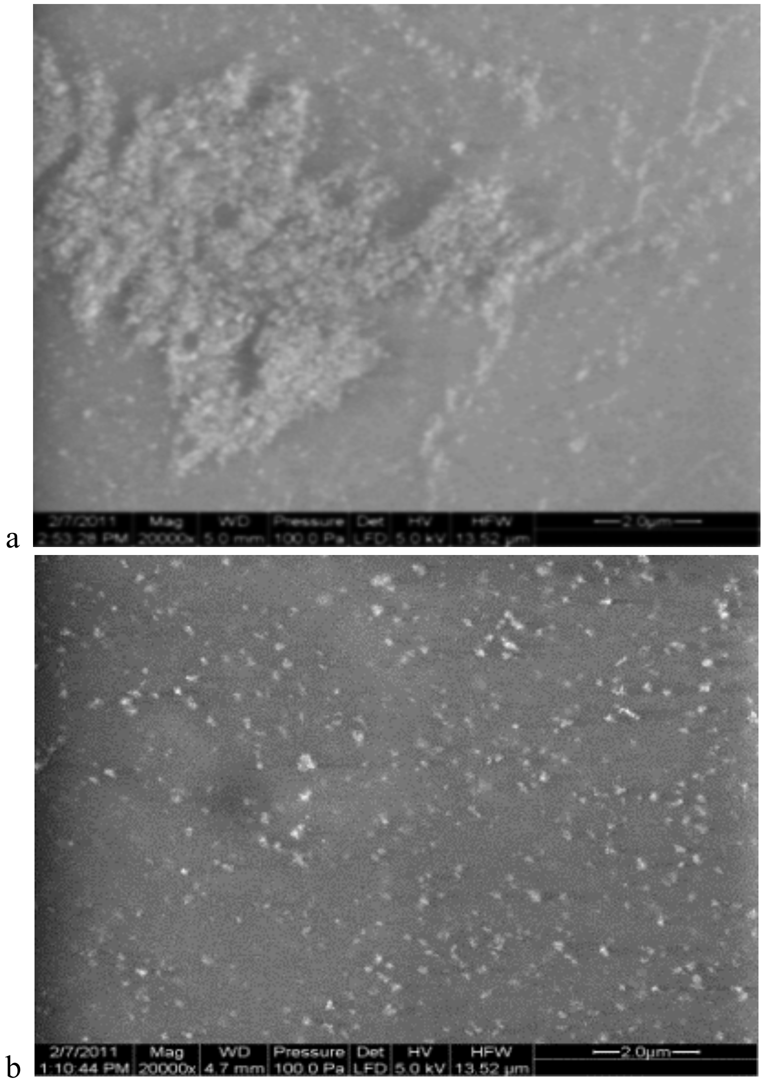

Figure A.21. Environmental SEM image of Alu C particles in SBR matrix: a – one of the first samples, inhomogeneous dispersion; b – one of the latest samples, homogeneous dispersion.

Figure A.22. Freeze-dry setup.

Figure A.23. Mold made of polyvinylsiloxane.